

Ground displacements in the Lower Namoi region

Pascal Castellazzi and Wolfgang Schmid

25 May 2020

Client: New South Wales Department of Planning, Industry and Environment



Acknowledgements

We acknowledge the partnership with the New South Wales Department of Planning, Industry & Environment (NSW DPIE) Water Group (in particular Susan Hamilton and Chris Rumpf). We also thank the NSW DPIE Water Group for sharing data and technical assistance.

Citation

Castellazzi P¹ and Schmid W² (2019) Ground displacements in the Lower Namoi region. Report. CSIRO, Australia.

¹CSIRO Land and Water, Urrbrae, SA

²CSIRO Land and Water, Floreat, WA

Copyright

© Commonwealth Scientific and Industrial Research Organisation 2020. To the extent permitted by law, all rights are reserved and no part of this publication covered by copyright may be reproduced or copied in any form or by any means except with the written permission of CSIRO.

Important disclaimer

CSIRO advises that the information contained in this publication comprises general statements based on scientific research. The reader is advised and needs to be aware that such information may be incomplete or unable to be used in any specific situation. No reliance or actions must therefore be made on that information without seeking prior expert professional, scientific and technical advice. To the extent permitted by law, CSIRO (including its employees and consultants) excludes all liability to any person for any consequences, including but not limited to all losses, damages, costs, expenses and any other compensation, arising directly or indirectly from using this publication (in part or in whole) and any information or material contained in it.

CSIRO is committed to providing web accessible content wherever possible. If you are having difficulties with accessing this document please contact csiroyenquiries@csiro.au.

Contents

Executive Summary.....	11
Summary of Recommendations.....	13
Part I Project Introduction	14
1 Problem Setting and Background.....	15
2 Objectives and Scope of CSIRO project milestones.....	15
3 Long-term Objectives.....	16
3.1 Other Basins in New South Wales.....	16
3.2 Land Subsidence Modelling.....	17
4 Area of Interest for InSAR and Benchmark Surveys.....	18
Part II Observing ground displacements using radar interferometry	20
1 Introduction.....	20
2 Available SAR images for Lower Namoi region.....	23
2.1 Older SAR data archives.....	23
2.2 Recent Sentinel-1 time-series.....	24
3 Processing.....	27
4 Results.....	28
4.1 InSAR-derived trends in ground level changes for 2016-2019.....	28
4.2 Temporal behaviour of ground levels.....	31
4.3 Comparison with results from PSI-INSAR.....	34
5 Summary.....	36
Part III Comparison of InSAR with in situ Benchmark data	37
1 Introduction.....	37
2 Time-periods of InSAR versus Benchmark Survey.....	37
3 Available in situ Benchmark Data.....	38
4 Processing.....	40
4.1 Processing of Benchmark Data for Comparison.....	40
4.2 Processing of InSAR Results for Comparison.....	41
5 Results.....	42

6	Summary.....	46
---	--------------	----

Part IV Correlating ground movements with auxiliary data 47

1	Introduction.....	47
2	Exploring temporal correlations.....	49
2.1	Hydraulic heads and benchmark deformation.....	49
2.2	Hydraulic heads and InSAR deformation.....	59
3	Exploring spatial correlations.....	68
3.1	Soil clay content.....	68
3.2	Land use.....	73
4	Summary.....	75

Part V Conclusions and Outlook 78

Appendix A	InSAR - Supplemental.....	84
Appendix B	Benchmark Surveys - Supplemental.....	89
Appendix C	InSAR-Benchmark Comparison – Supplemental.....	99
Appendix D	Correlating Ground Movement with Auxiliary Data – Supplemental.....	109
References	115

Figures

Figure 1 Study area for InSAR analysis and the benchmark survey of April 2019.....	19
Figure 2 Principle of the InSAR techniques: the phase difference observed by comparing two SAR images is used to infer satellite-to-ground distance changes.	21
Figure 3 Examples of spatial patterns in intermediary and final products of a simple InSAR processing: (A) Amplitude map of the Namoi region from one Sentinel-1 image; (B) Inteferogram generated using a pair of SAR images distant by 12 days; (C) corresponding InSAR coherence map, where lighter areas highlight good signal correlation; (D) corresponding unwrapped phase map, produced by applying an unwrapping algorithm on the interferogram (B). Note the correspondence between spatial patterns of (B) and (D). Also note that (B) and (D) are overlaid on the amplitude (A) for clearer visualization.	22
Figure 4 Temporal density of the SAR image stack showing the discontinuous SAR acquisition for the Lower Namoi region.	24
Figure 5 Sensing strategy used by Sentinel-1 satellite in order to cover a 250 km-wide ground footprint. This acquisition strategy is referred to as Terrain Observation with Progressive Scans SAR (TOPSAR; Source: ESA).....	25
Figure 6 Spatial coverage (A) and temporal density (B) of the SAR image stack processed for this study. The clear image on (A) shows the continuous SAR acquisition covering the study area, the dark image corresponds to the subset selected for InSAR processing.	26
Figure 7 Connection graph of the 94-images Sentinel-1 stack used to assess the feasibility of creating interferograms using the image stack. The Y axis present the 3D positioning of the satellite while acquiring the images (in reference to the master image) and the X axis presents the acquisition time-series.....	27
Figure 8 Ground level change along (A) the ground-satellite angle, referred to as Line Of Sight (LOS), and (B) projected along a vertical axis. Note that InSAR directly measures (A). (B) is inferred by considering the horizontal component of motion as being negligible (A). Due to the SAR acquisition geometry, velocity values in the horizontal direction are slightly higher than values measured along the LOS angle (≈ 35 degree). The groundwater model boundary is shown as black line.....	29
Figure 9 Example of velocity values along a North-South and an East-West transect.....	30
Figure 10 Example of velocity values along a North-South and an East-West transect.....	31
Figure 11 Amplitude of the absolute vertical velocities measured by InSAR for every year: (a-b) 2016; (c-d) 2017; (e-f) 2018.	32
Figure 12: Monthly precipitation anomaly over Wee Waa (-30.12; 149.32; source: http://www.bom.gov.au/ - station number 053034). Reference period is 2005-2015.	32
Figure 13 Time-series of vertical ground level changes over 3 random points located in the eastern part of the Lower Namoi region (black curves: ground level change; red curves: temporally-filtered ground level change signal.....	33

Figure 14 Similar to Figure 13, with three other points located in the western and central part of the Lower Namoi region.	33
Figure 15: Results from PSI analysis over the Southwestern corner of the study area, with the groundwater flow model boundary overlaid for spatial reference. (A) Takes into account the same SAR time-series as the ISBAS-InSAR analysis, and (B) only takes into account images from 2017.	35
Figure 16 Subsidence and Control Benchmarks in the Lower Namoi Region re-surveyed in April 2019	39
Figure 17 Example of calculation of Linear Trends of Subsidence from Benchmark Data	40
Figure 18 Evolution of the level of subsidence benchmarks from the late 1970's to 2019.	42
Figure 19 Vertical velocities of the subsidence benchmarks (top) incl. zoom-up (below). The numbering attributed to each subsidence benchmark is in correspondence with Table 3 and Table 8.	43
Figure 20 Time-series of Vertical Displacement [mm/yr] at Locations of Benchmarks with more than 2 mm/yr	44
Figure 21 Correlation between all annualised trends of vertical velocities for all subsidence benchmarks (in blue) and benchmarks with displacement > annualised measurement error (in red) with InSAR velocities derived at benchmark locations (in mm/yr) with a 15 x 15 kernel. ...	45
Figure 22 Design of Subsidence Benchmarks (adapted from Ross and Jeffery, 1991).....	48
Figure 23 Benchmark displacement trends using a measurement inaccuracy of ± 1 mm/yr, hotspots of InSAR displacement (only subsidence < -20 mm/yr shown), and distribution of modelled clay content over the top metre of soil.	50
Figure 24 Time-series of heads (WL) & critical heads (CH) at benchmarks with >2 mm/yr (original WLs and CHs derived from original WLs (a); averaged WLs and averaged CHs derived from original WLs – Method A (b); averaged WLs and CHs derived from average WLs – Method B (c)).....	52
Figure 25 Time-series of heads (WL) & critical heads (CH) with benchmark subsidence at benchmarks with >2 mm/yr (original WLs and BM subsidence (a); averaged CHs derived from original WLs with BM subsidence – Method A (b); CHs derived from average WLs with BM subsidence – Method B (c)).....	53
Figure 26 Individual time-series of heads & critical heads derived by different methods and subsidence recorded at 5 benchmarks >2 mm/yr.	54
Figure 27 Correlation between annual mean head (a) or annual mean critical head (derived from original heads) (b) or annual mean critical head (derived from averaged heads) with benchmark subsidence (c) using linear (left) or exponential (right) regression.	55
Figure 28 Critical head drop in piezometers (in m) during the entire period of water level recording (A) and during the InSAR observation period (B) and benchmark displacements trends (in cm/yr)	58

Figure 29 Water levels and critical heads at bores near the 5 benchmarks with subsidence trends of >2 mm/yr (black box: time window of InSAR analysis)	59
Figure 30 InSAR displacement trends near bores using a 5x5 averaging kernel (300m x 300m), hotspots of InSAR displacement (only subsidence < -20 mm/yr shown), and distribution of modelled clay content over the top metre	60
Figure 31 3D Scatter plot of critical head drop, proportion of clay in the surficial soil, and InSAR-derived deformation trend for manual data (left) or logger data (right) during the 3-year InSAR period (general (a); focus on relation between critical head drop and deformation (b); focus on relation between percent clay and deformation (c))	61
Figure 32 Histograms of critical head drop from bores with manual data (left) or logger data (right)	62
Figure 33 Time-series of heads and critical heads of selected piezometers with logger data (a) since recording started and (b) during the 3-year InSAR period.	63
Figure 34 Time-series of heads and critical heads of selected piezometers with manual data (a) since recording started and (b) during the 3-year InSAR period	64
Figure 35 Time-series of deformation and critical heads of selected piezometers with logger data (a) or manual data (b) during the 3-year InSAR period	65
Figure 36 Time-series of deformation and heads of selected piezometers with logger data (a) or manual data (b) during the 3-year InSAR period	66
Figure 37 Relation between drop in critical heads and deformation trends during the 3-year InSAR Period for select piezometers with non-zero critical head drop for logger data (a) and select maximal drop in critical heads (> 3 metres) for manual data (b).	67
Figure 38 Ground displacements in areas where clay content in the first meter of soil contains less than 45% of clay (A), and more than 45% of clay (B). The figure highlights the importance of considering high proportions of clays, which typically occurs in the valley, where most of the water is extracted. The red line shows the boundary of the groundwater model.	70
Figure 39 Absolute vertical displacement velocities as a function of the clay content in the first meter of soil for different periods considered in the InSAR time-series, with (in red) the 5, 50 and 95% percentile envelopes. The shape of the percentile curves (e.g. top graph) suggests a near-linear relation despite the shape of the scatter plot. The percentiles (red lines) are calculated for every 2.5% increment of clay content.	71
Figure 40 Correlation Relation between PSI-measured displacements and clay content for a multiple years PSI process (2015-2019; A) and a single (dry) year PSI process (2017; B). The low deviation observed on A indicates that only ground targets over built infrastructure (the only with high InSAR coherence in 2016) offers a relative protection to the influence of surficial clays. The percentiles (red lines) are calculated for every 2.5% increment of clay content. This figure was built from results shown on Figure 15.	73
Figure 41 Histograms of InSAR-derived vertical displacement velocities for each land use class (see nomenclature in Table 6) in percentage of the total observation for each class. Classes 330, 430 (cropping areas) and 620, 630 (near water bodies) present noisier InSAR results.	75

Figure 42 Vertical Displacement Trend in the Lower Namoi based on ISBAS-InSAR over a 3 year period (2016, 2017, 2018) with overlain Topography and location of Benchmarks.....	85
Figure 43 Generalised Surface Geology in the Lower Namoi for comparison with Vertical Displacement Trend in the Lower Namoi based on InSAR with overlain Topography and location of Benchmarks	87
Figure 44 Locality Plan – Namoi River Basin (Ross and Jeffery, 1991)	89
Figure 45 Locality Plan – Lower Namoi Valley (Ross and Jeffery, 1991)	91
Figure 46 Comparison of InSAR vertical displacement with benchmark trends using no measurement inaccuracy at all (white areas: below coherence threshold)	105
Figure 47 Comparison of InSAR vertical displacement with benchmark trends using a measurement inaccuracy of -1 mm/yr (white areas: below coherence threshold.....)	107
Figure 48 Correlation between drop in head (left)s or critical heads (right) and deformation trends during the 3-year InSAR Period for select piezometers with non-zero critical head drop for logger data.	111
Figure 49 Correlation between drop in head (left) or critical heads (right) and deformation trends during the 3-year InSAR Period for select maximal drop in critical heads (> 3 metres) for manual data.	113

Tables

Table 1 SAR mission with potentially available time-series usable for InSAR and observations regarding the result of the search (ESA: European Space Agency; CSA: Canadian Space Agency; MDA: MacDonald, Dettwiler and Associates Ltd.; JAXA: Japan Aerospace Exploration Agency).24	
Table 2 Main processing parameters	27
Table 3 Comparison of annualised trends of vertical velocities for subsidence benchmark (with displacement > annualised measurement error) with InSAR velocities derived at benchmark locations (in mm/yr).....	45
Table 4 Lookup table for estimated subsidence as a function of critical head for two selected piezometers using two different methods of deriving annual mean critical heads.....	57
Table 5 Estimation of the trend deviation due to the clay content in the first meter of soil. The trend estimation (curve fitting) accounts for all clay content values between 15 and 60%. Trend of the 5-95% red lines shown on Figure 39. To detect subsidence around the Benchmark 27 and 28 (Figure 28), the error estimates need to account for 50% of clay in the surficial soil.....	72
Table 6 Statistical analysis of the InSAR results per land use class. Classes representing more than 1% of the total coverage are marked in grey.	74
Table 7a Subsidence Benchmark Surveys 1974-1990 [m above AHD] (after Ross and Jeffery, 1991) and April 2019 - Results (Colour codes: see reverse side).....	95
Table 8 Comparison of annualised trends of vertical velocities for each subsidence benchmark with InSAR velocities derived at benchmark locations (in mm/yr).....	101

Acronyms and Abbreviations

BM	Benchmark
CH	critical head (historical minimum of head at which pre-consolidation occurred)
CSIRO	Commonwealth Scientific and Industrial Research Organisation
D-InSAR	Differential InSAR
EM	ElectroMagnetic
ENVISAT	"Environmental Satellite" Operated by the European Space Agency (ESA)
ERS	European remote sensing satellite consisting of two satellites (ERS-1 and ERS-2)
InSAR	Interferometric Synthetic Aperture Radar
(I)SBAS-InSAR	(Intermittent) Small Baseline Subset InSAR
LNM	Lower Namoi Model
LOS	Line-Of-Sight
NSW DPIE	New South Wales Department of Planning, Industry & Environment
OEH	Office of Environment and Heritage
PSI	Persistent Scatterer Interferometry
RTK	Real-time Kinematic survey technique
SAR	Synthetic Aperture Radar
TOPSAR	Terrain Observation with Progressive Scans SAR (TOPSAR)
WL	Water level
WSP	Water Sharing Plan

Executive Summary

CSIRO and the New South Wales Department of Planning, Industry, and Environment have assessed and quantified land subsidence and its relation to groundwater extraction in the Lower Namoi aquifer using a multi-source dataset from surveyed benchmarks, historical groundwater levels, and displacement-detection derived from space-borne radar imagery (Interferometric Synthetic Aperture Radar (InSAR)). The observations derived from analysing individual data sources and correlations and discrepancies between them are presented and interpreted.

The underlying purpose of the study is to provide a toolset for the determination or derived evidence of land subsidence or aquifer compaction in the Lower Namoi (and potentially for other NSW basins) that could be used for water level response management and as decision-support basis (e.g., Ministerial restrictions of bore extractions on presentation of evidence of land subsidence or aquifer compaction). The presented methodology and findings could also serve as an early warning system for land holders and regulators to monitor the impact of incremental effects of further groundwater extraction on deformation. Long-term benefits are the potential application of the provided novel subsidence monitoring methods in other areas of NSW and to inform and constrain the Lower Namoi and other NSW groundwater models with improved groundwater deformation data.

Due to the unavailability of remotely sensed ground displacement in the Lower Namoi over most of the 45-year benchmark observation period, displacement mapping derived from a dense time-series of space-borne radar images could only be used to monitor ground displacements from late-2015 to late-2018. The resulting displacement trend map appears to strongly follow cropping patterns, suggesting that short-term land movements are largely dominated by cropping cycles and its influence on the clay-rich soils occurring in the Lower Namoi. However, the Lower Namoi alluvium follows a contrasting land movement pattern in comparison with its non-alluvial surroundings characterised by lower clay content. Amplitudes of ground displacements are particularly strong during and following a wet (flood) year, as noted by previous studies. Another type of radar image processing was also tested and shows much less sensitivity to cropping activities or soil clay content. However, this technique can only be used to monitor displacements of coherent infrastructure (roads, buildings) and is not usable over crops. Displacements appear to show local instability along linear transportation corridors, as expected over clay-rich soils and as witnessed during a field visit. However, no well-defined subsidence pattern (e.g. which can be related to hydrogeological boundaries) could be found.

Benchmark data from a recent survey were compared with previous data from 1974 to 1990. Rates of ground-level change exceed -1 mm/yr in 8 out of 32 benchmarks and exceed -2 mm/yr in 5 out of 32 benchmarks. The maximum observed displacement trend is -8.5 mm/yr. We suggest the period between surveys to be at least six years to prevent a too dense frequency from yielding detection thresholds that are above any, even maximum, displacement trends. Displacements measured by comparing the last two surveys (2019 and the last one before that, usually 1990) are generally less than the trend based on all available data. While this seems to suggest a “slow-down” of the subsidence rates, the recent displacement of the last few years is hidden within the ≥ 29 -year gap between the last two surveys and, hence, is unknown.

Comparison between short-term (radar-based) and long-term (benchmark) displacement records are greatly limited by their different sensitivity to potential seasonal, annual, or multi-annual variations of ground level in relation to surficial clays and cropping activities. Unlike long-term trends from benchmark surveys, short-term radar-based trends are affected by noise from inter-

annual variations that are influenced by cropping and agricultural practices, swelling/shrinking clays, and climate variability. The longer and drier the radar-based periods are, the less is the derived displacement clouded by this noise.

The long-term relation between change in critical groundwater heads (historical minima of heads at which pre-consolidation occurred) and benchmark deformation is commensurate with the coincidence of periods of significant groundwater depletion (mid-1970s, early 1980s, mid-1990s) and can be described by a well-correlated empirical relationship. However, this prediction of subsidence as a function of dropping critical heads is specific for localised hydrogeologic conditions and the 45-year period of benchmark observations and cannot be spatially or temporally extrapolated. Contrastingly, correlations between short-term radar-based displacement data and temporally corresponding critical head or head changes are weak, further supporting the idea that short-term displacements are related to surficial processes rather than groundwater pressure change.

The lack of displacement patterns relatable to groundwater pressure loss in the short-term in radar-based displacement monitoring is supported by the hydraulic head analysis. First, it shows that no critical head drop occurred in $\approx 90\%$ of the bores with sufficient monitoring data during the radar monitoring period. Second, it is noted that no critical head drop occurred in and around the main long-term subsidence area detected through the benchmark surveys. Finally, the hydraulic head records show that a large number of critical heads over the valley were established in or prior to the 1990's. This suggests that no subsidence occurred during the short-term survey time-period (2015-2018), and that benchmark-derived displacement measurements are largely related to subsidence in or prior to the 1990's.

By exploring the spatial relations between clay content in soils and radar-derived displacement data, and by assuming that no other sources of displacement impact these data during the period of study, the sensitivity of radar-based displacement estimates toward surficial clay movements can be estimated. It is observed that the trend deviation in radar-based displacement data are of the order of 2 to 2.5 cm/yr when considering short-term monitoring (3 years) and strong climate variability in the study period (two dry years following a wet year). This estimation has to be considered conservative given the crop types, clay content, and generally low radar coherence observed over the Lower Namoi, compared to other tests performed over other areas (Murrumbidgee, Condamine). This observation informs on the reachable sensitivity of such technique to groundwater-related processes and is of great value in the perspective of deploying such radar-based techniques over other clay-rich alluvial valleys in NSW or elsewhere.

Summary of Recommendations

Further monitoring of ground displacement in the Lower Namoi through regular monitoring of installed benchmarks is sensible if at reasonable intervals. For a single survey to detect displacements trends that are beyond a cumulative error between surveys, we suggest benchmark survey intervals of at least six years.

Future InSAR monitoring should focus on longer time-series of at least 8 years, which increases the chances for the long-term subsidence trend not be obscured by measurement noise related to surficial clays. Alternatively, installation of corner reflectors at strategic locations would allow InSAR monitoring with a detection threshold finer than the long-term subsidence rates measured in this study. Future InSAR monitoring should also consider the strong climate variability of the region and focus on dry years, if possible, to reduce the sensitivity of InSAR-monitored surface displacement to the swelling of surficial clays during wet years. This will improve the accuracy of InSAR-monitoring and the chance of detecting groundwater-exploitation related land subsidence during this period.

Localised empirical functional relationships between dropping critical heads and benchmark displacement can be formulated but cannot be used to spatially extrapolate or temporally predict land subsidence. To overcome this limitation, three-dimensional numerical models are needed that are based as well on 3D-geological models, which represent the compressibility, thickness and storativity of the aquifer and fine-grained interbeds. Constraining the Lower Namoi groundwater flow model (LNM) by past and future critical head and subsidence observations from benchmarks and InSAR-monitoring would enable the evaluation of sustainable groundwater extraction levels and strategies to limit ground subsidence and its consequences. However, for that, the LNM needs to be updated in time (e.g., to include periods of critical head drop prior the current start of the model) and upgraded in methodology. While the lack of spatially distributed historic observations of significant vertical displacement may not permit a proper calibration of simulated deformation or estimation of elastic and inelastic storage coefficients, predictions of critical head drop and deformation that follow groundwater depletion within the LNM should still be considered for future scenarios.

A predictive LNM can be used for a risk analysis of 'worst-case' modelled land subsidence that unlikely exceeds a threshold to predict critical drawdowns that result in inelastic compaction or to determine where in space predictive uncertainty can be reduced by adding new InSAR and/or benchmark observations to the model. This approach of combining improved modelling methodology, observation data, and uncertainty analysis could be applied to other NSW-DPIE MODFLOW models in New South Wales that simulate groundwater systems with significant groundwater extraction and spatially distributed subsidence above detection thresholds.

Part I Project Introduction

The New South Wales Department of Planning, Industry & Environment (NSW-DPIE) and CSIRO Land and Water have entered into a consultancy project on the assessment of land subsidence over the Lower Namoi groundwater resource based on an analysis of available Synthetic Aperture Radar (SAR) imagery and comparison of displacement mapping derived from Interferometric SAR (InSAR) with surveyed benchmark data. An additional component includes the analysis of the correlation between land subsidence and groundwater level hydrographs, soils, and land use in the Lower Namoi region.

The Lower Namoi groundwater source has been selected for this study because of known, albeit minor, land subsidence that is potentially associated with groundwater extraction, dedicated benchmarks already installed in the field, and the existence of a previous Lower Namoi groundwater model potentially capable of simulating land subsidence.

The main purpose of the study is to measure land subsidence with SAR imagery and compile all other evidence of subsidence from auxiliary measurements. The results from this study may be used for water level response management and as a decision-support basis for the ministerial management or restriction of bore extractions as stipulated by the Water Sharing Plan (WSP) 2019. Secondly, correlations between land subsidence and critical groundwater head change in hydrographs could be utilised to set local groundwater level management targets and thresholds to forecast, prevent or limit irreversible sediment compaction and any associated land subsidence.

Thirdly, and beyond the scope of this project, long-term objectives of the improved ground deformation observations will be to better inform and constrain an updated and technically upgraded Lower Namoi MODFLOW model. Fourthly, this includes the quantification of ‘worst-case’ land subsidence that unlikely exceeds a threshold (based on the uncertainty of model input parameters) and the determination where model outcome uncertainty can be reduced by adding new InSAR and/or benchmark observations to the model. The primary use of such model could be the prediction and prevention of critical drawdowns that would result in inelastic compaction by setting groundwater level management targets. An upgraded model could also be used to manage the feedback and impacts of land subsidence on water-management related aspects, e.g. on aquifer storage capacity, environmental assets, surface / groundwater interactions, or integrity of infrastructure.

Current risk assessments of the Murray Darling Basin have highlighted a low confidence in data that inadequately identify the level of risk of sediment compaction and consequent land subsidence associated with groundwater extraction in the NSW alluvial groundwater systems. This is due to a lack of subsidence observation and proper models that can simulate feedbacks of groundwater-extraction related land subsidence on surface water systems. This will become exceedingly more important as pressure on groundwater extractions will most likely increase because of climate-change related surface-water shortage.

1 Problem Setting and Background

The Water Sharing Plan for the Upper and Lower Namoi Groundwater Sources 2019 (WSP 2019), includes an objective to “protect the structural integrity of the aquifers and groundwater quality, by ensuring groundwater extraction does not result in any aquifer compaction, aquitard compaction, land subsidence or change in the beneficial use of the aquifer.” Under section 324 of the NSW *Water Management Act 2000*, the Minister may prohibit or restrict the taking of water “If satisfied that it is necessary to do so—

- (a) to maintain or protect water levels in an aquifer, or
- (b) to maintain, protect or improve the quality of water in an aquifer, or
- (c) to prevent land subsidence or compaction in an aquifer, or
- (d) to protect groundwater-dependent ecosystems, or
- (e) to maintain pressure, or to ensure pressure recovery, in an aquifer.” (WMA,2000).

In the past, evidence of minor land subsidence or aquifer compaction in the Lower Namoi Valley of less than 50 mm had been observed by comparing levelling surveys from 1974 to 1990 (Ross and Jeffery, 1991) based on benchmarks installed in 1974 and 1981. In addition, a regional MODFLOW groundwater model had been created for the period 1980 to 1998 with simulated land subsidence (Ali et al., 2004) manually calibrated against the compaction observed at the benchmarks for the overlapping period between 1981 and 1990. Subsidence of between 0.08 and 0.21 metres was recorded for this period. This Lower Namoi Groundwater model was subsequently updated for the period from 1980 to 2012 (version 6) and is being updated by the NSW-DPIE groundwater modelling team for the period up until 2017 (version 7). However, land subsidence simulations have not been upgraded to include newest MODFLOW technology that allows for a feedback of simulated land subsidence on the movement and conjunctive use of water resources (Schmid et al., 2014, Hanson et al., 2014, Boyce et al., 2020), nor calibrated against new observations from remote sensing (InSAR) or new benchmark surveys.

Because of this lack of renewed benchmark surveys and of updated and re-calibrated subsidence modelling, risk assessments of Namoi Alluvium Water Resource Plan (NSW-DPIE, 2019) have identified a low confidence in data to inform the risk of sediment compaction associated with groundwater extraction across all alluvial groundwater systems. The overall objective of this study is to increase this confidence by improving the monitoring of potential land subsidence in the Lower Namoi using various techniques from remote sensing and a new benchmark survey conducted in April 2019.

2 Objectives and Scope of CSIRO project milestones

The primary objective is to assess the spatial and temporal patterns of ground displacements over areas of intensive agriculture within the Lower Namoi groundwater resource. Ground displacement observations are derived using available InSAR imagery for 2015-2018 using

Sentinel-1 satellites and then compared with historically (1974-1990) and recently (April 2019) surveyed benchmarks that were installed in the Lower Namoi in 1974 and 1981. The purpose of the recent survey is to verify whether any further land subsidence has occurred over the 28-years' time-gap without surveying, during which groundwater extraction has continued. The InSAR technique applied is the Intermittent Small Baseline Subset InSAR (ISBAS-InSAR; Bernardino et al., 2002; Sowter et al., 2013), which is the most suitable for agricultural areas with varying vegetated land-covers and, hence, lower coherence between images. Any evidence of land subsidence or aquifer compaction found by this study may be used for water level response management and as decision-support basis for the ministerial management or restriction of bore extractions as stipulated by the WSP 2019.

A secondary objective is to determine the critical groundwater head change that would potentially result in inelastic storage loss in the Lower Namoi aquifer. This information could be utilised to set local groundwater level management targets and thresholds to prevent or limit irreversible sediment compaction and any associated land subsidence. This involves analysing correlations between groundwater level hydrographs and land subsidence derived from benchmark surveys and from InSAR processing results near monitoring bores. Generally, such points are preferable in areas where no swelling/shrinking soils nor major land-cover changes occur, which however is quite prevalent in the Lower Namoi similar to the Liverpool Plains (Kirby et al., 2003). Infrastructure (e.g. roads, canals, etc.) or areas in the vicinity of infrastructure fit those criteria. Aside from the objective to study the impact of groundwater head change on land subsidence, this also allows determining which infrastructure is at risk.

A third objective is to investigate the potential relationships between seasonal compaction or expansion from InSAR and swelling/shrinking clayey soils. If possible, such influence on deformation will be used to better isolate the effect of groundwater abstractions (and the related release of groundwater from interbed storage) on ground level changes. Lastly, the type of land-use and related cropping and/or crop water supply (natural versus irrigation) may have an impact on seasonal or long-term land subsidence.

3 Long-term Objectives

3.1 Other Basins in New South Wales

This project undertaken by CSIRO in collaboration with NSW-DPIE uses remote sensing techniques to detect ground displacements that are potentially applicable to other valleys or aquifers in NSW. The advantage of using the Lower Namoi Valley as a first test case is to prove the concept on small subsidence rates and with limitations inherent to the techniques in areas of vegetation and low SAR signal coherence. That is, any other valley or aquifer where vegetation is similar or sparser will have better InSAR coherence, hence the InSAR technique will be expected to work similarly or better than over the Lower Namoi valley.

3.2 Land Subsidence Modelling

Newest land subsidence simulation capabilities of MODFLOW include the feedback of impact of aquifer compaction/expansion on surface deformation, the dependency of aquifer-hydraulic properties on mesh deformation, and deformation-dependent surface-water/groundwater interaction & conjunctive use (Schmid et al., 2014; Hanson et al., 2014, Boyce et al., 2020). Such techniques can be used to manage the feedback and impacts of land subsidence on water-management related aspects, such as impacts on environmental assets, surface / groundwater interaction, or the integrity of infrastructure (e.g. surface-water conveyance). Therefore, it would be desirable not just to update the Lower Namoi Model (LNM) to recent as currently undertaken by the NSW-DPIE groundwater modelling team, but also to upgrade it by using such new subsidence simulation techniques and to keep the model current on a regular basis.

Ultimately, the modelled displacement of the improved, updated, upgraded, and kept-current LNM will need to be recursively recalibrated from time to time by utilising equally improved observations derived from InSAR (upscaled to MODFLOW resolution) in conjunction with benchmark survey data. Better monitoring will help inversely estimate subsidence-related model input, such as skeletal elastic and inelastic storage coefficients, and output, such as surface deformation.

However, even model results of a better informed and constrained LNM will always remain uncertain to some degree. Options to address this uncertainty are (A) to analyse and quantify the range of probable subsidence outcomes or (B) to reduce the uncertainty in model by specifically analysing the effect of uncertainty reduction in specific areas of the model by adding new InSAR or benchmark subsidence observations.

The probability analysis would be based on the uncertainty of subsidence model parameters and evaluate a conservative 'worst-case' subsidence that unlikely exceeds a threshold. While the InSAR analysis in this report gives some evidence of technique-dependent detection thresholds, the subsidence threshold can also be defined by the regulator. Outcomes of this analysis can be either contour maps of spatially varying worst-case subsidence rates or of varying probabilities of subsidence rates exceeding a particular threshold.

Areas where the InSAR analysis confirms or contradicts subsidence can be candidates for benchmark surveying either to be continued or discontinued and/or for a linear uncertainty analysis that studies the effect of any planned future monitoring on the uncertainty reduction in the upgraded/updated LNM ('data worth analysis'). In addition, this type of uncertainty analysis provides evidence of whether subsidence input parameters are well or not well constrained by the InSAR or benchmark observations ('identifiability analysis'), which will help construct an as parsimonious subsidence model as necessary.

If successful, this approach of combining improved modelling methodology, observation data, and uncertainty analysis could potentially be applied to other NSW-DPIE MODFLOW models in NSW simulating groundwater systems with significant groundwater extraction.

4 Area of Interest for InSAR and Benchmark Surveys

The primary criterion for the delineation of the study area was to include the eastern half of the management area, i.e. between Narrabri and Burren Junction, an area where NSW-DPIE surveyed the benchmarks dedicated to land subsidence monitoring and installed in the 1980's.

The secondary criterion was to include as much of the model domain of the Lower Namoi Model version 7 that is currently upgraded by the NSW-DPIE groundwater modelling team, so that, in the future, observations derived from InSAR and benchmark surveys can help calibrate the model against simulated subsidence and estimate subsidence-related parameters, such as skeletal elastic and inelastic storage coefficients. The model domain of the LNMv7 is delineated by the outline of the groundwater source. However, the westernmost tip of the groundwater source could not be covered by the InSAR analysis as it exceeds the used satellite imagery by a minor amount.

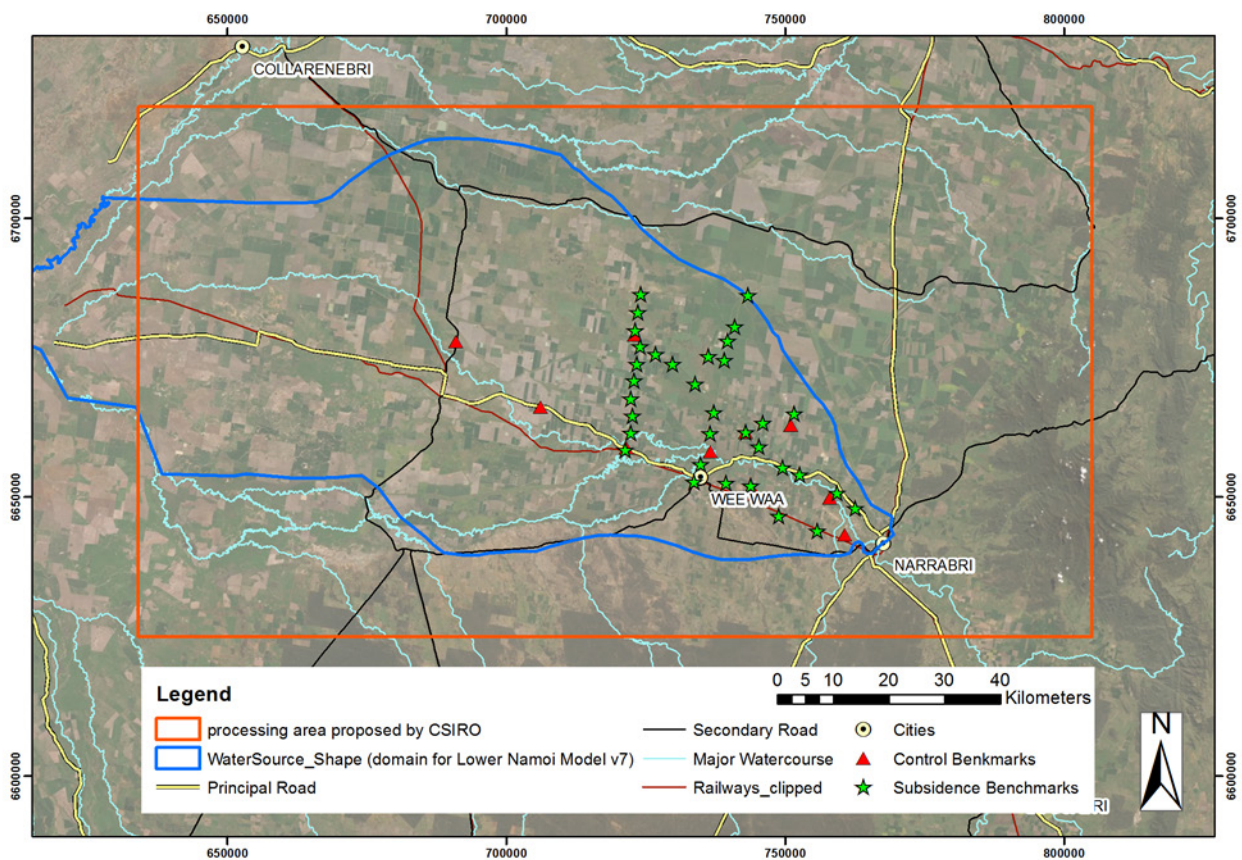
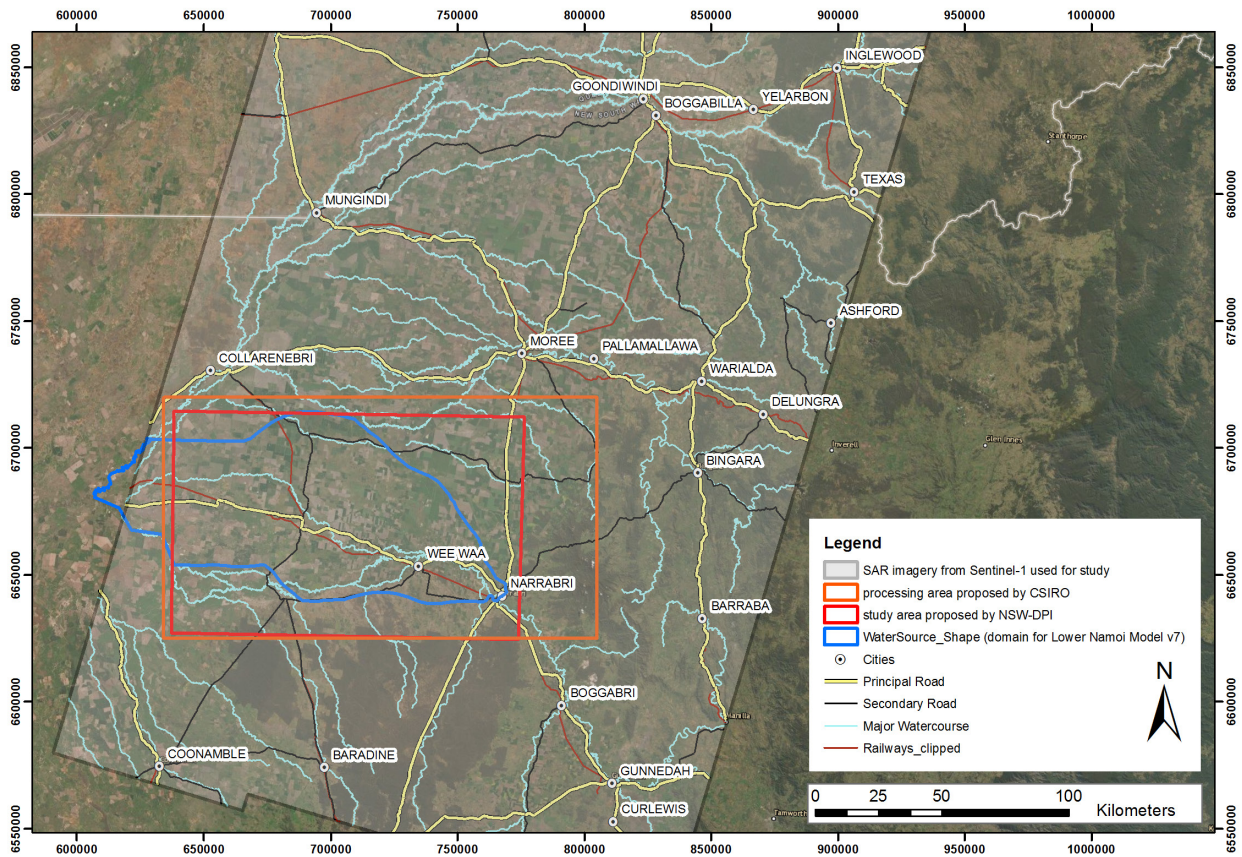


Figure 1 Study area for InSAR analysis and the benchmark survey of April 2019.

Part II Observing ground displacements using radar interferometry

One objective of this study is to derive ground movement for the Lower Namoi region from SAR imagery. The results are to be compared with in-situ benchmark data (Part III) over a period of up to 45 years, since the mid-1970s. This section discusses the type, availability, and suitability of SAR imagery for the Lower Namoi region. Among the SAR missions, and due to the low temporal density of radar imagery acquired over the study region during previous missions, only the most-recent radar imagery products from the Sentinel-1 mission proved to be useful. We discuss the derivation of vertical displacement trends from Sentinel-1 using SBAS-InSAR as well as the spatial and temporal behaviours of these displacements.

1 Introduction

Synthetic Aperture Radar satellites orbit Earth along a polar orbital track, passing by both poles on every path, and are capable to emit ElectroMagnetic (EM) waves toward Earth from a distance of around 700 km. These waves react with Earth's surface and the return signal is sensed by an antenna aboard the satellite. An image is formed by representing information about the return signal over ground footprint units, referred to as pixels. The information contained in images is related to the strength (usually called intensity or amplitude) or the phase value of the return signal.

The ground reflects the signal differently depending on its surface roughness, composition, humidity, hence these parameters can be assessed through SAR images. Ground 'targets' such as buildings and vegetation also respond to the signal and are clearly visible in SAR images. The phase information can be compared in time, along a time-series of images acquired from the same orbital position and with the same acquisition parameters (resolution, angle of view etc.). This allows to monitor changes in the satellite-to-ground distance. These techniques, called Interferometric SAR or InSAR (Massonet and Feigl, 1998), are particularly useful in civil engineering, seismology, and volcanology. They have also been applied to groundwater science either alone (Castellazzi et al., 2016, 2017) or in conjunction with other methods such as geophysics (Martel et al., 2018).

Several InSAR techniques exist, although they all follow the same basic principles. The phase value of the EM signal returning to the sensor, ranging from $+\pi$ to $-\pi$, is compared along two or more SAR images (Figure 2). A displacement of the ground is detected through a variation of the phase value between two images.

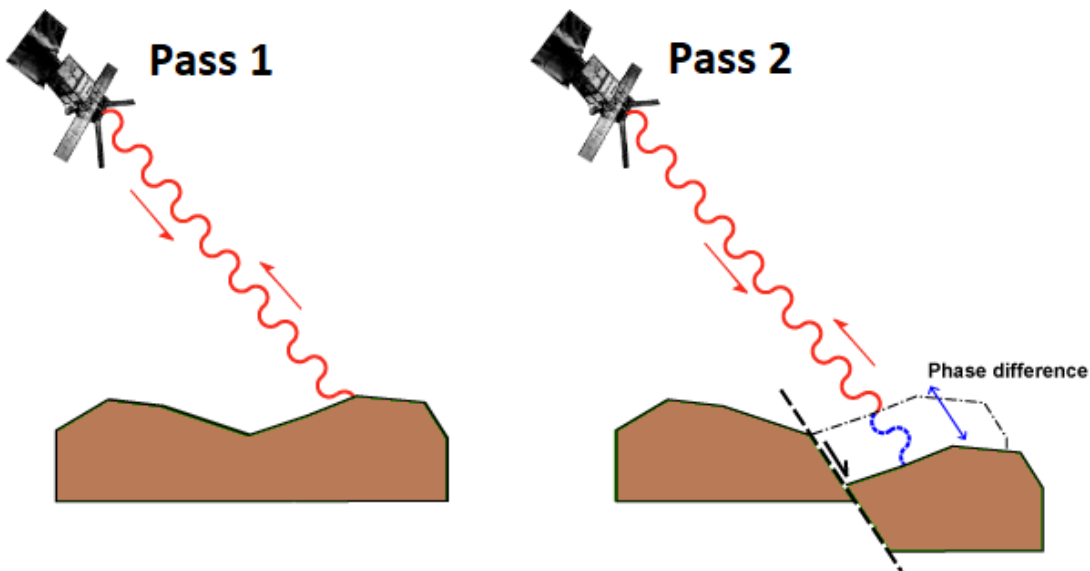


Figure 2 Principle of the InSAR techniques: the phase difference observed by comparing two SAR images is used to infer satellite-to-ground distance changes.

The InSAR analysis is always performed from SAR images acquired along the same orbital track and from identical orbital positions. To be comparable, the ground footprint of all pixels in both images have to perfectly correspond. The SAR images are co-registered, which implies that the second is resampled to be perfectly compatible with the first. For this, the two intensity images (Figure 3A) of the pair are analysed spatially and a deformation equation is applied on one of the image for spatial resampling. Once the two images are co-registered, the phase information from the two images is used to create a phase difference map (called interferogram, Figure 3B) and a coherence map (Figure 3C). The former provides information about the phase shifts observed by comparing the two images, the latter provides information about the comparability of the images and is a proxy for the noise level of the phase information. The coherence map is used to gain information about the reliability of the interferogram, and sometimes, to mask noisy areas in an interferogram. Finally, the interferogram is unwrapped by developing the phase shifts (which signal is wrapped over 2π) to create an absolute shift map ('unwrapped interferogram'; Figure 3D).

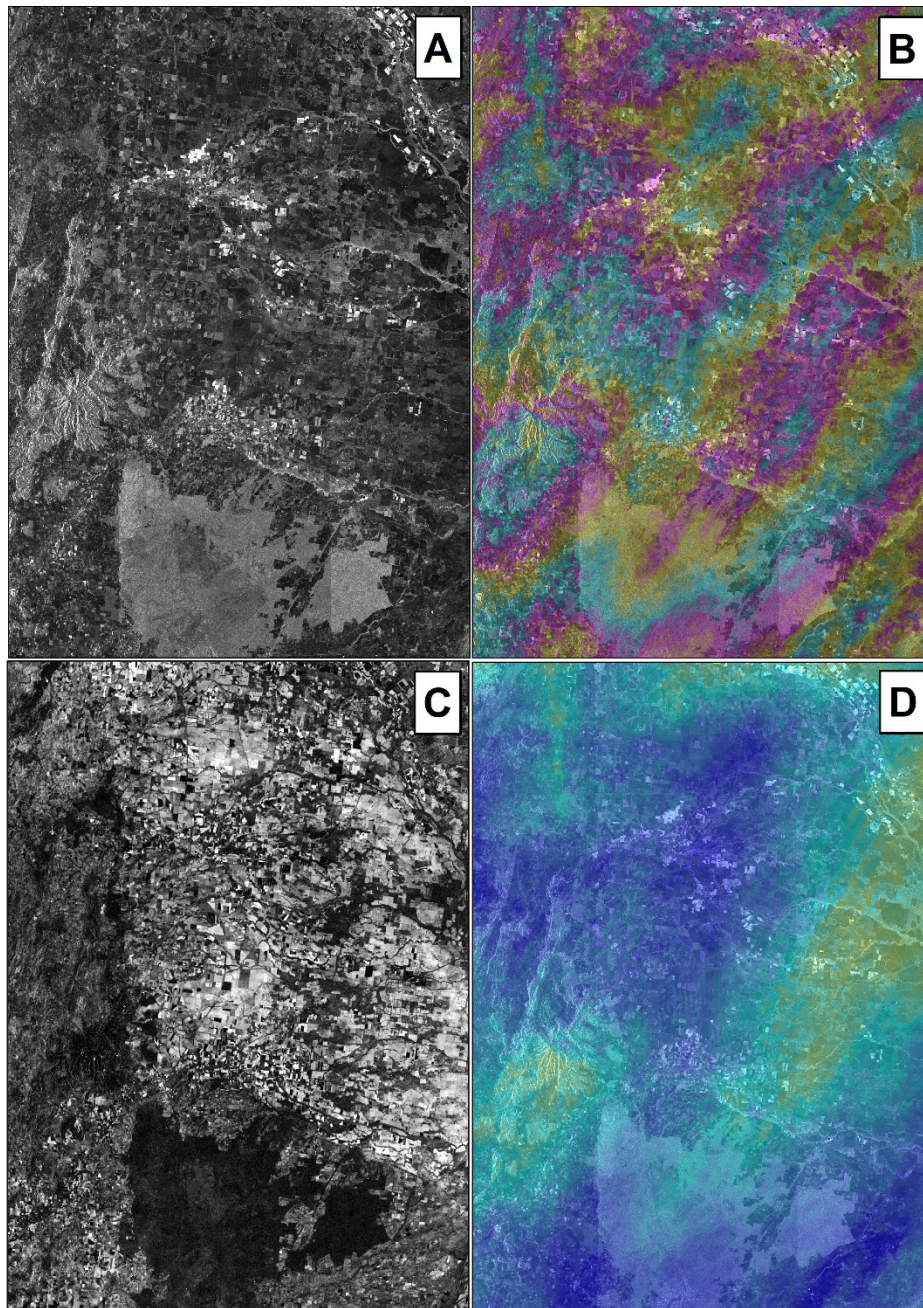


Figure 3 Examples of spatial patterns in intermediary and final products of a simple InSAR processing: (A) Amplitude map of the Namoi region from one Sentinel-1 image; (B) Interferogram generated using a pair of SAR images distant by 12 days; (C) corresponding InSAR coherence map, where lighter areas highlight good signal correlation; (D) corresponding unwrapped phase map, produced by applying an unwrapping algorithm on the interferogram (B). Note the correspondence between spatial patterns of (B) and (D). Also note that (B) and (D) are overlaid on the amplitude (A) for clearer visualization.

While Differential-InSAR was originally created in the late-1990s (Massonnet and Feigl, 1998) after the launch of ERS-1/2 satellites, the stacking techniques, or advanced InSAR, only appeared in the early 2000s. They allow integrating information from numerous interferograms created from a co-registered image stack (Ferretti et al., 2001; Berardino et al., 2002). Nowadays, beside several specific applications, these stacking techniques largely supplemented the one-interferogram approach (Figure 3) for detection of progressive movements, such as subsidence related to groundwater pumping. A comprehensive explanation and comparison between InSAR techniques is provided by Crosetto et al. (2016).

InSAR techniques differ by the strategy adopted to select a set of interferograms from a SAR image time-series. They also differ by the strategy to isolate signal from noise. In all cases, the displacement is measured along the satellite Line-Of-Sight (LOS) angle (referred to as 'LOS angle', usually between 20 and 45 degrees). This measurement can be either directly converted to a vertical displacement, if the horizontal component is negligible, or can be decomposed in horizontal and vertical components if a measurement produced along a different LOS angle is available.

SBAS-InSAR (Berardino et al. 2002), or Small Baseline Subset InSAR, is directly inspired by the first generation of InSAR techniques. A preliminary analysis of a SAR image time-series allows to identify image pairs able to produce coherent interferograms. Generally, it consists in selecting image pairs with short temporal and spatial baselines among all possible pairs in a SAR image stack. The pairs are selected by considering the time gap between the two acquisitions ('temporal baseline'), and the spatial gap in satellite positioning while acquiring the images ('spatial baseline'). A particularity of SBAS-InSAR is that the resolution of the images is reduced prior to creating the interferograms, which reduces the local variance and partially smooth out the noise. The resolution decrease factor is generally between 3 to 10. Using Sentinel-1 images, the final resolution of the process would then be of the order of 20 to 90 m. All interferograms are also spatially filtered and the phase is 'unwrapped' (as shown on Figure 3D). This step allows generating a map of satellite-to-ground distance change from an interferogram with phase shift values ranging from $-\pi$ to $+\pi$. Finally, all interferograms are integrated into an inversion strategy separating signal (phase shifts related to displacements) from noise (any other contributors, such as atmospheric phase shifts) for every date of the original SAR image time-series. This technique is efficient for detecting progressive movements in low to medium coherence areas, such as agricultural/farming areas.

PSI, or Persistent Scatterer interferometry (Ferretti et al. 2001) proposes a different approach where only the signal over high quality ground targets such as building, walls or uncovered rocks is used. A master image is selected at the temporal centre of the image stack, and the phase shift is analysed in time in reference to the master image and only over these targets. This technique is particularly suited for urban areas, where good quality (coherent) ground targets are numerous. It provides better precision in space and vertical accuracy than SBAS-InSAR. However, the low spatial density of good quality targets over natural settings challenges the use of PSI away from urban areas.

2 Available SAR images for Lower Namoi region

2.1 Older SAR data archives

Several SAR missions acquired images during the 1990's and 2000's. Generally, unlike Europe and North America, Australia was not well covered by these missions. Archives from these missions were searched for time-series compatible with InSAR analysis, which were acquired along a consistent orbital path. The list of archive datasets that were search is provided in Table 1.

Table 1 SAR mission with potentially available time-series usable for InSAR and observations regarding the result of the search (ESA: European Space Agency; CSA: Canadian Space Agency; MDA: MacDonald, Dettwiler and Associates Ltd.; JAXA: Japan Aerospace Exploration Agency).

Missions	Organisations	Time period	Data availability over Lower Namoi region
ERS 1/2	ESA	1991-2000 and 1995-2011	Three time-series of 8, 16, and 4 images (paths 109, 259, 338) with large temporal gaps above 90 days
RADARSAT-1	CSA/MDA	1995-2013	No usable time-series
ENVISAT	ESA	2002-2012	Two time-series of 8 and 10 images (paths 216 and 488) between 2003 and 2006
ALOS-1	JAXA	2007-2011	No usable time-series
RADARSAT-2	CSA/MDA	2008-now	

While every effort was made to determine if older SAR imagery during the 1990s and 2000s would allow InSAR analysis of displacement, clearly, as Figure 4 shows, the temporal density of images is very discontinuous. Hence, the objective to derive displacement from SAR for a period overlapping with the period of subsidence benchmark surveys (between 1974 and 2019) could not be met.

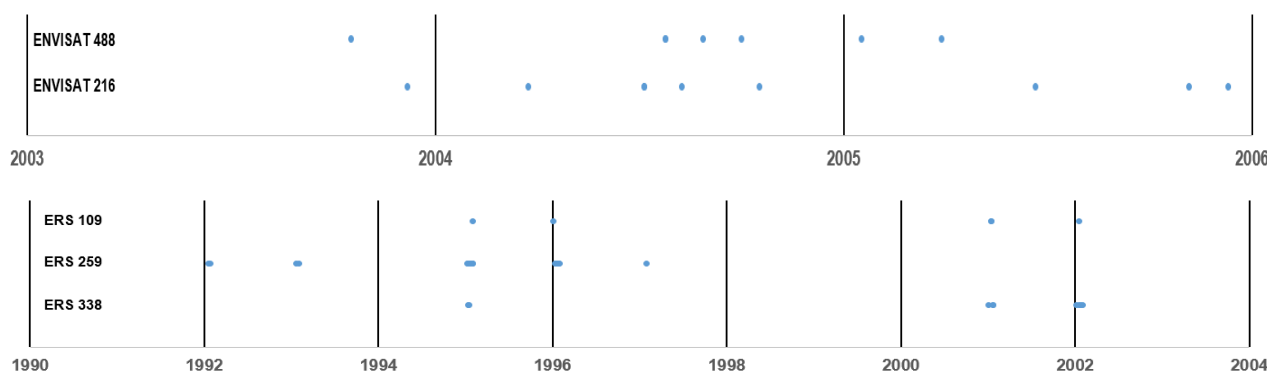


Figure 4 Temporal density of the SAR image stack showing the discontinuous SAR acquisition for the Lower Namoi region.

2.2 Recent Sentinel-1 time-series

Sentinel-1 mission is part of ESA’s Copernicus program and consists of two SAR satellite on the same orbital track. It is the first globally acquiring SAR system. It provides SAR time-series usable for InSAR with a 6-day temporal density over Europe and 12-day over the rest of the World. It is a game-changer, as the data it provides to InSAR users largely improves data availability for development in InSAR science and applications. It is particularly true over Australia, where archive datasets are often insufficient for most applications requiring SAR time-series (Table 1). In order to cover the world, Sentinel-1 has a wide swath acquisition mode, referred to as Terrain Observation with Progressive Scans SAR (TOPSAR; De Zan et al. 2006). Data is acquired in bursts by cyclically switching the antenna beam between multiple adjacent sub-swaths (Figure 5). The different sub-swath acquired by Sentinel-1 satellites can be merged in one single image. However, joints between swaths might remain visible even after merging.

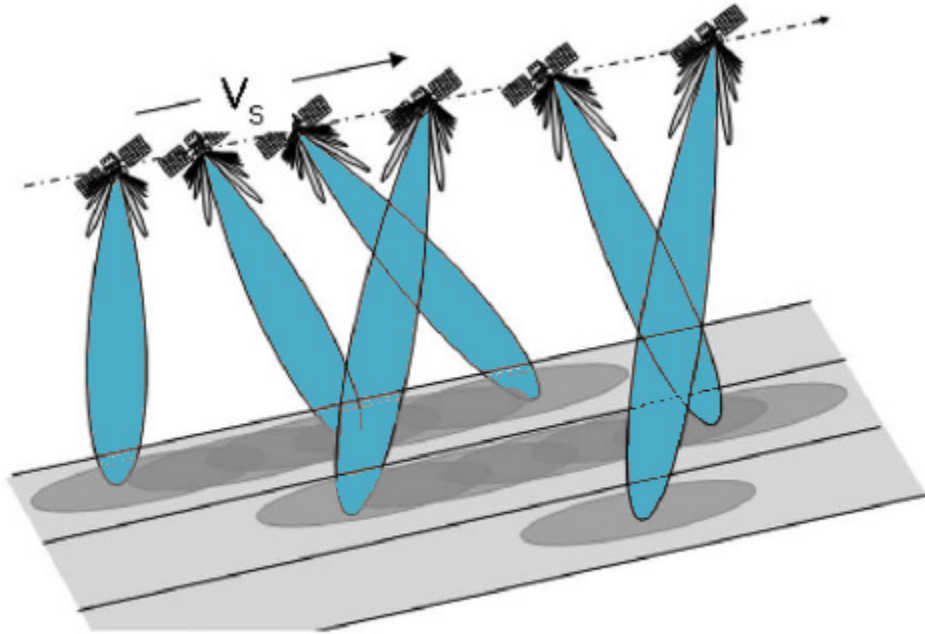


Figure 5 Sensing strategy used by Sentinel-1 satellite in order to cover a 250 km-wide ground footprint. This acquisition strategy is referred to as Terrain Observation with Progressive Scans SAR (TOPSAR; Source: ESA).

Sentinel-1 data are available online as tiles corresponding to a ground coverage of 250km (width) by 200 to 250 km (length). Three tiles were merged for all acquisitions dates in order to produce a spatially continuous SAR image with no spatial gaps. A spatial subset was then created (Figure 6A) and 94 images (Figure 6B) were cut according to the selected footprint. The resulting SAR time-series comprises 94 images acquired between 03/10/2015 and 28/11/2018, which correspond to around 3 years with ≈ 30 images per year.

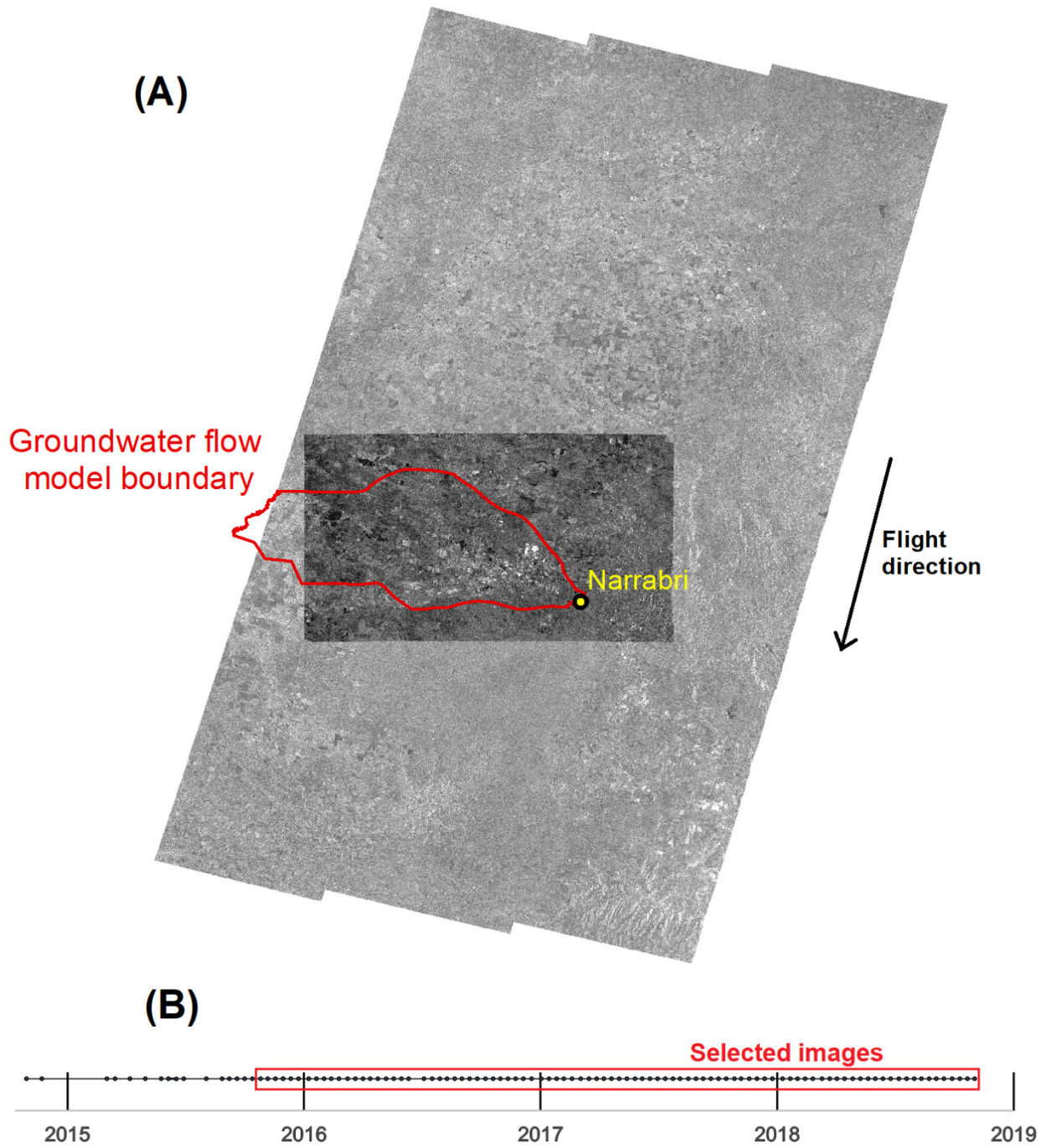


Figure 6 Spatial coverage (A) and temporal density (B) of the SAR image stack processed for this study. The clear image on (A) shows the continuous SAR acquisition covering the study area, the dark image corresponds to the subset selected for InSAR processing.

3 Processing

The 94 Sentinel-1 images stack was processed using SARSCAPE 5.5 and following the SBAS-InSAR approach (Berardino et al., 2002). Given the vegetation occurring throughout the study area, the adaptation of the Intermittent-SBAS-InSAR approach proposed by Sowter et al. (2013) was implemented. This approach considers the signal over areas where intermittent signal coherence occurs. In other words, it allows areas where high variation of coherence might happen, for example due to seasonal changes of land cover, to be integrated into the SBAS inversion at the cost of a higher noise level in the final results. The connection graph, which defines the interferograms produced from the stack of SAR images, is shown on Figure 7.

Table 2 presents the main processing parameters, which will be useful if more SBAS-InSAR processing is needed in the future.

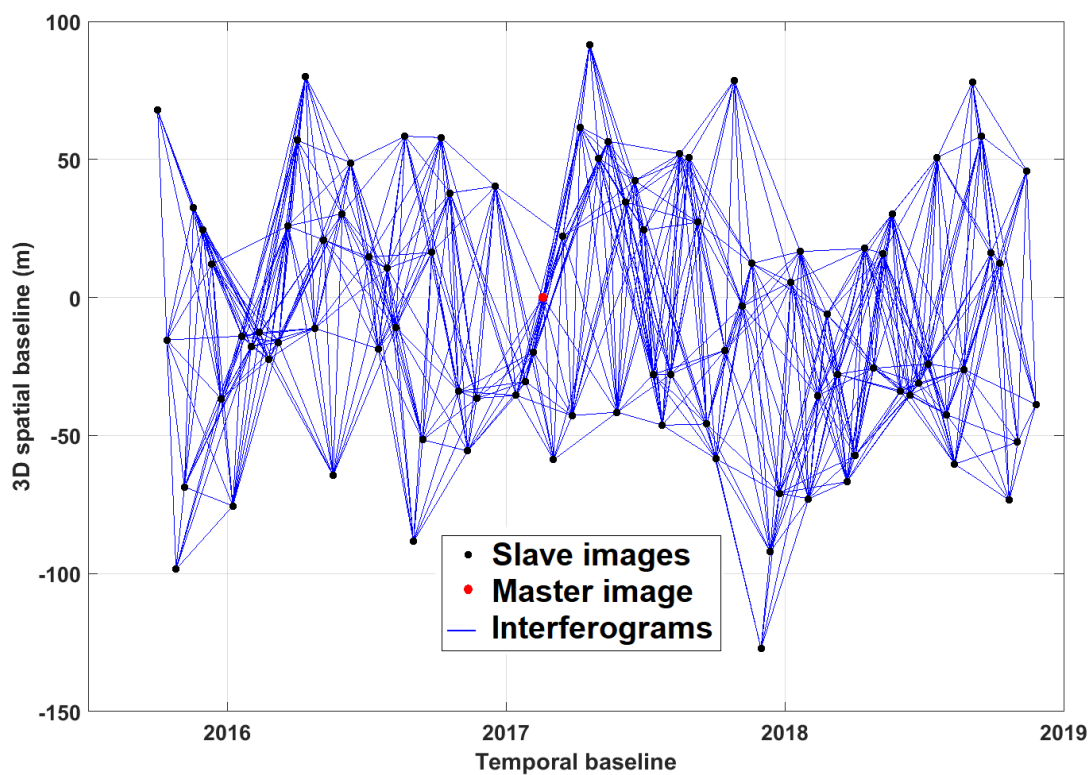


Figure 7 Connection graph of the 94-images Sentinel-1 stack used to assess the feasibility of creating interferograms using the image stack. The Y axis present the 3D positioning of the satellite while acquiring the images (in reference to the master image) and the X axis presents the acquisition time-series.

Table 2 Main processing parameters

Number of images	94
Multi-looking factors	Range 16 / Azimuth 4
Number of interferograms generated	633
Coherence threshold	0.2
Allowance below the Coherence threshold (images)	60%
Allowance below the Coherence threshold (interferograms)	60%
Unwrapping strategy	Minimum Cost Flow

4 Results

4.1 InSAR-derived trends in ground level changes for 2016-2019

The ISBAS-InSAR approach used in this study produces a space(x,y)-time(t) data-cube, with each time layer corresponding to the changes in the ground-to-satellite distance along the Line-Of-Sight angle (≈ 35 degree from nadir, over a descending path east of the study area, the satellite is right-looking). All values of ground-to-satellite distance change are in reference to the first image, which shows no displacement. Note that, because of coherence thresholds masking out noisy sections of the image, blank areas occur in the final results. Figure 8A presents the trend estimation calculated for every pixel of the data-cube overlaid on a SAR intensity map. Figure 8B presents the same map after conversion of LOS angle displacement into vertical displacement, assuming the horizontal component of displacement as negligible. This vertical displacement map can also be found as a zoomed-in version (Figure 42 in Appendix A.1) with the overlain topography and the location of subsidence benchmarks, which we will compare the InSAR displacement trends against in Part III.

The trend map produced using the InSAR-derived data-cube shows a clear delineation between the Lower Namoi quaternary alluvial basin and its more consolidated pre-quaternary hard-rock surroundings (around and south of the southern border of the groundwater source boundary, e.g. towards the Pilliga Forest, and southeast of Narrabri towards Mount Kaputar) (compare Figure 42 and Figure 43 in Appendix A.1). The quaternary alluvial basin shows varying values of displacements of from ± 60 mm/yr, while the hard-rock formation surroundings are usually below ± 10 mm/yr. This gives confidence in the InSAR results as no displacement is expected where no compressible sediments occur.

Spatial pattern of displacements is dominated by high spatial frequencies. The crop footprints can often be seen on the trend map, which suggest that a large part of the detected displacements is attributable to work on different adjacent crops types.

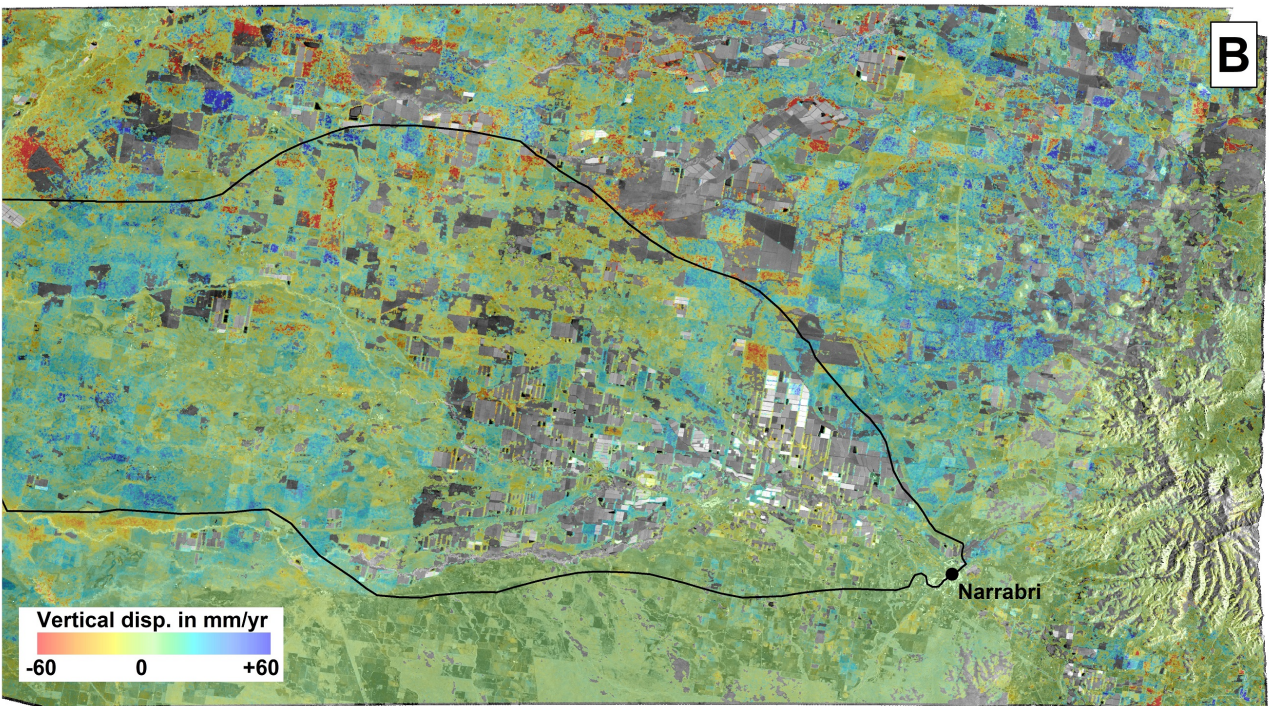
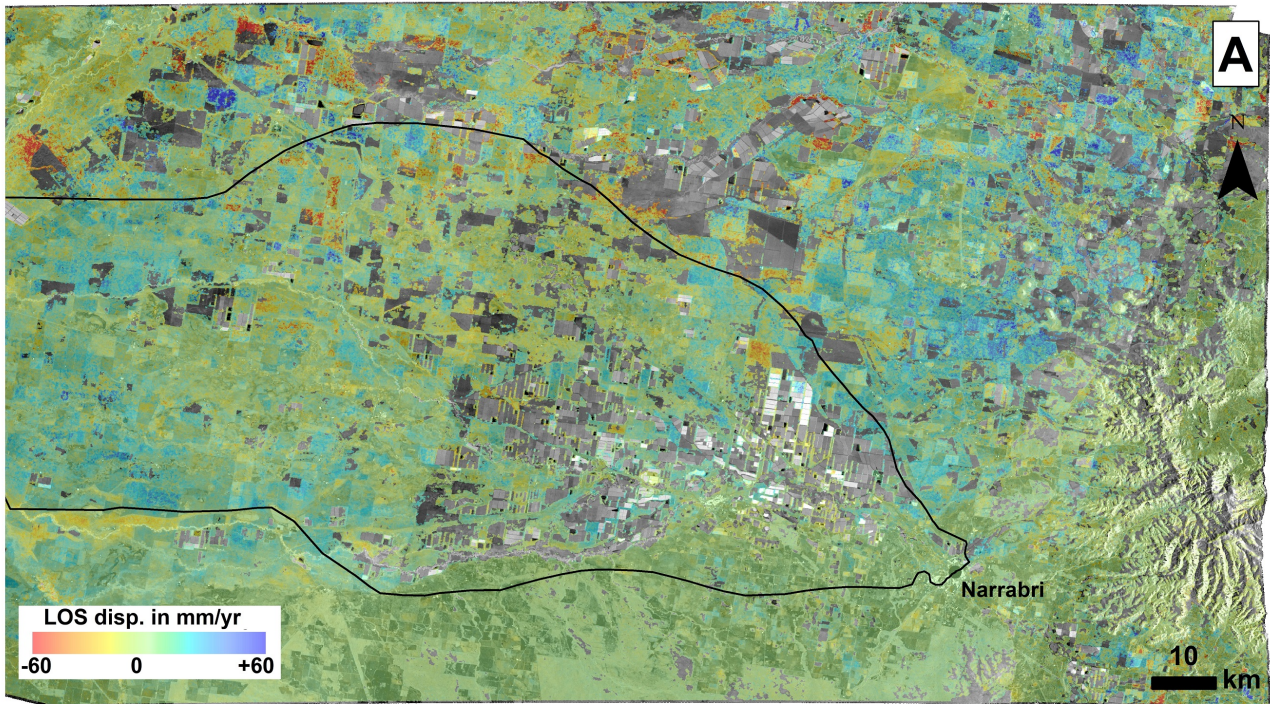


Figure 8 Ground level change along (A) the ground-satellite angle, referred to as Line Of Sight (LOS), and (B) projected along a vertical axis. Note that InSAR directly measures (A). (B) is inferred by considering the horizontal component of motion as being negligible (A). Due to the SAR acquisition geometry, velocity values in the horizontal direction are slightly higher than values measured along the LOS angle (≈ 35 degree). The groundwater model boundary is shown as black line.

Figure 9 and Figure 10 present four transects selected over the LOS vertical velocity map (Figure 8B). They show that the amplitude of InSAR-detected vertical displacements reaches 40 mm at certain locations. The spatial frequency of these peaks suggest that they are not related to aquifer hydraulic pressure changes, but rather to cropping activities. By applying a spatial moving mean filter of ≈ 10 km (corresponding to ≈ 5 km on both sides of each pixels, for each transects) this effect

is decreased. This relies on the assumptions that the filter is of significant size to encompass multiple crops and smooth out the effects of the work applied on them. Most of the vertical velocities applied after applying the filter are of the order of ± 10 mm/yr, with some isolated peaks reaching 20 mm/yr.

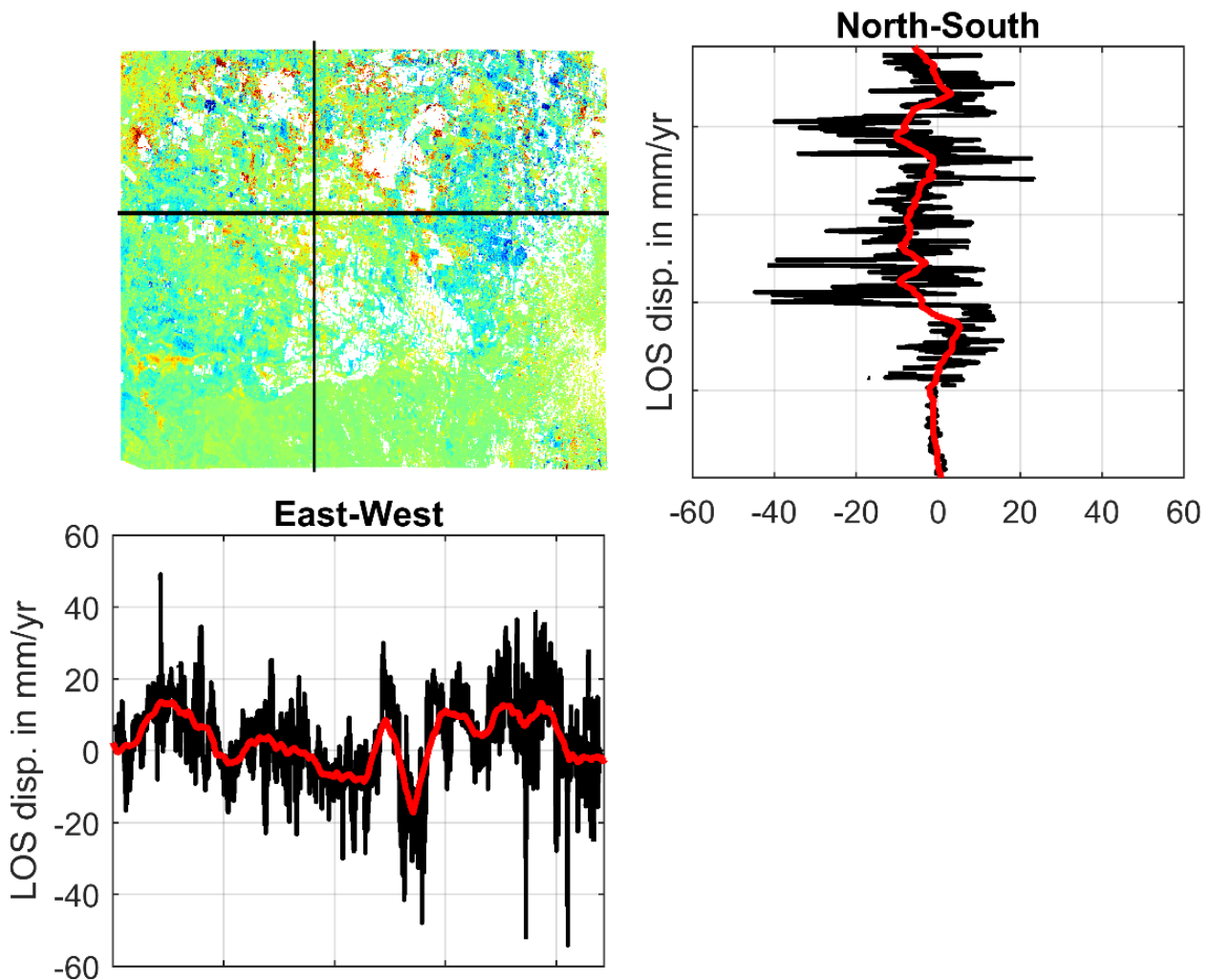


Figure 9 Example of velocity values along a North-South and an East-West transect.

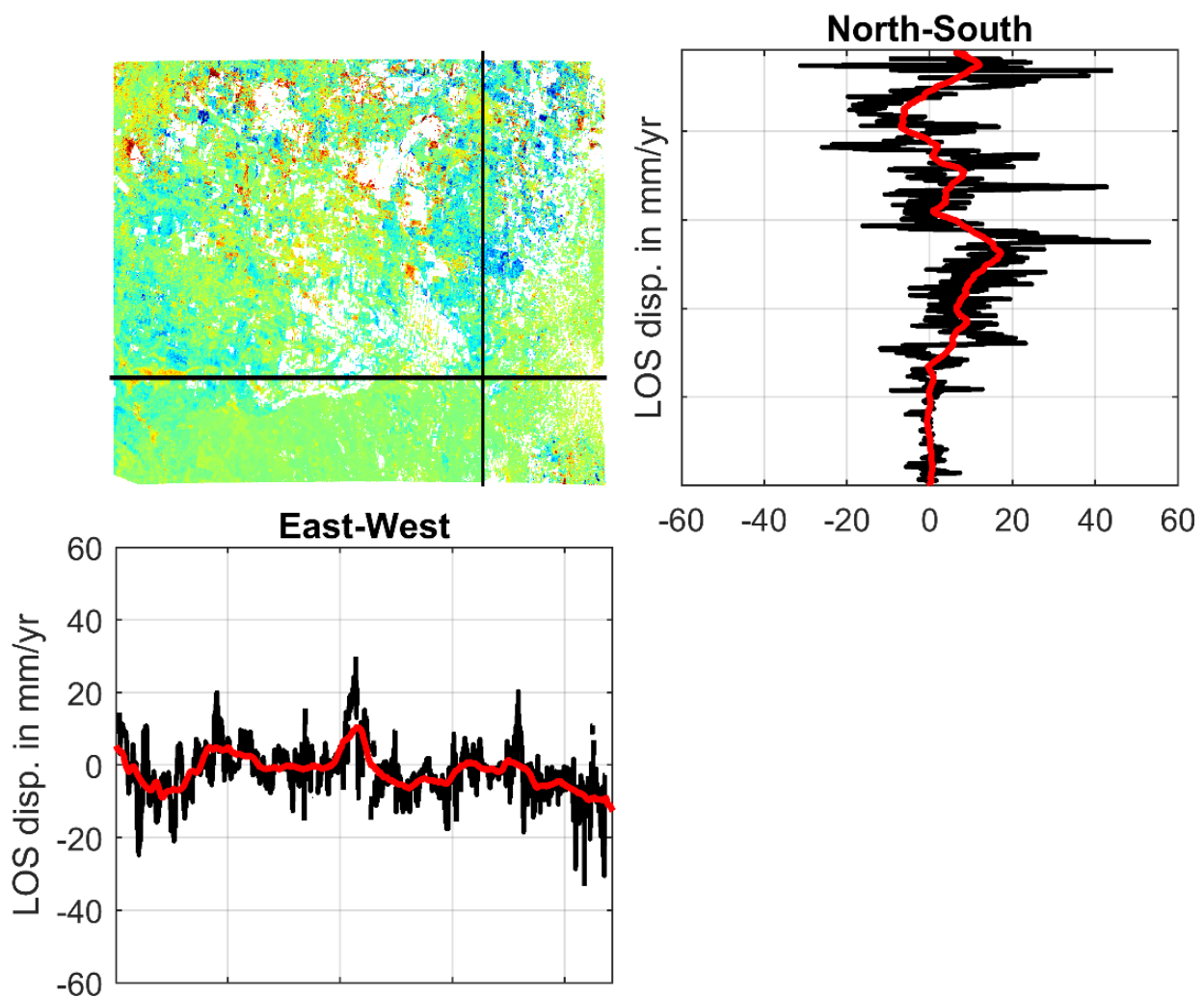


Figure 10 Example of velocity values along a North-South and an East-West transect.

4.2 Temporal behaviour of ground levels

The trend maps presented in the previous section were created using the full length of the InSAR time-series, i.e. from 03/10/2015 and 28/11/2018. In order to better understand how the trends in ground levels have evolved during this period, the yearly amplitude of displacements was computed (Figure 11). We observe that the contribution to the total displacements measured through InSAR decreased through the years from 2016 (Figure 11a/b) to 2018 (Figure 11e/f). Most of the total change in ground level is detected in 2016, and the velocity values are progressively decreasing in 2017 and 2018. This coincides with precipitation, which are higher in 2016 than 2017 or 2018, as shown in Figure 12. This might be related to climate variability. Floods may decrease ground levels through erosion or increase ground level as a result of groundwater recharge and elastic expansion. Conversely, water usage may potentially decrease during drought years, due to decreased cropping activities and intensity, decreasing subsidence rates occurring during these years. At this time, little is known about the dominating factors controlling the ground level response to climate variability. The consideration of multiple years is expected to reduce these effects in the final results.

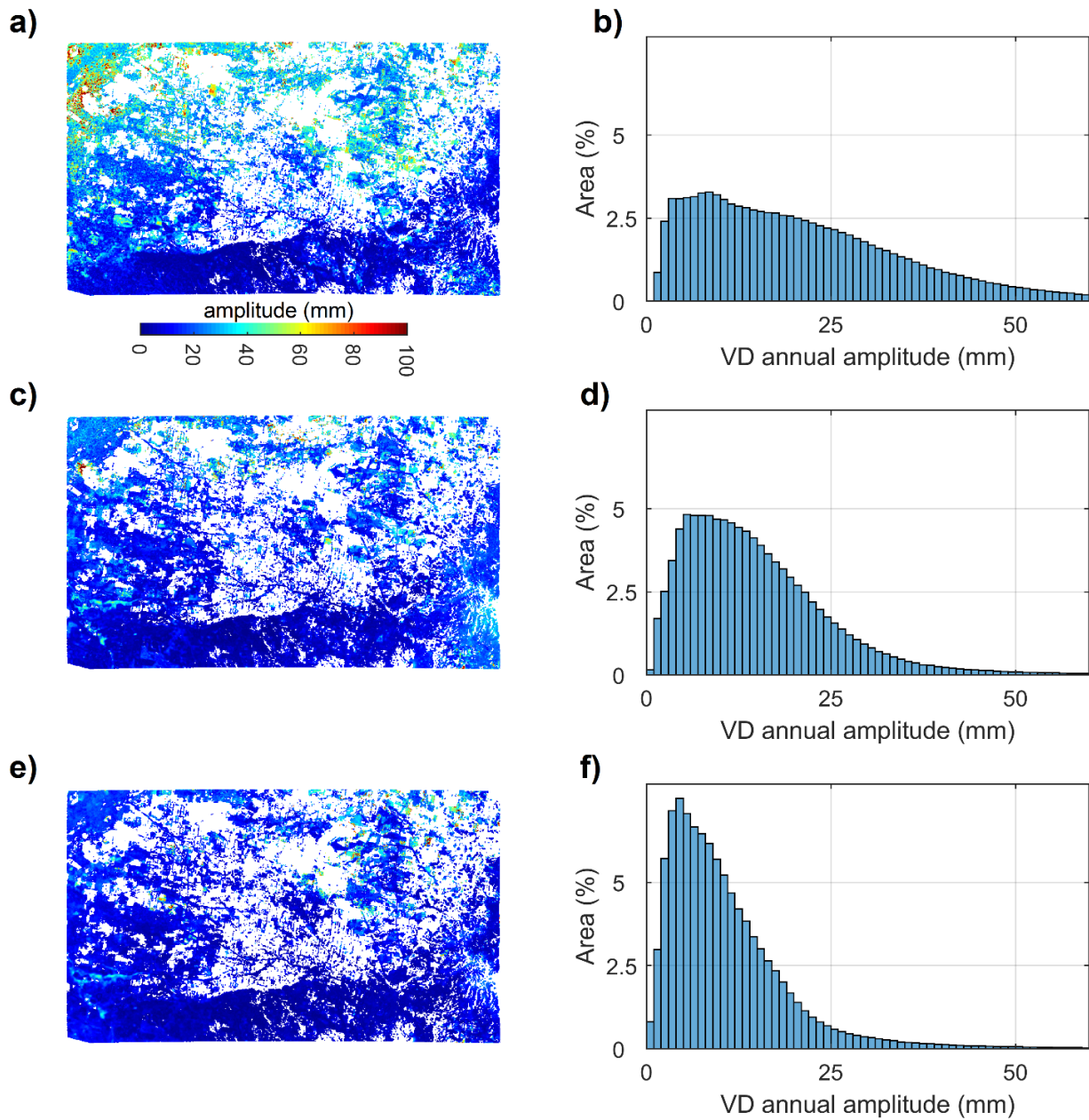


Figure 11 Amplitude of the absolute vertical velocities measured by InSAR for every year: (a-b) 2016; (c-d) 2017; (e-f) 2018.

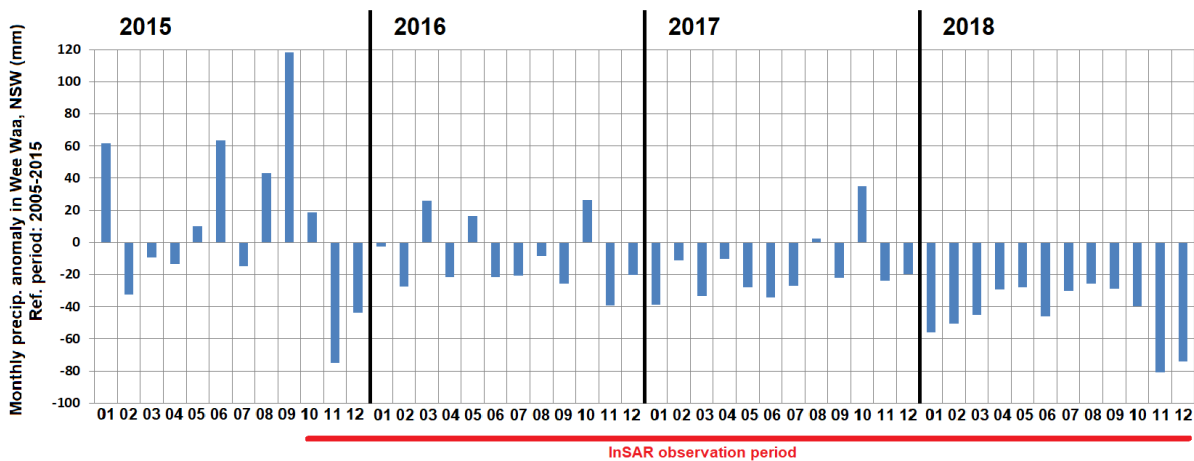


Figure 12: Monthly precipitation anomaly over Wee Waa (-30.12; 149.32; source: <http://www.bom.gov.au/> - station number 053034). Reference period is 2005-2015.

Time-series of LOS vertical displacement were created for six random points. The first set of three points are located in the eastern portion of the study area outside the Lower Namoi groundwater source and stretch from the Pilliga forest across Narrabri to an area of positive ground displacement (Figure 13).

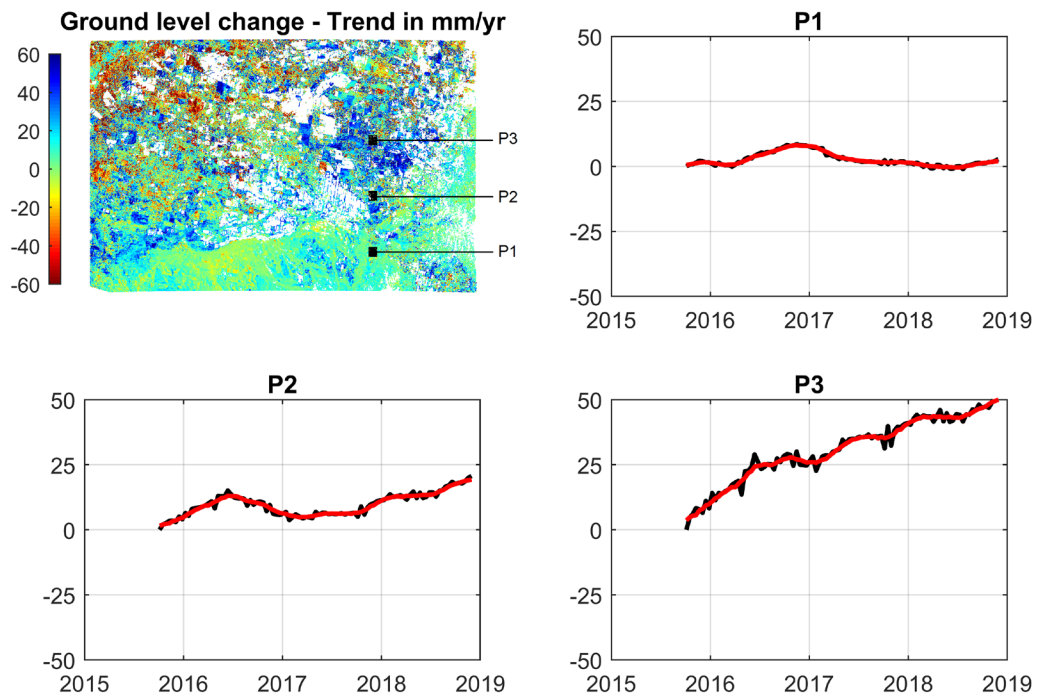


Figure 13 Time-series of vertical ground level changes over 3 random points located in the eastern part of the Lower Namoi region (black curves: ground level change; red curves: temporally-filtered ground level change signal).

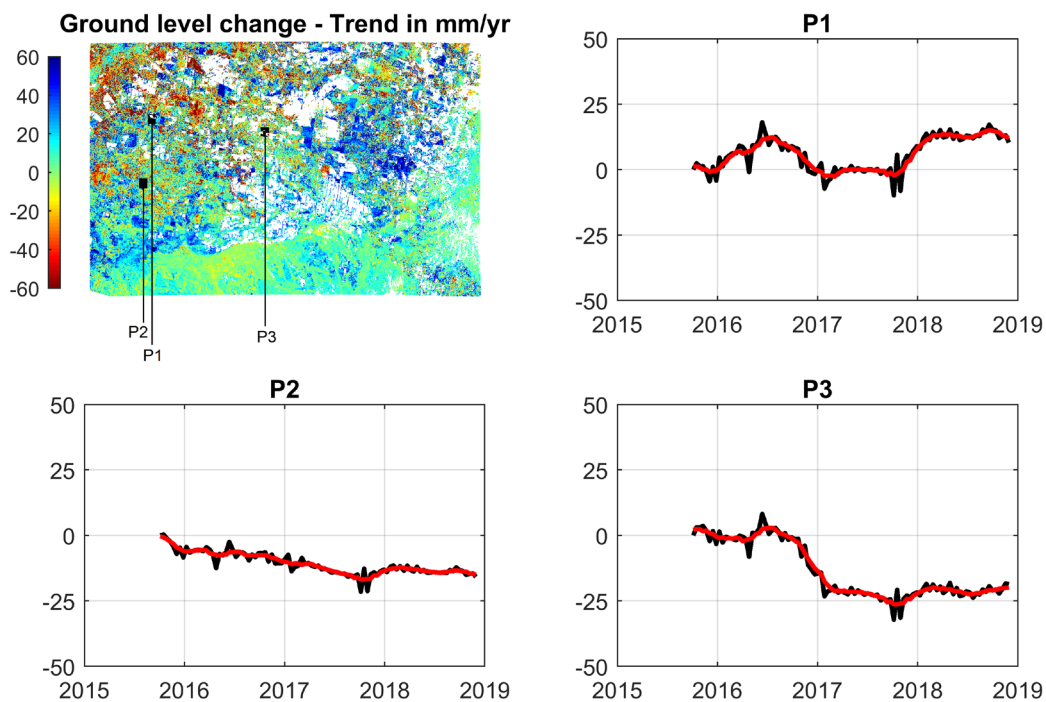


Figure 14 Similar to Figure 13, with three other points located in the western and central part of the Lower Namoi region.

To no surprise, the points just south and north of Narrabri (P1, P2; Figure 13) show relative stability, while P3 in the area of ground level rise shows seasonal patterns superimposed on a rising trend.

The second set of three points are located in the western part of the study area but inside the boundary of the Lower Namoi groundwater source (Figure 14) deliberately west of the subsidence benchmarks (as this area will be compared separately in Part III). P1 and P3 (Figure 14) indicate positive and negative ground displacement, respectively. P3 is the only point that demonstrates a significant decline in ground levels near the Merah North Section of subsidence benchmarks. Both points show a most likely climate-related relative rise in 2016 and again in 2018. Interestingly, this is analogous to an observation of Ross and Jeffery, 1991, who report ‘widespread rise in ground surface (...) following two wet seasons.’

4.3 Comparison with results from PSI-INSAR

Persistent Scatterer Interferometry (PSI) is an InSAR technique allowing greater vertical accuracy than ISBAS-InSAR. However, as it focuses on interpreting the phase shifts only over the most coherent ground targets, its spatial coverage can be limited. These targets usually correspond to hard surfaces such as roads or buildings. Rarely, coherent targets can also be found on rock outcrops or bare soils. The technique is not particularly suitable for vegetated areas such as the Lower Namoi region. However, PSI results can complement ISBAS-InSAR with a potential to reduce the influence of surficial clays and provide better accuracy over built infrastructure.

Two PSI computations were performed over a subset of the study area (Figure 15). The first (Figure 15A) includes the same SAR image time-series as the one used for the ISBAS-InSAR processing (94 images, see Figure 6). The second only includes a total of 30 images acquired in 2017. A coherence threshold of 0.75 was selected for the first computation, and a lower threshold of 0.7 was selected for the second to maximize coverage and the quantity of measurement points, at the cost of a slightly lower overall accuracy.

Results indicate no major displacement patterns along linear transport infrastructure during the 2015-2018 era (Figure 15A). When considering the full SAR images time-series, it is also observed that persistent targets are limited to built infrastructure (Figure 15A), illustrating the limits of using PSI techniques to sufficiently cover such vegetated regions over long periods. By only accounting for images taken in 2017 (Figure 15B), more ground targets are detected and the final coverage expands to the several stable bare-soil areas. Results for 2017 show movements from surficial clays and potentially its effect on hard structures. However, no spatially defined subsidence patch potentially coinciding with lithological or hydraulic pressure change boundaries appears. This supports the observations drawn from ISBAS-InSAR that no major groundwater-related subsidence occurred during the 2015-2018 era. It is however apparent that the high clay content of the soil surface creates local instability, which is illustrated on Figure 15B.

These two tests confirm the usability of the PSI technique during the driest years (2017), but also show its limits when applied over a long time-series including at least one wet year (2016). Indeed, as the technique relies on interpreting the phase shifts over ground targets that are highly coherent throughout the time-series, one episodic flood event is sufficient to prevent any detection over bare-soils along the whole time-series. The technique is of great interest to

complement ISBAS-InSAR observations and monitor infrastructure stability with greater accuracy. It is perfectly usable as long as the limited spatial extent illustrated on Figure 15B is acceptable, and the time-series does not encompass any flooding episode.



Figure 15: Results from PSI analysis over the Southwestern corner of the study area, with the groundwater flow model boundary overlaid for spatial reference. (A) Takes into account the same SAR time-series as the ISBAS-InSAR analysis, and (B) only takes into account images from 2017.

5 Summary

One objective of this study was to derive long-term ground movement for the Lower Namoi region from SAR for the purpose of comparing it with in-situ benchmark data over a period of up to 45 years since the mid-1970s. In the 1970s and 80s, no SAR remote sensing was present. During early SAR missions in the 1990s and 2000s, older ENVISAT and ERS SAR imagery existed for the Lower Namoi region, but proved to be unusable, because, unlike Europe and North America, Australia was not well covered with a very low temporal density of images.

Starting in 2015, data of the Sentinel-1 mission are available for the Lower Namoi region with a high, 12-day, temporal density. For all acquisition dates, three 250km-wide tiles were merged to produce a spatially continuous SAR image. A subset of this image was analysed for the study area. The resulting SAR image time-series comprises 94 images acquired between October 2015 and November 2018 (around 3 years with ≈ 30 images per year). The stack of 94 Sentinel-1 images was processed using SARSCAPE 5.5 and the ISBAS-InSAR approach (Berardino et al., 2002; Sowter et al. (2013)). While vegetation, aside from ground movement, also responds to the signal and is clearly visible in the SAR images, ISBAS-InSAR can account better than other InSAR techniques for lower or a high variation of coherence in areas with spatial or seasonal changes in cropping or land cover.

Using the ISBAS-InSAR approach produced a space(x,y)-time(t) data-cube. Each time layer corresponds to the changes in the ground-to-satellite distance but includes also blank areas because of coherence thresholds masking out noisy sections of the image. The line-of-sight (LOS) angle displacement was converted into vertical displacement, assuming the horizontal component of displacement as negligible. The vertical displacement was then compared against displacement observed in-situ in Part III.

The trend map derived from the InSAR data-cube revealed a clear delineation between the Lower Namoi quaternary alluvial basin with a higher amplitude (\pm max. 60 mm/yr) and its more consolidated pre-quaternary surroundings with a lower (\pm around 10 mm/yr) amplitude of ground movement. However, in areas of intensive cropping, the detected displacement is also attributable to work on the crops (with oscillations across spatial transects of up to ± 40 mm/yr). However, this effect was reduced to ± 10 mm/yr by a spatial moving-mean filter based on the assumption that the filter is large enough to encompass multiple different crops. Yearly amplitudes of displacement decreased from 2016 to 2018, which might be related to climate variability (e.g. ground level decrease as a result of erosion due to flood or increase following expansion due to recharge) or agricultural work during these events or following years (e.g. reconstruction of trenches and canals).

Six time-series of LOS vertical displacement show relative stability or a rising trend in the eastern part of the study area and positive and negative ground displacement in the western and central part. All series with significant rise or decline are superimposed with seasonal, most likely climate-related, patterns (esp. in 2016 and again in 2018), which is analogous to an observation of Ross and Jeffery, 1991, who report 'widespread rise in ground surface (...) following two wet seasons.'

Part III Comparison of InSAR with in situ Benchmark data

1 Introduction

In the past, evidence of minor land subsidence or aquifer compaction in the Lower Namoi Valley of less 50 mm had been provided in form of several benchmark surveys from 1974 to 1990 (Ross and Jeffery, 1991) of benchmarks installed in 1974 and 1981. The overall objective of this study is to increase this confidence by improving the monitoring of potential land subsidence in the Lower Namoi using various techniques from remote sensing (see Part II) and a new benchmark survey conducted in April 2019.

The primary objective is to assess the spatial distribution and temporal trends of land subsidence over areas of intensive agriculture within the Lower Namoi groundwater source. Ground displacement observations from remote sensing (radar interferometry) are derived using available InSAR imagery for certain years with good data from the Sentinel-1 satellite (see Part II) and then compared with historically surveyed (1974-1990) and only recently re-surveyed benchmarks (April 2019) that were installed in the Lower Namoi in 1974 and 1981. The purpose of the resurvey is to ascertain whether any further land subsidence has occurred over the intervening 28 years during which groundwater extraction has continued.

Any evidence of land subsidence or aquifer compaction found by this study may be used for water level response management and as decision-support basis for the ministerial management.

2 Time-periods of InSAR versus Benchmark Survey

When comparing the long-term “inelastic” subsidence between InSAR and benchmark survey data, issues of temporal and spatial incompatibility arise. While the benchmark data span a period of 45 years from 1974 to 2019, the period of usable “good” newer generation InSAR from Sentinel-1 starts in late 2015 until recent, i.e. includes only around 3 years (Figure 5). Older generation InSAR imagery from ERS and ENVISAT for the Lower Namoi does overlap more with the benchmark data from 1992 to 2006 (Figure 4). However, unfortunately, this imagery is temporally and spatially very discontinuous and, hence, could not be used for this comparative analysis.

Therefore, the only way land subsidence trends of the up to 45 years of benchmark data can be compared with trends from just 3 years of InSAR-derived data is by annualising the trends per year.

At the very outset, this comparison needs to be treated with caution as strong inter-annual and seasonal variations that result from variations in climate and land management will influence the 3-year trend of the InSAR data much more than up to 45-years of benchmark data.

3 Available in situ Benchmark Data

In the past, evidence of minor land subsidence or aquifer compaction in the Lower Namoi Valley of less 50 mm had been provided in the form of several benchmark surveys from 1974 to 1990 (Ross and Jeffery, 1991) of benchmarks installed in 1974 and 1981. After a survey gap of 29 years, a new benchmark survey for 41 subsidence and 10 control benchmarks was conducted in April 2019 by SMK Consultants Pty Ltd for the NSW-DPIE as part of this project.

The data for 41 subsidence and 10 control benchmarks were subsequently provided to CSIRO for comparison with InSAR-derived vertical displacement. Results of all previous and recent benchmark surveys are compiled in Table 7 a and b in Appendix B.2. Further details of the survey can be obtained from the NSW-DPIE Water Group. Out of the 41 surveyed subsidence benchmarks, 9 benchmarks could not be used for this study as they could no longer be located, were destroyed or damaged leading to possible errors in the result. 32 benchmarks were usable and used for comparison with InSAR results (see Figure 16 notes in Table 7b).

Prior to the survey, the measurement method and accuracy for control and subsidence benchmarks was given by the surveyor as “STATIC/Logged” with ± 10 mm and “Realtime Kinematic (RTK)” with ± 15 mm, respectively. In the interest of time, the technique with a higher accuracy “STATIC” was chosen for control benchmarks to prevent error propagation of control onto subsidence benchmarks. The slightly higher inaccuracy of “RTK” was chosen for individual subsidence benchmarks.

After the survey, the surveyor reported the following statements in a 2-page report called “Methodology for Survey of Benchmarks:”

- *“The STATIC survey technique involves logging a minimum of 4 control marks at the same time to determine the connections between each other station. Logging times are dependent on length of surveyed lines as set by the Surveyor General for control surveys. The accuracy of a static survey in an unconstrained least squares adjustment of all observations in the network is less than 15mm horizontal and less than **30 mm vertical**. This is consistent with those estimated accuracies by the Surveyor General of NSW for GNSS Control network results.*
- *The RTK technique involves logging of data over three minutes and then a separate independent observation at a different time of the day to eliminate possible satellite errors as recommended by the Surveyor General’s Directions for Control Surveys. The estimated accuracy of the RTK technique is 20 mm horizontal and **35 mm** (Surveyor General).”*

In another 1-page PDF-sheet called “19-91 Control Network Adjustment Report,” the surveyor lists another ‘elevation error’ for the 10 control benchmarks that ranges between 21 and 29 mm, i.e. ± 10.5 to ± 14.5 mm, which is within the error margin of 30 mm, i.e. ± 15 mm reported above.

There appears to be a discrepancy between pre-survey accuracy assumptions and post-survey accuracy reports. If, potentially, 30 mm vertical for STATIC and 35 mm for RTK translates into a measurement error of ± 15 mm for control benchmarks and ± 17.5 mm for subsidence benchmarks, then that would mean that a post-survey reported cumulative error of ± 32.5 mm is slightly higher than the previously assumed ± 25 mm.

Due the uncertainty around what the measurement error for the 2019 survey was, for this report and the following comparison with InSAR data, we applied for the 2019 survey a cumulative error of ± 25 mm. We also assumed that historic surveys were not more accurate and applied the same accuracy assumption to previous surveys. Based on that assumption, the differential subsidence between two surveys would be at least ± 50 mm.

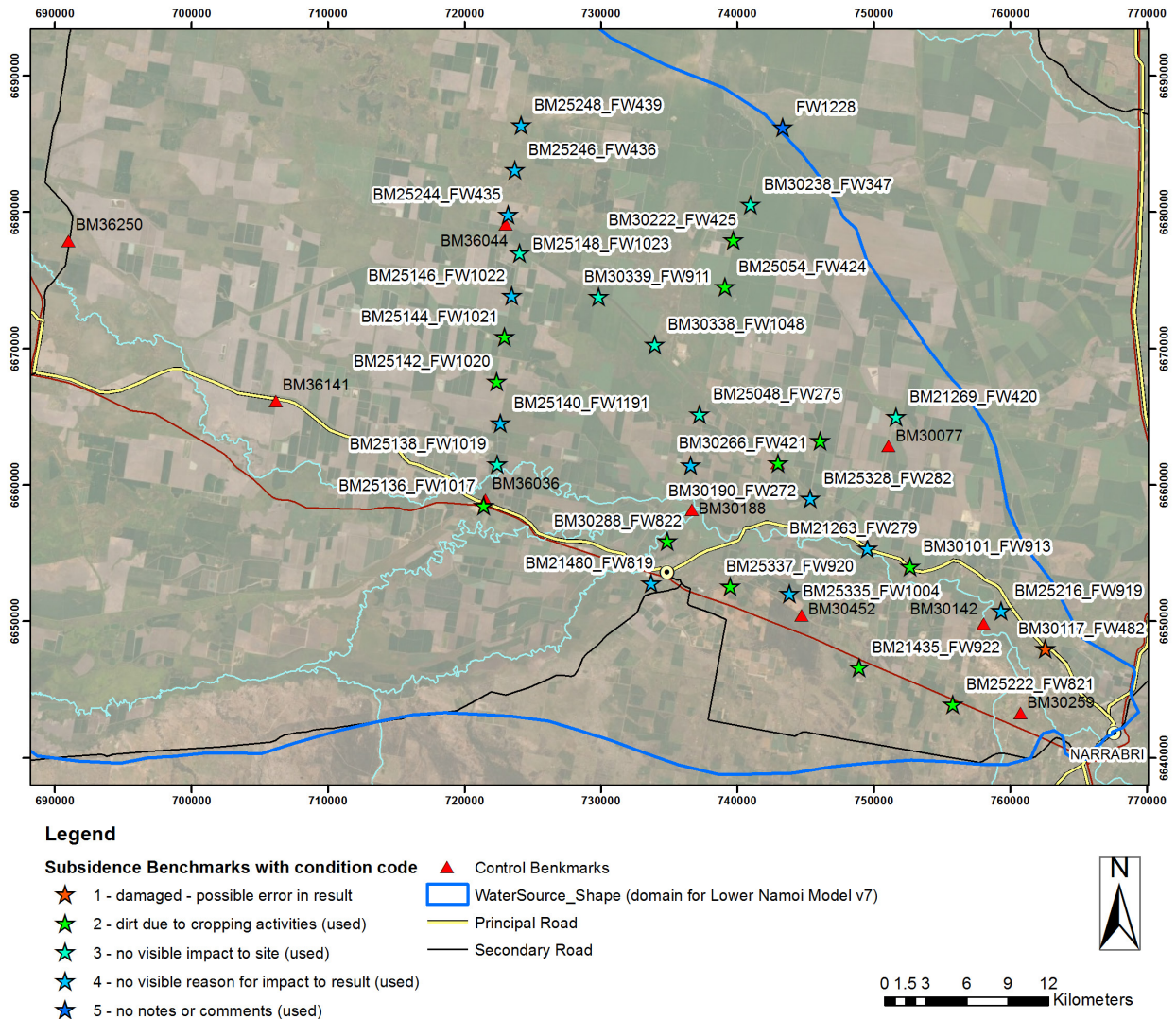


Figure 16 Subsidence and Control Benchmarks in the Lower Namoi Region re-surveyed in April 2019

4 Processing

All measurements available from Ross and Jeffery (1991) were compiled together with the latest survey performed in April 2019 into one database (Table 7). Time-series of compaction or expansion for each benchmark are displayed in Figure 18.

4.1 Processing of Benchmark Data for Comparison

A linear curve was fitted using a least mean square approach applied on all available measurements for each location (Table 3 and Table 8; column “linear trend using all avail. data”). The trend value was extracted from the equation of the fitted line (a represents the trend in the linear equation of the fitted line $y = ax + b$). This approach has the advantage of providing consistent and comparable estimation of the ground level change. However, the total number of measurements (i.e. number of surveys per benchmark) and, hence, the reliability of the calculated trend varies between benchmarks. The large time gaps between the last survey in 2019 and the previous one (1990 or older) suggest that the trend represents a secular and progressive change in ground level rather than a seasonal or spatially limiting signal related to the work on the crops or the seasonal expansion/contraction of the clays.

For comparison, we also calculated the linear trends just between the last two surveys (2019 survey and the last one before that) and between the last and first one (2019 and initial survey in 1974, 1975, 1980, or 1981). On the basis of one example, Figure 17 shows that the trend that is only based on the last two surveys is generally less than the trend based on just the total movement between the last and the first or the trend based on all available data. However, as the most recent trend of the last few years is hidden within the 29-year gap, no conclusion of a slow-down of the rate of decline can be drawn from the lesser trend for the current rate of decline based on just the last two surveys.

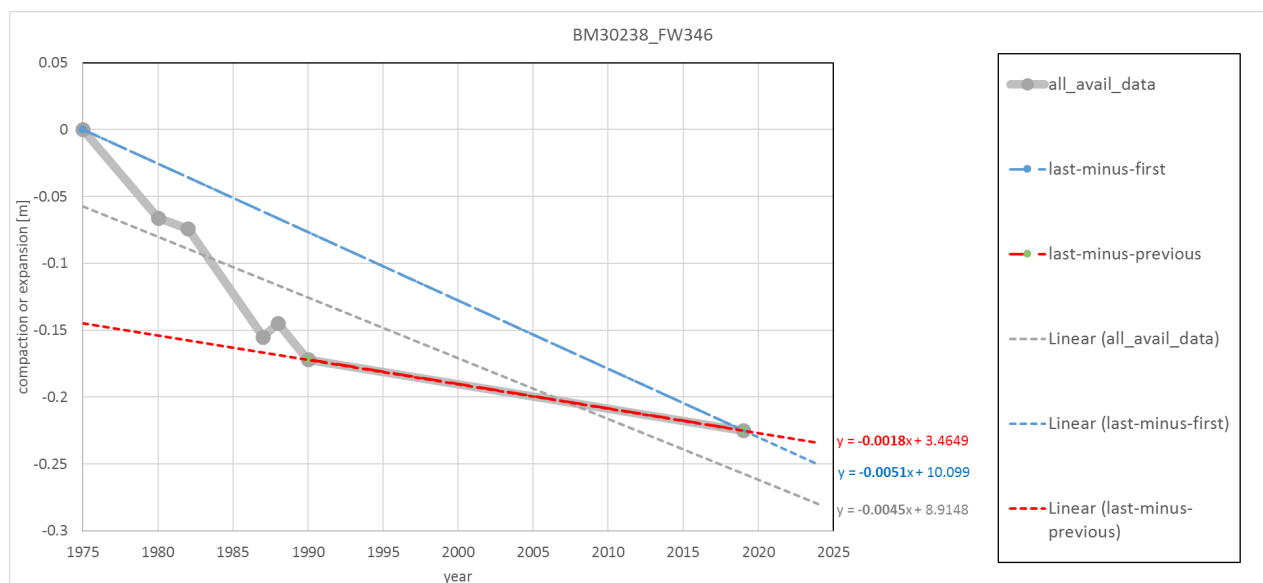


Figure 17 Example of calculation of Linear Trends of Subsidence from Benchmark Data

4.2 Processing of InSAR Results for Comparison

In order to compare the annualised trends of land subsidence based on up to 45 years of benchmark data trends have also been generated for the 3-year period of InSAR-derived data vertical velocities.

A first trend calculation based on a down-sampled ISBAS InSAR data-cube with no buffer area was conducted, but not very meaningful, as spatial smoothing occurs. The concept of buffer is important. When computing a trend using the 2016-to-2019 time-series extracted from one particular pixel in the data-cube, the result becomes representative of the 3-year evolution of that very pixel. This can create problems in certain locations, where other processes were active aside from groundwater extraction that may also lead to displacement. Alternatively, the displacement for any given point is better retrieved using a spatial averaging kernel for each date of measurement (e.g. 15 by 15 kernel used for annualised trends in (Table 3 & Table 8 and time-series and Figure 20). Table 8 in Appendix C.1 also provides trend for each of the 3 years (2016, 2017, 2018).

The spatial resolution of the data-cube is $\approx 60\text{m}$. That is, the kernel is roughly a square of 900m each-side, or $\approx 450\text{m}$ on either side of the benchmark point. Note that when no-data (non-coherent) values appear close to the benchmark, this pixel is not considered in the calculation, so not all trends come from a 15×15 pixel time-series, and many have less.

5 Results

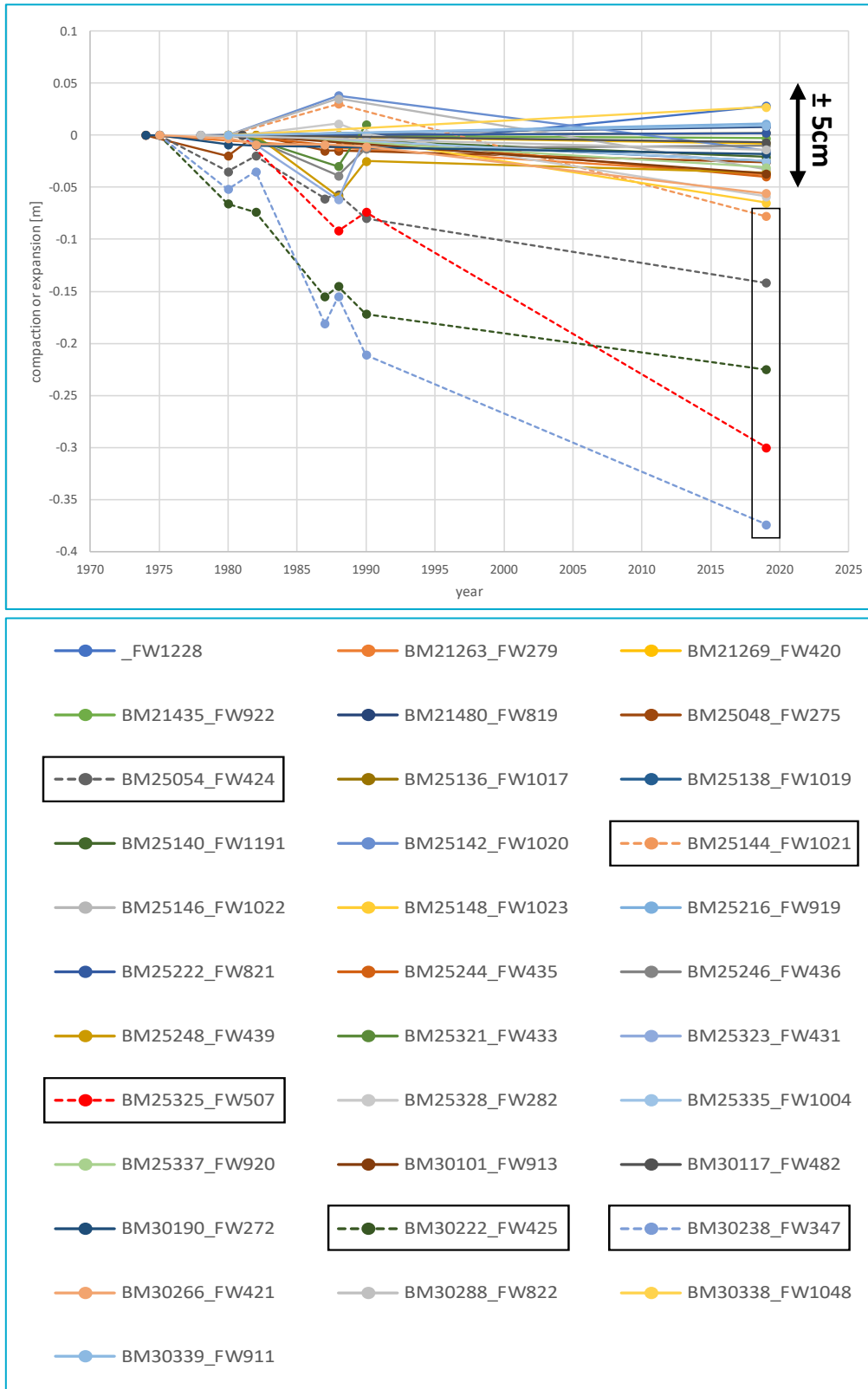


Figure 18 Evolution of the level of subsidence benchmarks from the late 1970's to 2019.

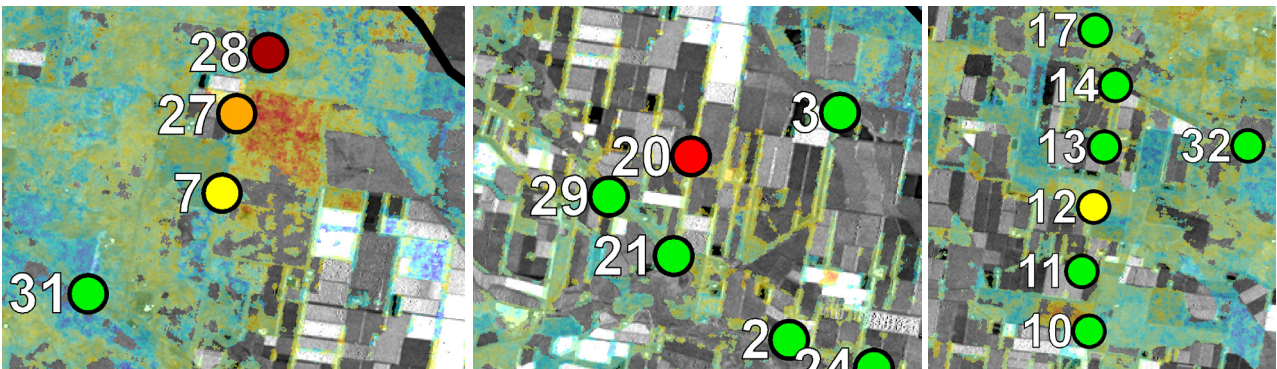
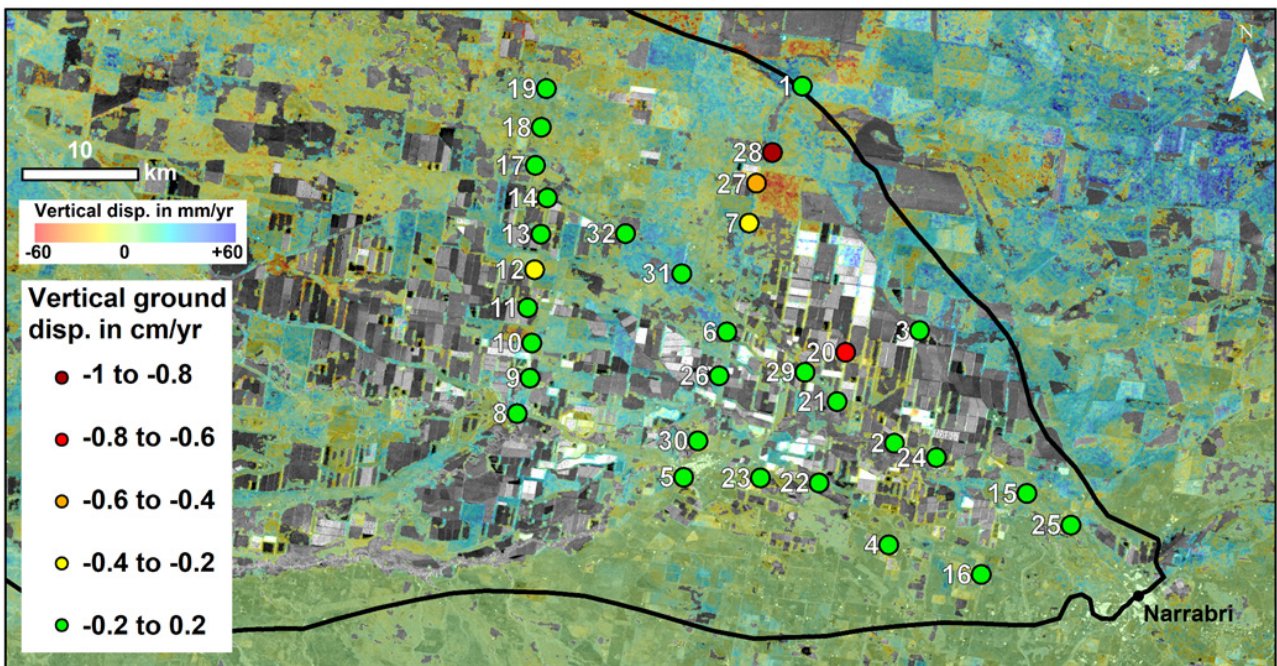


Figure 19 Vertical velocities of the subsidence benchmarks (top) incl. zoom-up (below). The numbering attributed to each subsidence benchmark is in correspondence with Table 3 and Table 8.

In Figure 18 and Figure 19, we observe five subsidence benchmarks with vertical displacement above 2 mm/yr. For the locations of these five benchmarks, time-series of InSAR vertical displacement are displayed in Figure 20 for comparison based using a 15x15-pixel spatial averaging kernel for each date of measurement.

Eight of the 32 subsidence benchmarks are above the annualised margin of error specific to each benchmark (error of $\pm 50 \text{ mm} / \text{number of years between first and recent survey}$) (Table 3) (Figure 47 in Appendix C.3). More information is given in Table 8 in Appendix C.1. The vertical displacement trends from surveys and InSAR are contradictory for a historically important benchmark 28 (FW347) that has been reported with a maximum subsidence of 21 cm since surveying started in Ross and Jeffery, 1991 and now, in 2019, revealed 37 cm. However, while this benchmark historically shows the biggest subsidence trend with surveys between 1975 and 2019 (44 years), in contrast, InSAR shows uplift at this location. This may be due to any localized surface movements caused by agricultural or infrastructure work. However, as stated earlier, we are indeed comparing a total magnitude of nearly 40 cm of subsidence over 44 years measured with benchmark surveys to a total magnitude of around 5 cm of uplift over the last 3 years derived from InSAR.

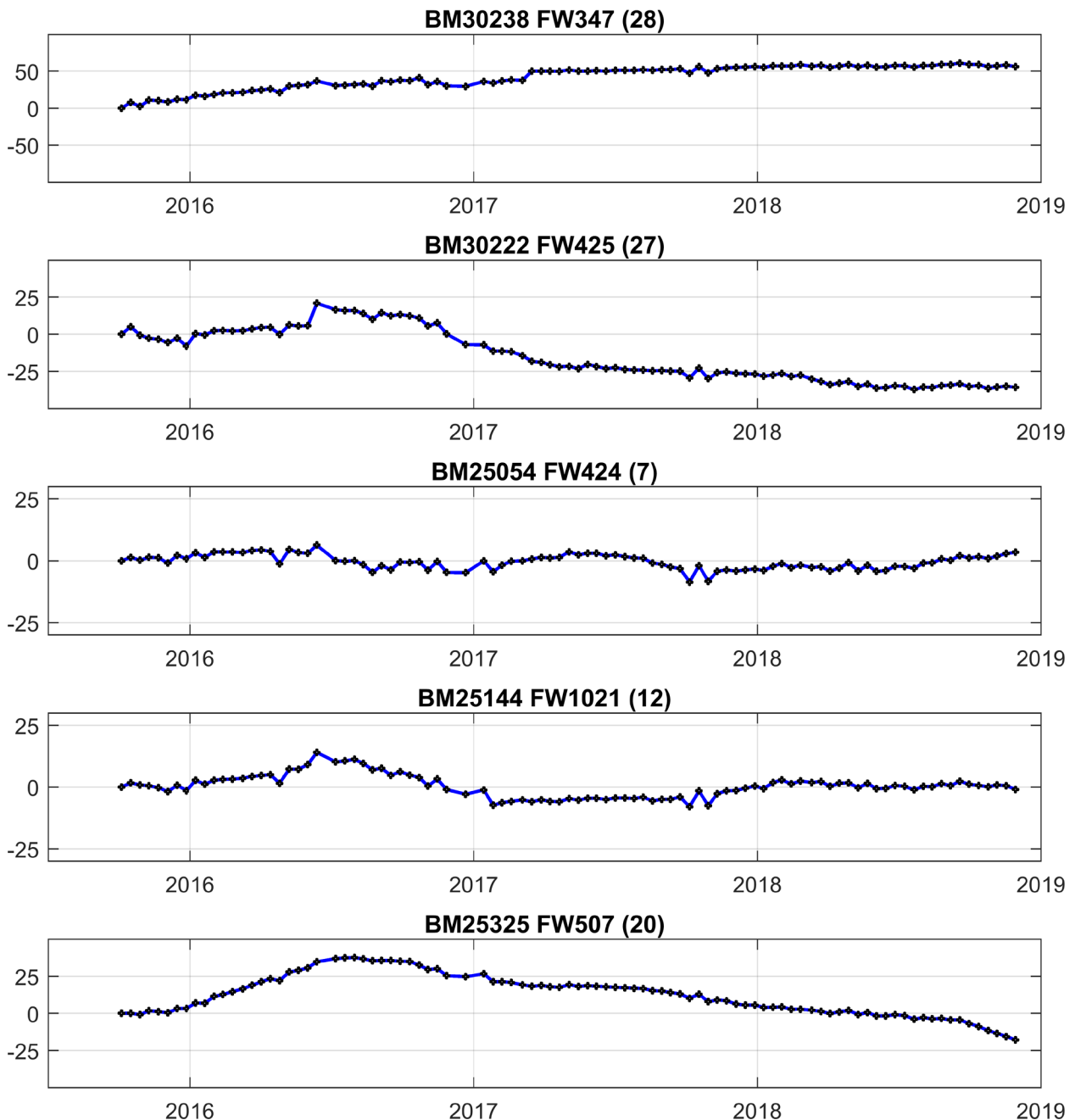


Figure 20 Time-series of Vertical Displacement [mm/yr] at Locations of Benchmarks with more than 2 mm/yr

When excluding benchmark 28 from a correlation between benchmark and InSAR trends for the other 7 benchmarks with trends beyond the assumed margin of error, one can observe a positive relationship with InSAR vertical displacement of around 1.5 times the vertical displacement from benchmarks. Notably, this correlation is very weak as it only rests on 7 data points. Hence, a discernible trend between benchmark and InSAR displacement cannot be confirmed.

Reasons for this weak correlation can be firstly, that InSAR is affected by surficial movements, and benchmarks generally are not. Secondly, an InSAR-trend calculated over 3 years does not necessarily correspond to a trend calculated over a period of up to 45 years of benchmark surveys. This is particularly true when strong inter-annual variations occur, which can be seen in the per-year trend evaluation (Figure 20).

Table 3 Comparison of annualised trends of vertical velocities for subsidence benchmark (with displacement > annualised measurement error) with InSAR velocities derived at benchmark locations (in mm/yr).

Id map	name	Benchmark Year of		cumulative annualized margin of error *	Benchmark Vertical Displacement trend [mm/yr]			InSAR Velocity 3-year trend [mm/yr]	
		first Survey	last survey before 2019		between 2019 – last	between 2019 – first	linear trend using all avail. data	InSAR VV (no buffer)	InSAR VV (15 x 15 kernel)
7	BM25054_FW424	1975	1990	1.14	-2.14	-3.23	-3.10	5.91	-0.29
12	BM25144_FW1021	1980	1988	1.28	-3.48	-2.00	-2.42	-8.10	-1.48
14	BM25148_FW1023	1980	1988	1.28	-1.67	-1.67	-1.79	0.01	-8.83
20	BM25325_FW507	1981	1990	1.32	-7.79	-7.89	-7.60	-6.06	-8.53
21	BM25328_FW282	1981	1990	1.32	-2.07	-1.55	-1.80	-3.05	-0.87
27	BM30222_FW425	1975	1990	1.14	-1.83	-5.11	-4.54	-18.03	-16.30
28	BM30238_FW347	1975	1990	1.14	-5.62	-8.50	-8.52	29.54	14.93
29	BM30266_FW421	1975	1990	1.14	-1.55	-1.27	-1.30	-15.02	-8.68

* cumulative annualised error per year = (10 mm for control BM + 15 mm for subsidence BM) x 2 (for comparison between two or more surveys) / number of years of BM survey record.

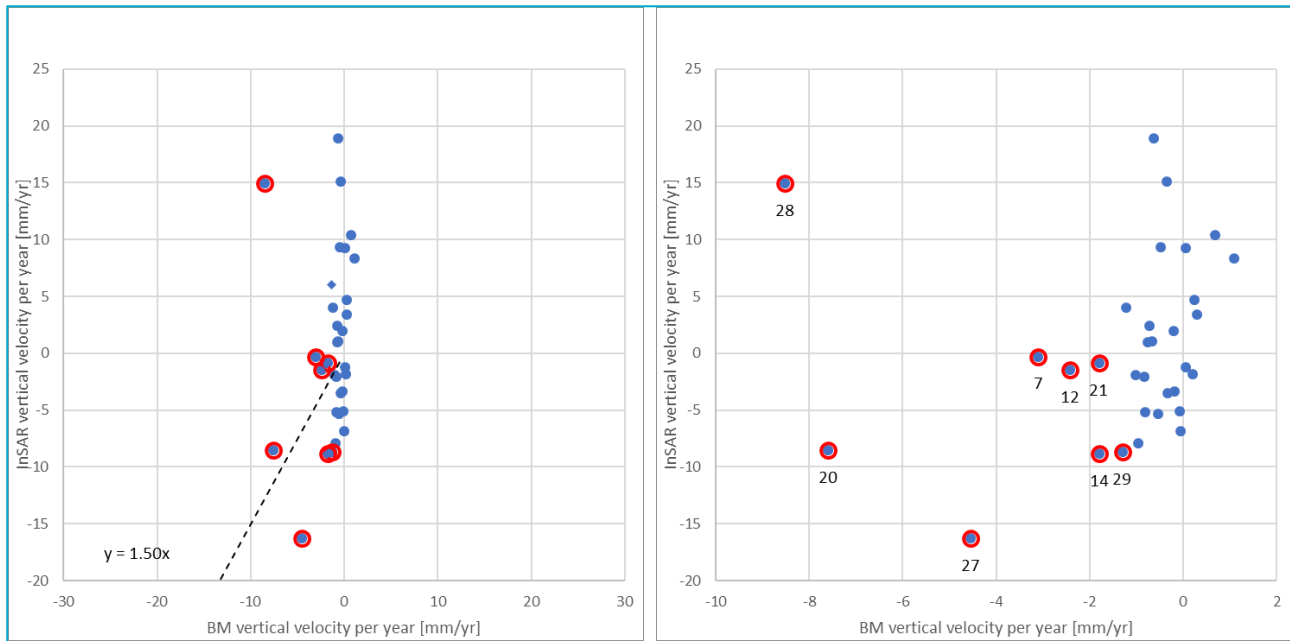


Figure 21 Correlation between all annualised trends of vertical velocities for all subsidence benchmarks (in blue) and benchmarks with displacement > annualised measurement error (in red) with InSAR velocities derived at benchmark locations (in mm/yr) with a 15 x 15 kernel.

6 Summary

The comparison of “inelastic” subsidence between short-term InSAR (Sentinel-1; 2015 until recent) and long-term benchmark survey data (up to 45 years from 1974 to 2019) requires a normalisation by creating annualised trends. While this approach is the only way these otherwise incompatible periods and methods can be compared, the basic problem is that strong inter-annual and seasonal variations resulting from variations in climate and land management can influence the 3-year trend of the InSAR data relatively more than up to 45-years of benchmark data.

Benchmark data of a recent survey (conducted in April 2019 by SMK Consultants Pty Ltd for the NSW-DPIE Water Group as part of this project) were compiled together with previous data from 1974 to 1990 from Ross and Jeffery, 1991. There is some uncertainty around the survey accuracy of this and previous surveys. Prior to the recent survey, the measurement method and accuracy for control and subsidence benchmarks was given by the surveyor as ± 10 mm for control and ± 15 mm for subsidence benchmarks. However, after the survey, the surveyor reported slightly different post-survey accuracy reports (30 mm for control and 35 mm for subsidence benchmarks, i.e. assuming a measurement error of ± 15 mm for control and ± 17.5 mm for subsidence benchmarks). That is, the post-survey reported cumulative error of ± 32.5 mm is slightly higher than the previously assumed ± 25 mm. Due to the measurement error uncertainty, we accounted for the pre-survey measurement accuracy while interpreting results of the 2019 survey. We also assumed that historic surveys were not more accurate and applied the same accuracy assumption to previous surveys. Based on that assumption, the differential subsidence between two surveys would be at least ± 50 mm.

Linear trends were calculated for time-series of compaction or expansion for each benchmark using all available data. Since this trend is based on a large time gap between the last two surveys (2019 and 1990 or older), the trend represents a progressive change in ground level rather than a seasonal or spatially limiting signal related to work on the crops or the seasonal expansion or contraction of clays. A simple trend based on just the last two surveys (2019 survey and the last one before that) is generally less than a trend based on all available data. However, as the most recent trend of the last few years is hidden within the 29-year gap, no conclusion of a “slow-down” of the rate of decline can be drawn based on just the last two surveys.

For each subsidence benchmark, annualised trends of land subsidence, based on up to 45 years of benchmark data, were compared to trends generated for the 3-year period of InSAR-derived data vertical velocities, based on a down-sampled ISBAS InSAR data-cube using a spatial-averaging kernel for each date of measurement (e.g. 15 by 15 kernel). Eight of the 32 subsidence benchmarks are above the annualised margin of error specific to each benchmark, which is generally between 1 and 2 mm/yr. When applying a more conservative error of 2 mm/yr, the vertical displacement of only 5 benchmarks remains outside the margin of error with one historically important benchmark (FW347) that shows nearly 40 cm since the inception of surveying, but an inverse correlation with InSAR trend, which shows an uplift of around 5 cm at this location. Given the incompatibility of the time-periods for benchmarks and InSAR, it is possible that a short-term uplift is hidden within a 44-year subsidence trend.

Part IV Correlating ground movements with auxiliary data

1 Introduction

Critical groundwater depletion, drainage and head change can potentially result in inelastic storage loss in the Lower Namoi aquifer if changes in stresses on the fine-grained aquitards or interbed exceed preconsolidation thresholds. Inelastic subsidence occurs while head levels reaches unprecedented historical lows, meaning that the hydrostatic pressure in the aquifer is beyond the maximum effective stress that it has experienced in the past, called the pre-consolidation stress.

Theoretically, the determination of this information may be utilised to set local groundwater level management targets and thresholds to prevent or limit irreversible sediment compaction and any associated land subsidence. However, in the Lower Namoi, ground movement can potentially not only be influenced by long-term inelastic and seasonal elastic aquifer compaction or expansion resulting from changes in aquitard or fine-grained interbed storage, but also by seasonal swelling and shrinking of vertosol soils, as well as land-use and related cropping and/or crop irrigation.

In order to derive relationships between head change and deformation derived from benchmark surveys, we assume the observations to be independent of swelling/shrinking of vertosols and land-use changes. The benchmark results are assumed to represent deformation as the differential between the measured movement of a steel rod driven into the bottom of 20' deep PVC-cased bore holes for as far as possible or at least 5' beyond the bottom of the hole and any background movement measured at control benchmarks (Ross and Jeffery, 1991)(Figure 22). The assumption is that the steel rod is isolated from any near-surface movement related to swelling/shrinking montmorillonite clays (commonly referred to as black soils or vertosols) in the upper 20' of the soil profile and the alluvium. Based on that assumption, we ignore the influence of these clays on the deformation across the aquifer from below 20' down to the bottom of the aquifer. Hence, only groundwater heads that represent aquifer dewatering were used to analyse potential correlation with benchmark deformation (Section 2.1).

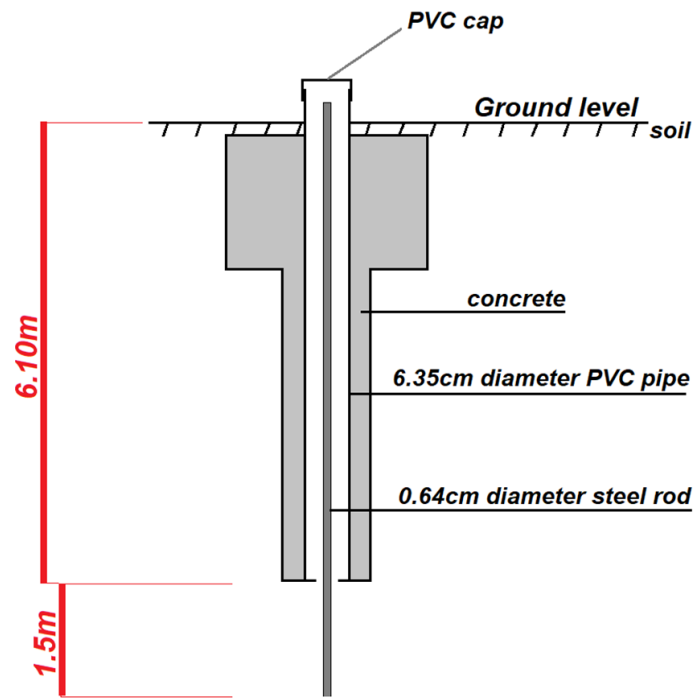


Figure 22 Design of Subsidence Benchmarks (adapted from Ross and Jeffery, 1991)

In contrast, InSAR-derived ground movements are impacted by all three types of auxiliary data and are ignorant of the cause, whether related to swelling/shrinking clays, or aquifer compaction/expansion, or high InSAR noise level related to the vegetated land cover. Therefore, InSAR versus water level correlation analysis would generally be preferable at points where no swelling/shrinking soils nor major land-cover changes occur. However, swelling/shrinking clays are known to be quite prevalent in the Lower Namoi similar to the Liverpool Plains (Kirby et al., 2003). Hence, a multi-factorial correlation between InSAR deformation and groundwater heads as well as clay content becomes necessary to better isolate the effect of groundwater abstractions (and the related release of groundwater from interbed storage) on ground level changes from the impact of swelling/shrinking clays (Section 2.2).

The clay fraction in the Lower Namoi is slightly less (around 60%) compared to the Liverpool Plains (around 80%). Therefore, also the annual amplitude of swelling and shrinking is expected to be less than in the Liverpool Plains, where it reaches up to ± 15 cm/yr (Ringrose-Voase 2020), especially considering that vertical shrinkage amounts to only about one third of the volumetric shrinkage. Since the annual amplitude of swelling and shrinking is unknown, a correction of surface deformation from InSAR for those surface effects to obtain an approximation of aquifer compaction is not possible. As an approximation of the spatial distribution of the percentage of clay near the surface, we generated a soil clay content map defining the volumetric proportion of clay in the first meter of soil from ‘modelled soil properties’ available from eSPADE v2.0 (NSW and Office of Environment and Heritage (OEH) 2020), as depth-weighted average from ‘Clay %, 0-30 cm’ and ‘Clay %, 30-100 cm.’ eSPADE is a Google Maps-based information system that allows free access to soil and land information from across NSW. The readily downloadable rasters of modelled soil properties on eSPADE include percent, clay, sand, and silt for three depth intervals (0-5 cm, 0-30 cm, and 30-100 cm). The modelling methods and data sources are described in NSW & OEH (2018).

The clay content of the first metre is just an approximation of the near-surface clay content but is utilized firstly to allow the above-mentioned three-dimensional temporal correlation analysis between InSAR-derived ground movement in the vicinity of bores, drop in head or critical head in related piezometers, and clay content at those points, but also to conduct a statistical analysis of the spatial distribution of clay content and InSAR-derived ground displacement (Section 3.1).

Lastly, we investigate the impact that the type of land-use and related cropping and/or crop water supply (natural versus irrigation) may have on seasonal or long-term land subsidence (Section 3.2). For that we sourced land use of 2017 also downloadable from eSPADE (NSW & OEH 2020) and compared land use classes against InSAR results and also observations drawn from PSI (Part III, section 4.3).

2 Exploring temporal correlations

2.1 Hydraulic heads and benchmark deformation

In order to study the effect of aquifer dewatering on deformation, benchmark subsidence can be compared with critical heads that represent the historical minimum of head level at which pre-consolidation occurred. Any water level fluctuation above those critical heads is assumed to solely influence elastic compaction and expansion. Any new drop of water levels to below previous critical heads established new critical heads and may impact inelastic subsidence.

It is important to note that the delay of the subsidence reaction is unaccounted for in the analysis. For example, a sudden critical head drop followed by a quick recovery might not be sufficiently long to allow for full consolidation of compressible sediments. In this case, subsidence potentially occurs later if hydraulic head drops again down to historical minimum, even though the critical head stays the same.

While earliest water level hydrographs go back to 1906, hydrographs for the 5 bores that are paired with benchmarks of subsidence rates of more than 2 mm/year start at the earliest in mid-1968 (Figure 24a). For these 5 bores, hydrographs of piezometers with the deepest drawdowns since inception of each respective benchmark survey were analysed, assuming that they drive dewatering and vertical leakage from fine-grained interbeds in the aquifer (Figure 23; 7 = BM25054, 12 = BM25144, 20 = BM25325, 27 = BM30222, 28 = BM30238).

Note that the nomenclature for piezometers used in this report henceforward is as follows: GWxxxxx-y-z, with xxxxx being the bore site ID paired with the benchmark of equivalent site ID, y being the hole ID, and z being the pipe ID. The piezometers with deepest drawdowns within each bore paired with benchmarks are GW25054-1-2, GW25144-1-3, GW25325-5-6, GW30222-2-2, and GW30238-2-2.

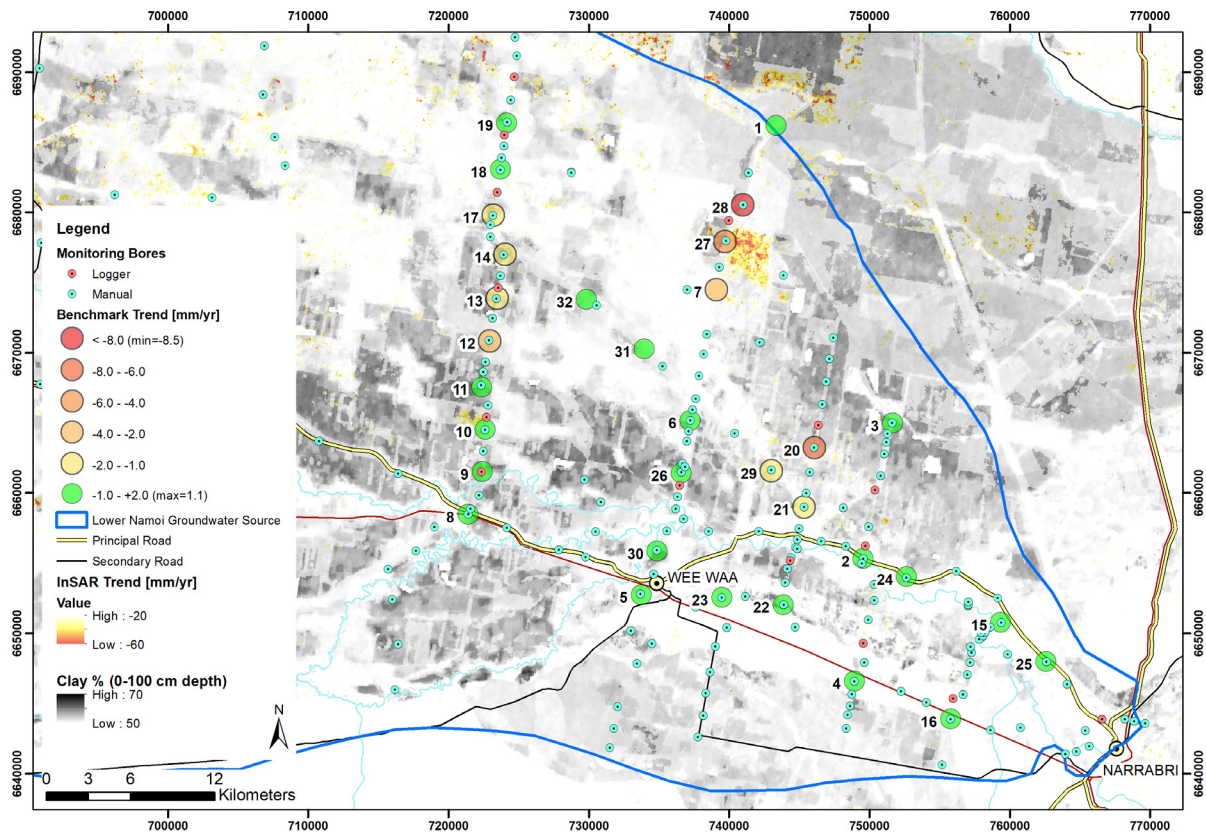


Figure 23 Benchmark displacement trends using a measurement inaccuracy of ± 1 mm/yr, hotspots of InSAR displacement (only subsidence < -20 mm/yr shown), and distribution of modelled clay content over the top metre of soil.

When deriving time-series of critical heads from the original water level hydrographs of these 5 piezometers, we assume no pre-consolidation prior the beginning of the water level records. We can observe significant groundwater depletion with associated drop in critical head in the mid-1970s and early 1980s (Figure 24a), particularly for piezometers GW030222-2-2, GW025325-5-6, and GW030238-2-2, which also showed maximum subsidence of 22, 30, and 37 cm over the total period of ≈ 45 years. While these periods of depletion apparently resulted in consolidation and, hence, new pre-consolidation heads, infrequent minimum heads which may not be always representative for a longer period of drawdown or may even be manual measurement errors will also cause the critical head to drop to new minima (Figure 24a).

The comparison between benchmark subsidence and critical heads is further complicated, because the exact dates of the benchmark surveys are unknown to the authors. Yet, even if the dates were known, and as stated before, subsidence always occurs with some delay to the change in stress and cannot be correlated based on exact dates. For simplicity, in this study, benchmark findings of particular survey years are compared against average water levels or average critical heads for each survey year. However, annual mean critical heads can be obtained either by first finding the minima of the original heads and then annually-averaging the resulting critical heads afterwards (Method A, Figure 24b), or by first averaging the original heads and then finding the minima of averaged heads (Method B, Figure 24c).

Method A will honour the influence of any short-term drop of heads on the establishment of new pre-consolidation heads regardless of whether those are based on single value water level

measurements or longer periods of depletion and dewatering. A single value measurement, in this respect, may have no effect on critical heads because it is either a measurement error or of extremely short duration insufficient to cause actual, often delayed, dewatering of fine-grained interbeds in the aquifer. However, longer, often seasonal, depletion will indeed cause a drop in critical heads, which, in this case, will remain constant during any potential recovery in the following season.

Method B will discard the influence of the above described short-term drop of heads as critical heads are derived from annual averages, except in the case where a short-term drop of head is the only measurement in the year. However, when deriving critical heads from already averaged heads, the effect of seasonal drawdown may be compensated by subsequent recovery, and, in this case, would have a false zero effect on critical heads.

This results in a much lesser drop in critical heads in the mid-1970s using Method B, where sharp seasonal drawdowns are followed by quick and full recovery (Figure 24c). As a consequence, critical heads remain at a significantly higher level when compared to Method A and experience a new drop in critical head in the mid-1990s. Unlike in Method A, when using Method B, pre-consolidation heads were already achieved in the early 1980s, and, hence no further drop in critical head can be observed during the 1990s. However, after the 1990s, pre-consolidation heads remain more or less stable for both approaches. This indicates that, while the actual time of occurrence of the most recent incremental land subsidence within the 19-year gap between the last two surveys is unknown, measurements of the recent benchmark survey may indeed be related to dewatering activities in the mid-1990s. Any later dewatering during specific periods (e.g. 2001 to 2003) may have caused sporadic (and potentially low amplitude) deformation, but because preceding rises in head caused elastic expansion, that deformation would have been also elastic and not inelastic.

In summary, true pre-consolidation head hydrographs most likely will be somewhere between the two approaches, as both are extreme in the sense that critical heads obtained before averaging are influenced by single values of water level measurements, while critical heads derived from already averaged water levels may ignore heavy seasonal depletion and dewatering if compensated again with recovery during following seasons. Therefore, in this study, correlations between benchmark subsidence and both types of annual mean critical heads were analysed.

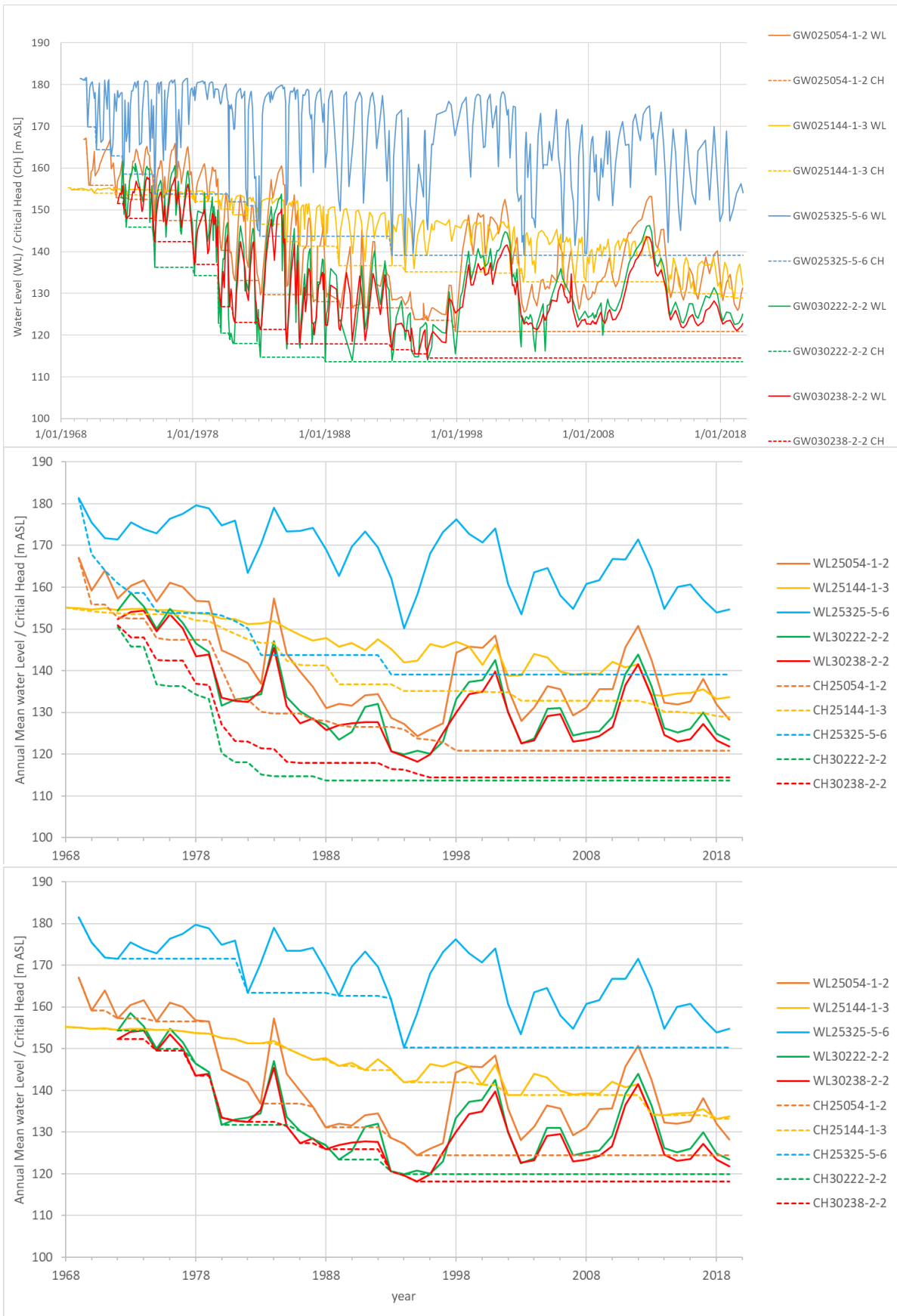


Figure 24 Time-series of heads (WL) & critical heads (CH) at benchmarks with >2 mm/yr (original WLs and CHs derived from original WLs (a); averaged WLs and averaged CHs derived from original WLs – Method A (b); averaged WLs and CHs derived from average WLs – Method B (c))

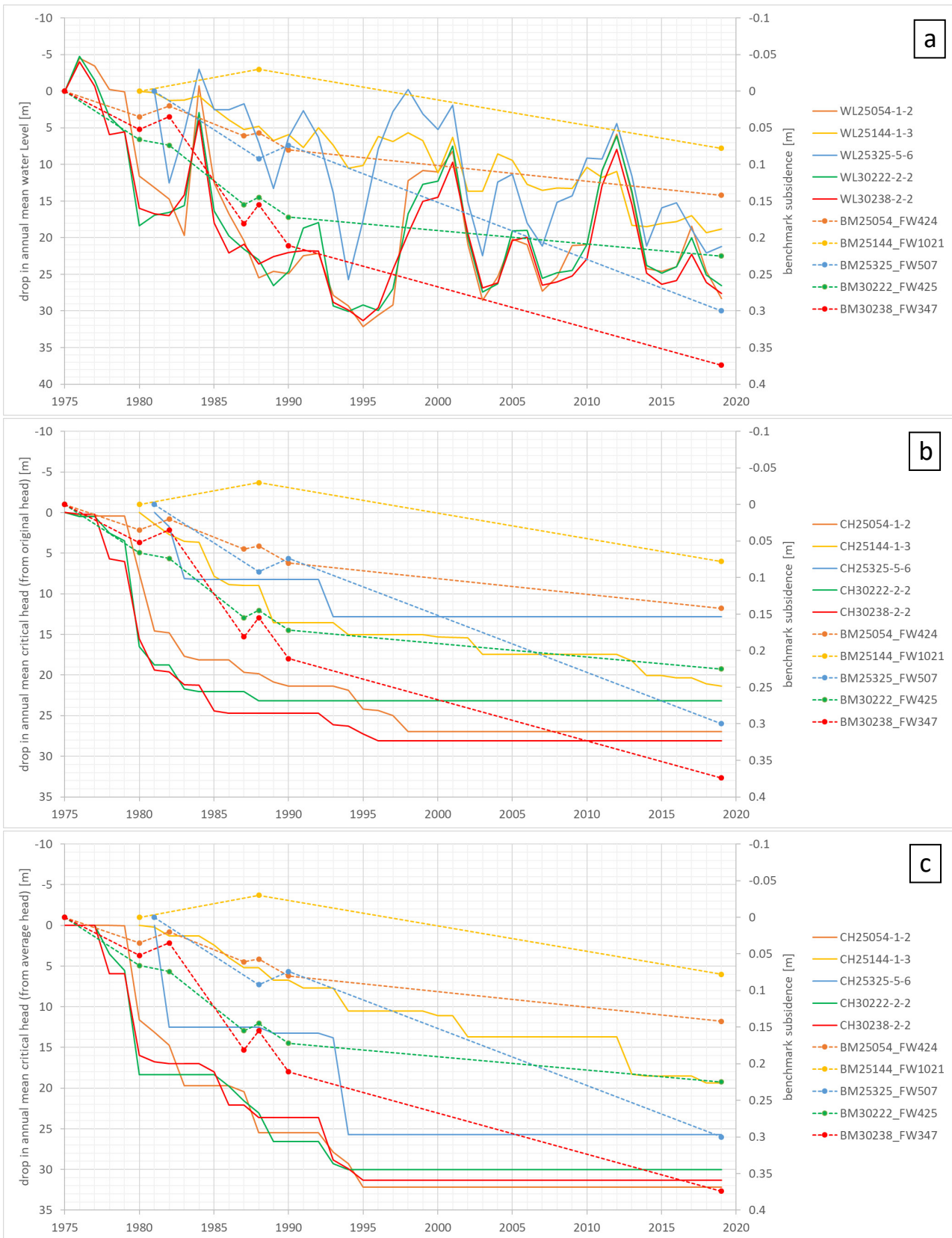


Figure 25 Time-series of heads (WL) & critical heads (CH) with benchmark subsidence at benchmarks with >2 mm/yr (original WLS and BM subsidence (a); averaged CHs derived from original WLS with BM subsidence – Method A (b); CHs derived from average WLS with BM subsidence – Method B (c))



Figure 26 Individual time-series of heads & critical heads derived by different methods and subsidence recorded at 5 benchmarks >2 mm/yr.

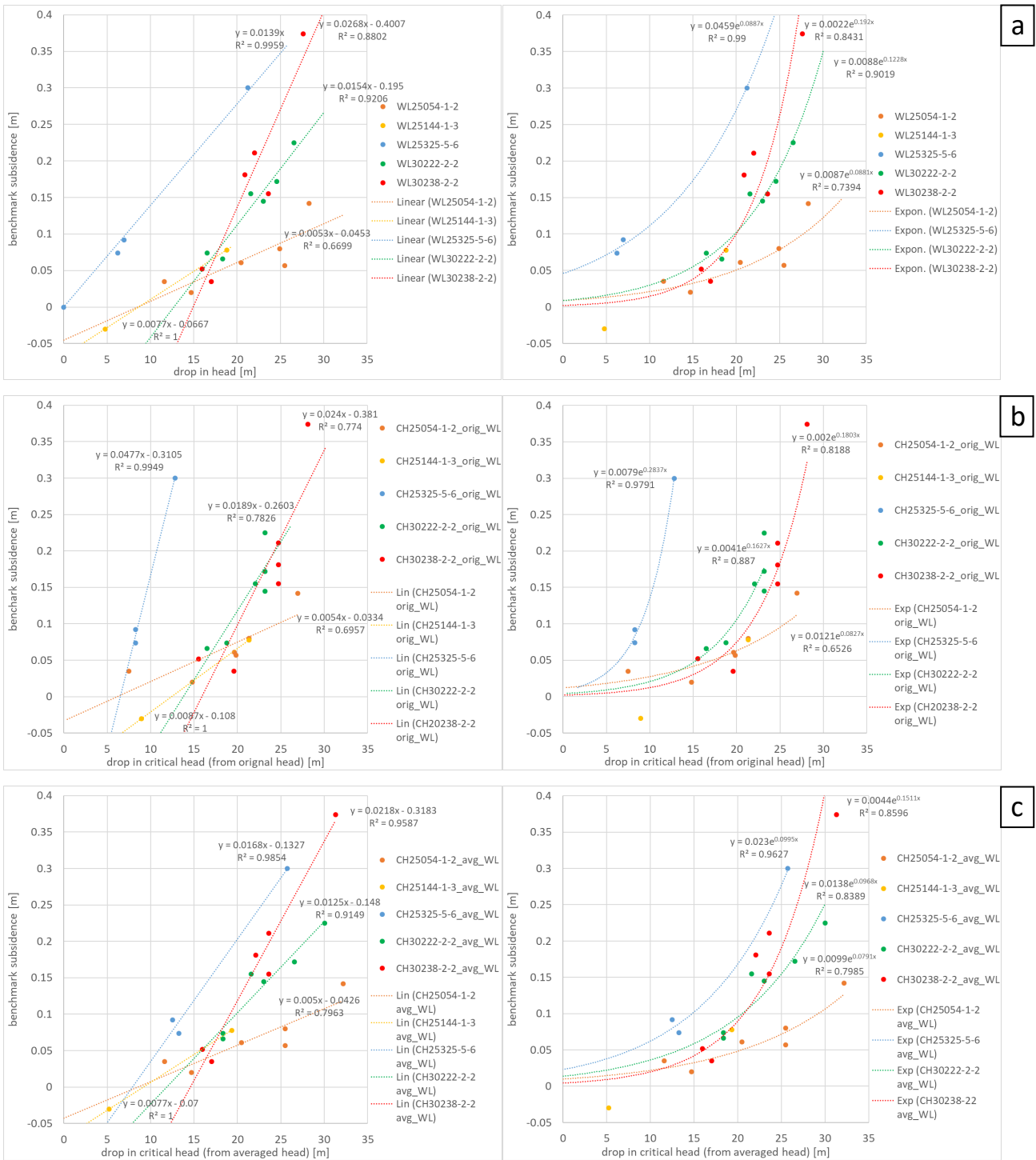


Figure 27 Correlation between annual mean head (a) or annual mean critical head (derived from original heads) (b) or annual mean critical head (derived from averaged heads) with benchmark subsidence (c) using linear (left) or exponential (right) regression.

Linear regression between head drop and critical head drop is generally associated with a good correlation (Figure 27 left), but meaningless unless forced into a zero intercept, because head drop and critical head drop start at zero at time of the first survey, when also benchmark subsidence was zero. When forced into zero intercept, correlation deteriorates (not displayed). That is, a simple linear relationship between head drop or critical head drop and benchmark subsidence cannot be formulated. However, exponential regressions appear to be more closely reflecting the reaction of subsidence to a drop in critical head which drives inelastic subsidence (Figure 27 right).

Particularly for two piezometers that show the deepest drawdown and drop in critical head (GW030222-2-2, GW030238-2-2; Figure 25 and Figure 26), a very similar correlation pattern demonstrates initially little to no subsidence for a smaller drop in annual mean critical head, but then increasing rates of subsidence for a deeper drop in critical head (Figure 27b). One possible reason for that may be that annual mean critical heads derived from original water levels were established already at the beginning or even before the benchmark surveys began. That is, after the initial drop in critical head and initial subsidence, pre-consolidation heads remained, and new subsidence followed with some delay.

However, when using critical heads that are derived from annual mean heads, short-term drops in heads in the early to mid-1980s are ignored and only sustained drawdown in the mid-1990s leads to the establishment of newer, deeper preconsolidation heads. Therefore, the slopes between critical head drop and benchmark subsidence are less compared to using annual mean heads derived from the original heads (Figure 27c).

The very similar empirical exponential relationship for GW030222-2-2, GW030238-2-2 most likely reflects the proximity of only around 3 km between them. We can expect that similar hydrogeology, including stratigraphy of aquitards and aquifers and their respective compressibility and thickness, will result in a similar reaction of subsidence to a similar drop in critical head. In contrast, the more distant piezometer GW025325-5-6, whose associated benchmark experiences the second biggest total subsidence of around 30 cm over a period of 38 years, shows a very different behaviour (blue curves in Figure 27 b and c) with a lesser drop in critical heads leading to subsidence comparable to GW030238-2-2.

The coefficients in the exponential relationship **subsidence** = $b \times e^{a \times \text{Head drop}}$ in Figure 27 may be explained as follows:

- **a** - Curvature (or exponential slope if in lin-log) expresses the sensitivity of the subsidence to the critical head drop;
- **b** – Offset expresses the magnitude of subsidence independent of the critical head.

In Figure 27, GW030222-2-2 (green) and GW030238-2-2 (red) have about the same **a**-coefficient 0.16 vs. 0.18, but a factor of 2 in between them for the **b**-coefficient, suggesting that GW030222-2-2 reaches a higher subsidence with the same critical heads or needs a smaller drop in critical heads to achieve the same subsidence (Table 4). Indeed, GW030238-2-2 reached a much higher total subsidence of 37 cm compared to GW030222-2-2 with 22 cm.

Using the annually-averaged critical head record, which is derived from the average head, more correctly reflects the total subsidence. An **a**-coefficient of 0.15 versus 0.097 means that critical head for GW030238-2-2 in the mid-1990s dropped relatively more than for GW030222-2-2 resulting in more inelastic subsidence.

Note that any such empirical relationship is specific for localized hydrogeologic conditions, and for the 45-year period of benchmark observations. Any spatial extrapolation to other areas or temporal prediction of subsidence as a function of continuously dropping critical heads cannot be made based on those relationships. While for the 5 benchmarks (with subsidence trends of >2 mm/yr) subsidence is well correlated with critical head drop, other benchmarks remain stable despite significant drop in critical head (e.g. Merah Section and Wee Waa Section north of Wee

Waa in centre of Figure 28A). Therefore, a drop in critical head cannot be used as a qualitative proxy for potential subsidence.

Table 4 Lookup table for estimated subsidence as a function of critical head for two selected piezometers using two different methods of deriving annual mean critical heads

	GW030222-2-2	GW030238-2-2	GW030222-2-2	GW030238-2-2
	Using critical head (from original heads)		Using critical heads (from averaged heads)	
b-coeff	0.004	0.002	0.014	0.004
a-coeff	0.16	0.18	0.1	0.15
CHdrop [m]	Benchmark Subsidence since start of Surveys [m]			
5	0.01	0.00	0.02	0.01
10	0.02	0.01	0.04	0.02
15	0.04	0.03	0.06	0.04
20	0.10	0.07	0.10	0.08
25	0.22	0.18	0.17	0.17
30	0.49	0.44	0.28	0.36
35	1.08	1.09	0.46	0.76
40	2.41	2.68	0.76	1.61

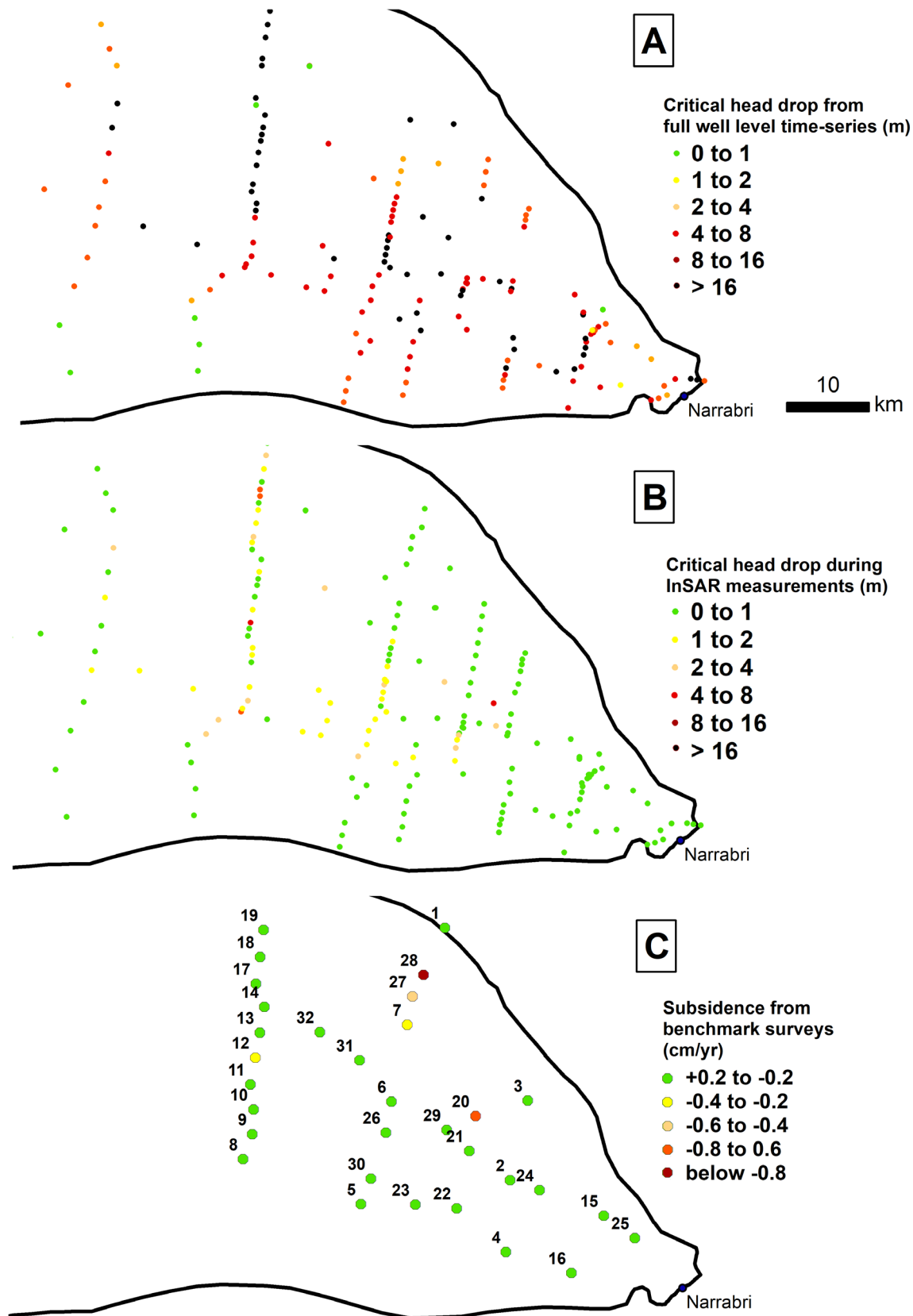


Figure 28 Critical head drop in piezometers (in m) during the entire period of water level recording (A) and during the InSAR observation period (B) and benchmark displacements trends (in cm/yr)

2.2 Hydraulic heads and InSAR deformation

Critical heads of piezometers with deepest drawdowns within each bore do show significant drops over the entire period of record in some areas (Merah Section and Wee Waa Section north of Wee Waa in Figure 28A). A much lesser or no drop in critical heads of these piezometers can be found during the InSAR period from the end of 2015 to the end of 2018 (Figure 28B). Consistent with that finding, also critical heads of all deep piezometers at the 5 benchmarks with subsidence trends of >2 mm/yr remain constant over the InSAR period (compare Figure 28B with Figure 28C, Figure 29; dashed lines) most likely because previous pre-consolidation heads were established long before the 3-year InSAR period between the early 1980s to the mid-1990s. This suggests that the most reactive part of the aquifer near Benchmark 27 and 28 (in terms of the hydraulic pressure drop to subsidence reaction) did not undergo sufficient head drop during the InSAR observation period to create subsidence detectable by InSAR. It also suggests that other sections of the aquifer do not show major subsidence even if critical heads drop significantly (Figure 28). A '3-way' correlation analysis between benchmark subsidence, InSAR deformation, and critical heads at just the 5 benchmarks with subsidence trends of >2 mm/yr is not possible.

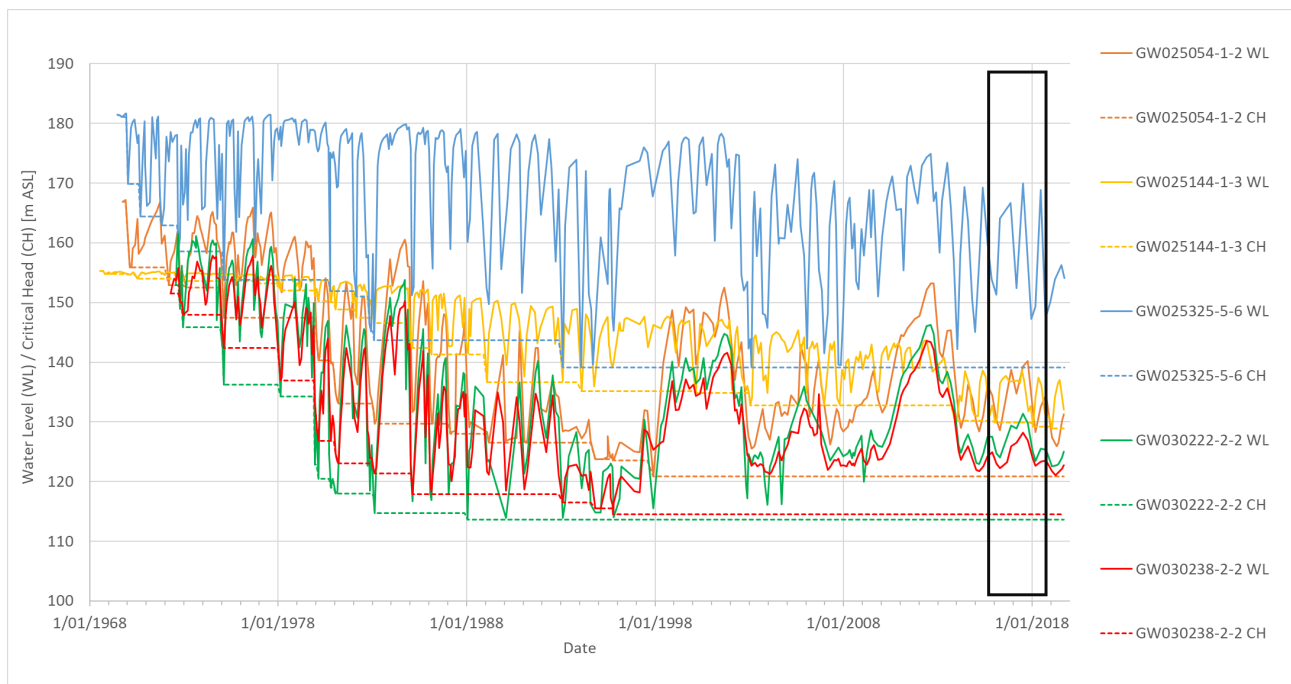


Figure 29 Water levels and critical heads at bores near the 5 benchmarks with subsidence trends of >2 mm/yr (black box: time window of InSAR analysis)

Instead, a correlation analysis of InSAR-derived subsidence at the vicinity of 589 piezometers belonging to 254 bores in the study area is presented. For that, we applied a 5-by-5 pixels averaging kernel (which corresponds to 300m x 300m) around each bore on the InSAR-derived vertical displacement map (Figure 30). We considered the measurement as invalid when less than 75% of the pixels were above the coherence threshold. Since manually recorded water levels time-series have varying time-steps, we resampled the time-series during the period of the InSAR analysis (03/10/2015 until 28/10/2018), with similar time-steps than the InSAR time-series. Thus, the process of calculating critical heads time-series is performed as follows:

1. computing the historical minimum along each head time-series to obtain critical heads, taking into account the full time-series and initial record sampling frequency for each well;
2. resampling the resulting head and critical head time-series over a synthetic, uniform time-vector to precisely cut temporal windows (12-days steps, as the InSAR time-series);
3. computing the change in critical heads occurring during the InSAR era;

Following this procedure, resampled time-series of heads and critical heads for all 589 bores could then be compared to time-series from InSAR. However, it should be noted that many correlations between time-series of resampled water levels or critical heads with equal time-stepping of InSAR series are problematic due to the sparsity of manually recorded water level data. Many bores had none or just a few water level measurements during the InSAR period, which results in interpolation artefacts across either the entire period between measurements that fall outside the InSAR period or across long periods within the InSAR period. For that reason, bores with less than 3 measurements during the InSAR era were not considered in the analysis.

Expansion and compaction derived from InSAR velocities can be observed during the 3-year InSAR period at levels of up to around ± 20 mm/year (Figure 31a left, z-axis) for 483 piezometers belonging to 227 bores (Figure 31a right and Figure 32 left) when using piezometers with more than 3 measurements during the 3-year InSAR period, which accounts for manual data (Figure 30). For 33 piezometers belonging to 23 bores only with logger data comprising of more than 1100 measurements, expansion and compactions ranges around ± 15 mm/year (Figure 31a right, z-axis and Figure 32 right).

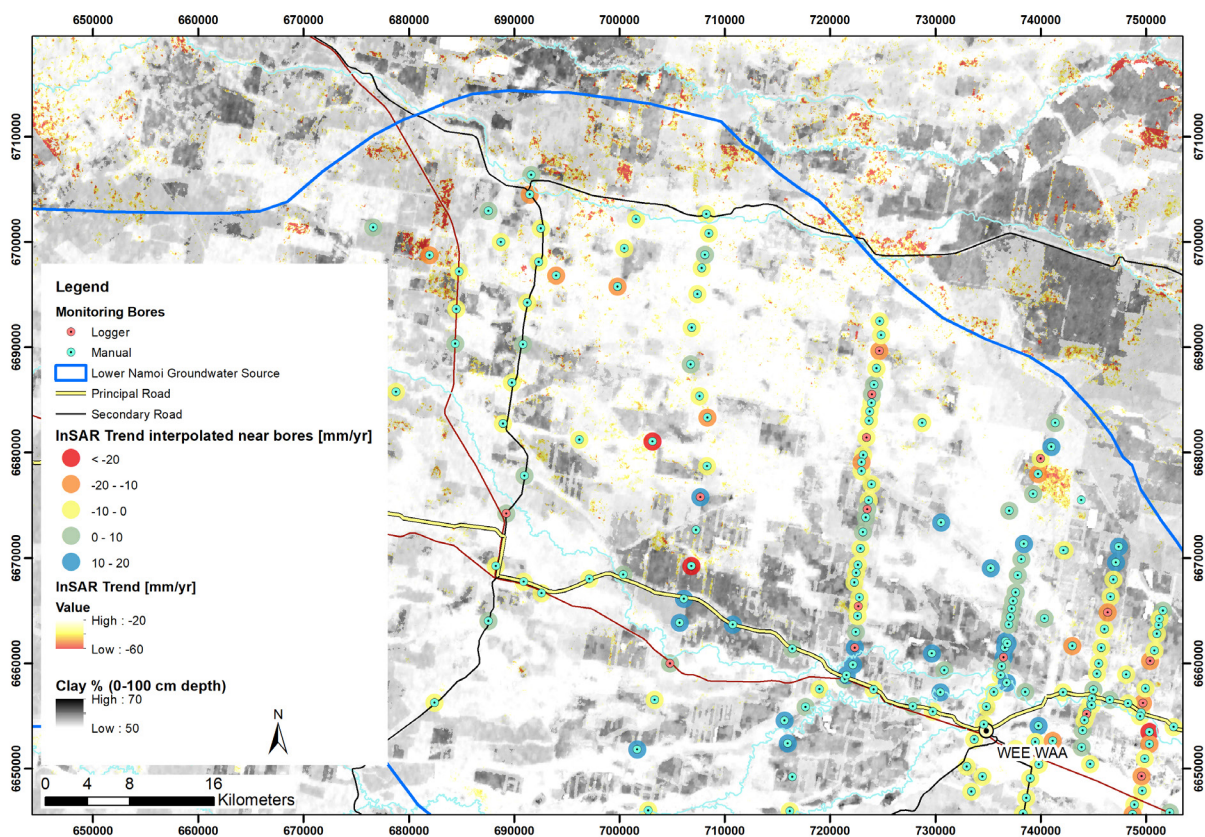


Figure 30 InSAR displacement trends near bores using a 5x5 averaging kernel (300m x 300m), hotspots of InSAR displacement (only subsidence < -20 mm/yr shown), and distribution of modelled clay content over the top metre

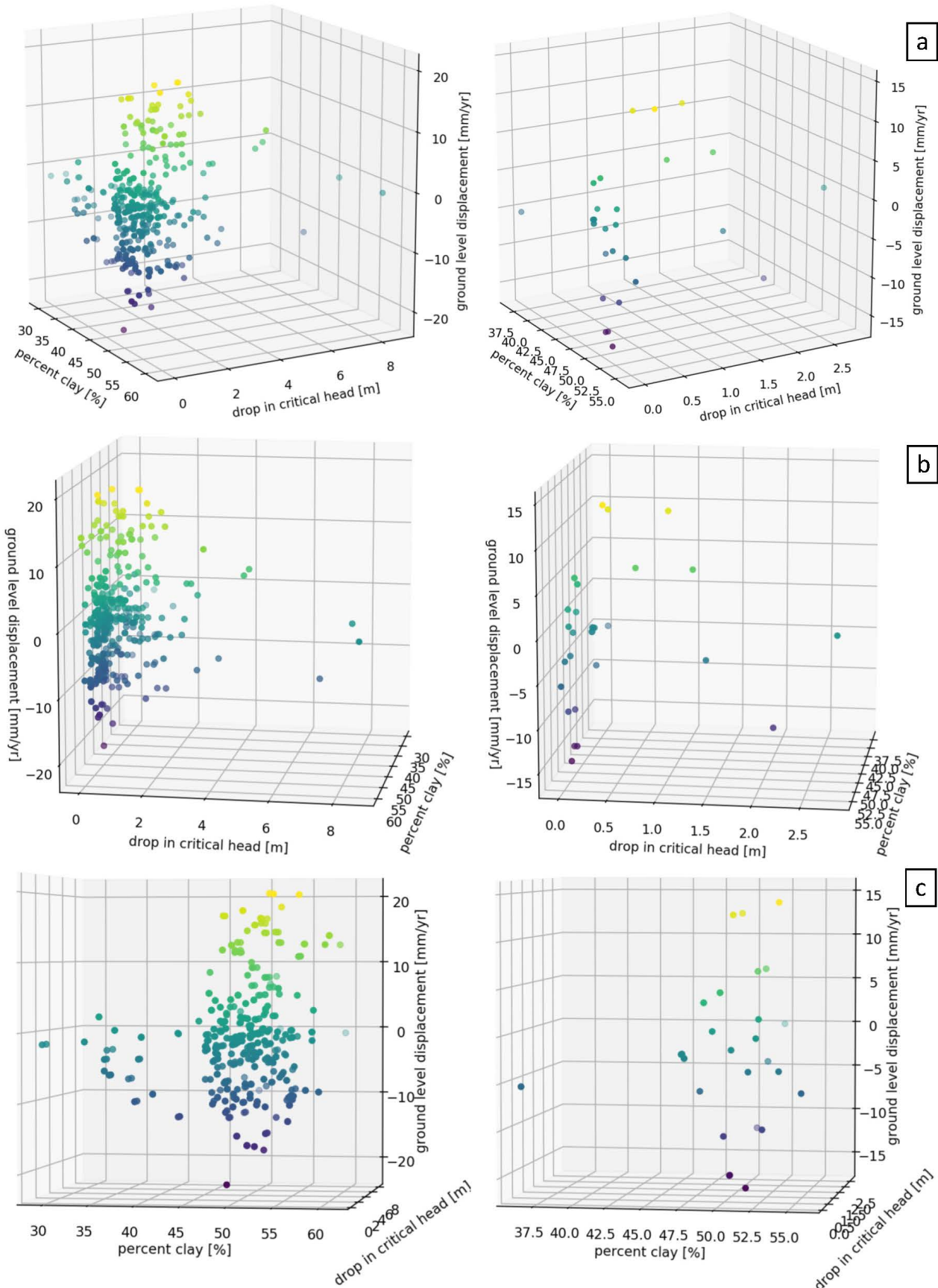


Figure 31 3D Scatter plot of critical head drop, proportion of clay in the surficial soil, and InSAR-derived deformation trend for manual data (left) or logger data (right) during the 3-year InSAR period (general (a); focus on relation between critical head drop and deformation (b); focus on relation between percent clay and deformation (c))

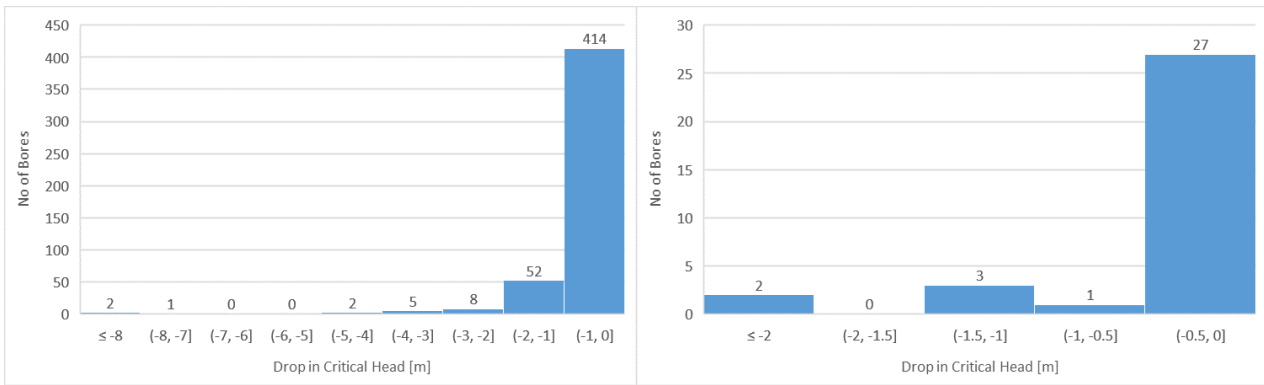


Figure 32 Histograms of critical head drop from bores with manual data (left) or logger data (right)

Most of those piezometers did not reveal any or only minimal drop in critical heads (Figure 31b, Figure 32) during the 3-year InSAR period (Figure 31b, Figure 32, Figure 33b, Figure 34b) most likely because pre-consolidation was established long before the 3-year InSAR period (Figure 33a, Figure 34a). That is, the InSAR-derived surface movement in the 300-m vicinity of those piezometers may not be attributable to inelastic subsidence, but rather to either swelling and shrinking of clays in the vertosol soils, to InSAR measurement errors due to low-coherence, or to elastic compaction and expansion of fine-grained inter bed or aquitard portions of the aquifer that are above pre-consolidation head.

However, few bores seem to indicate a decline in critical heads during the 3-year InSAR period. When using all bores with more than 3 measurements (i.e. comprising both manual and logger data), 69 piezometers did show a decline in critical heads from 1 to 9 metres (Figure 31b left, 'drop in critical head' axis; Figure 32 left). Yet, a few piezometers may have errors in the manual measurements, such as recording negative instead of positive depths below measuring point, association with incorrect 'above sea levels', or simply typos resulting in large offsets. While most of the error have been corrected, even a remaining isolated false low value could be misinterpreted as a drop in head that leads to a newly established, but false, pre-consolidation head (e.g. suspected errors in GW036227-1-2, GW036280-1-1, GW036542-1-1 in Figure 34b). When only accounting for logger data, only 6 piezometers showed a drop in critical head of more than half a metre and up to nearly 3 metres (Figure 31b right, 'drop in critical head' axis; Figure 32 right) in early 2017 and early 2018 (Figure 33b).

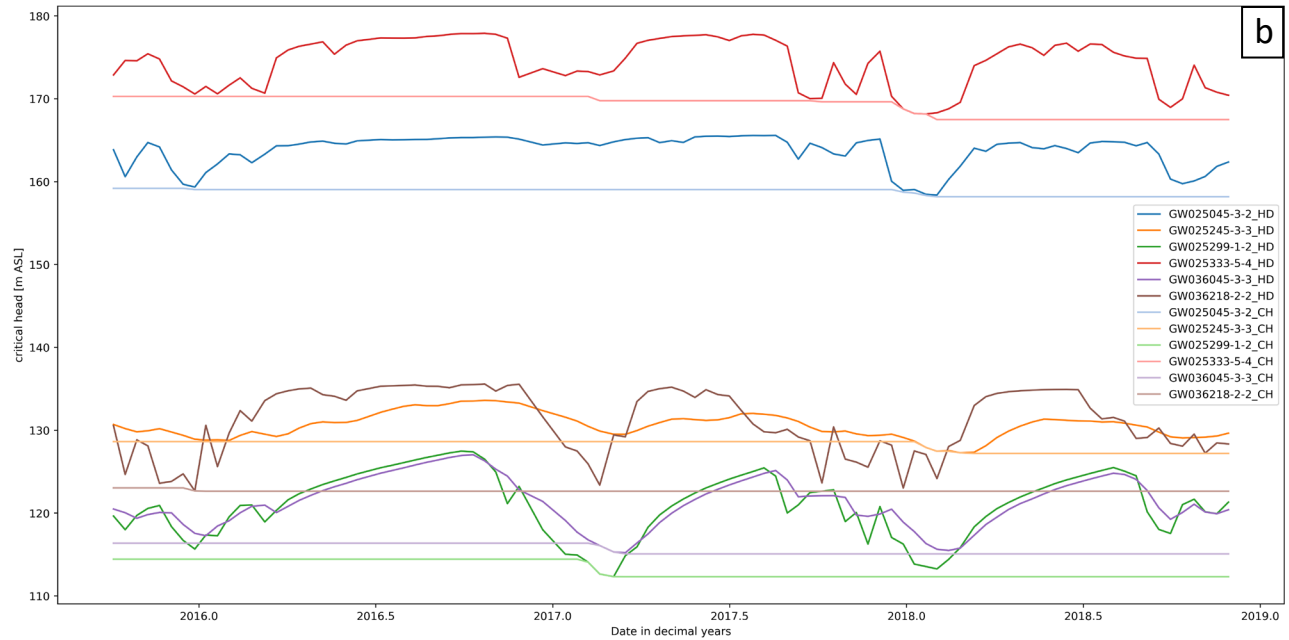
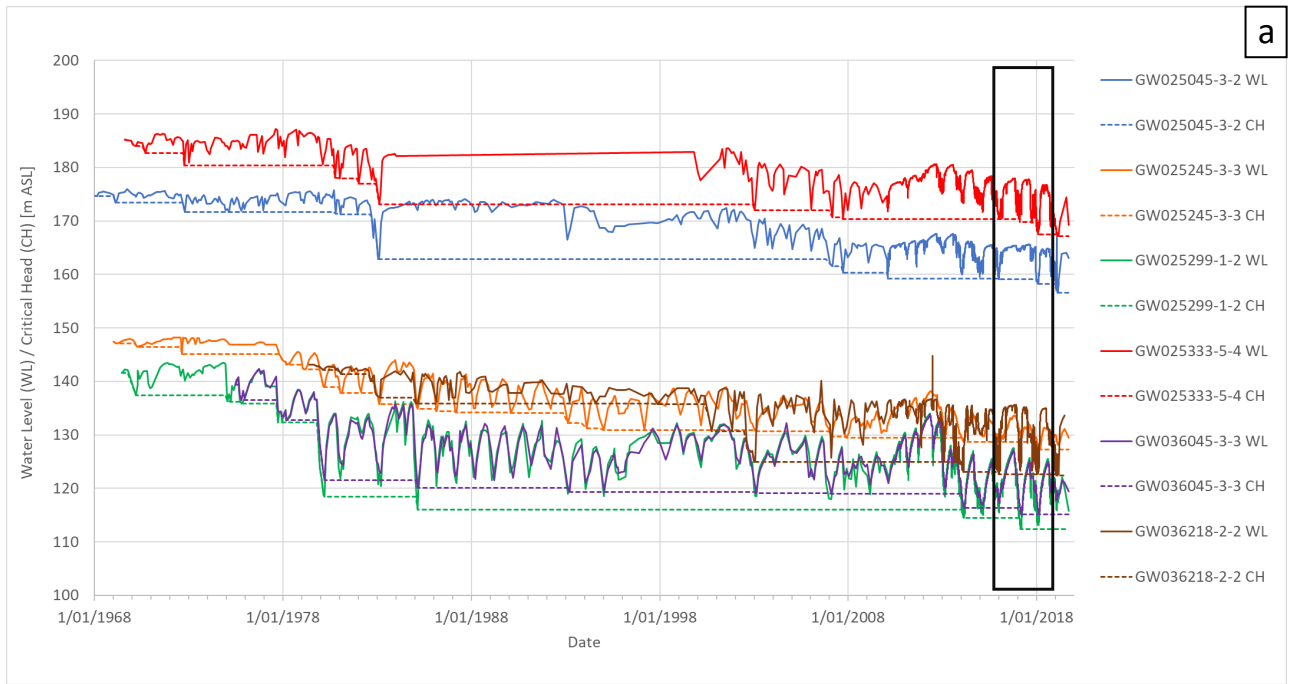


Figure 33 Time-series of heads and critical heads of selected piezometers with logger data (a) since recording started and (b) during the 3-year InSAR period.

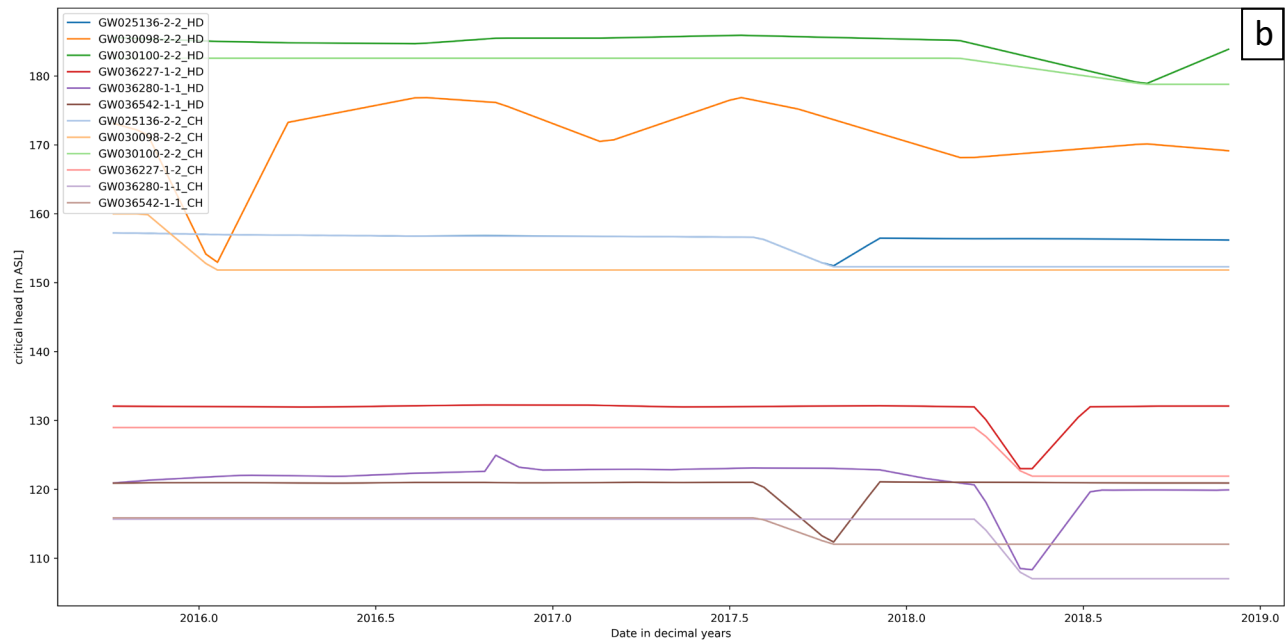
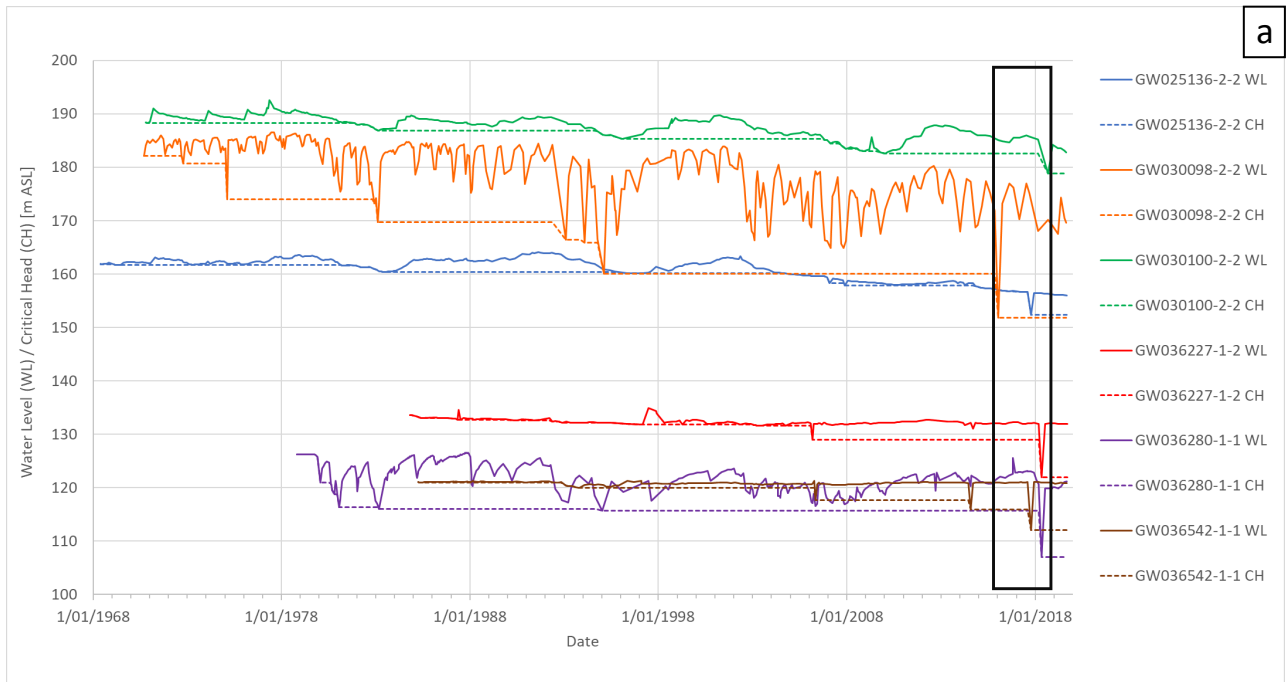


Figure 34 Time-series of heads and critical heads of selected piezometers with manual data (a) since recording started and (b) during the 3-year InSAR period

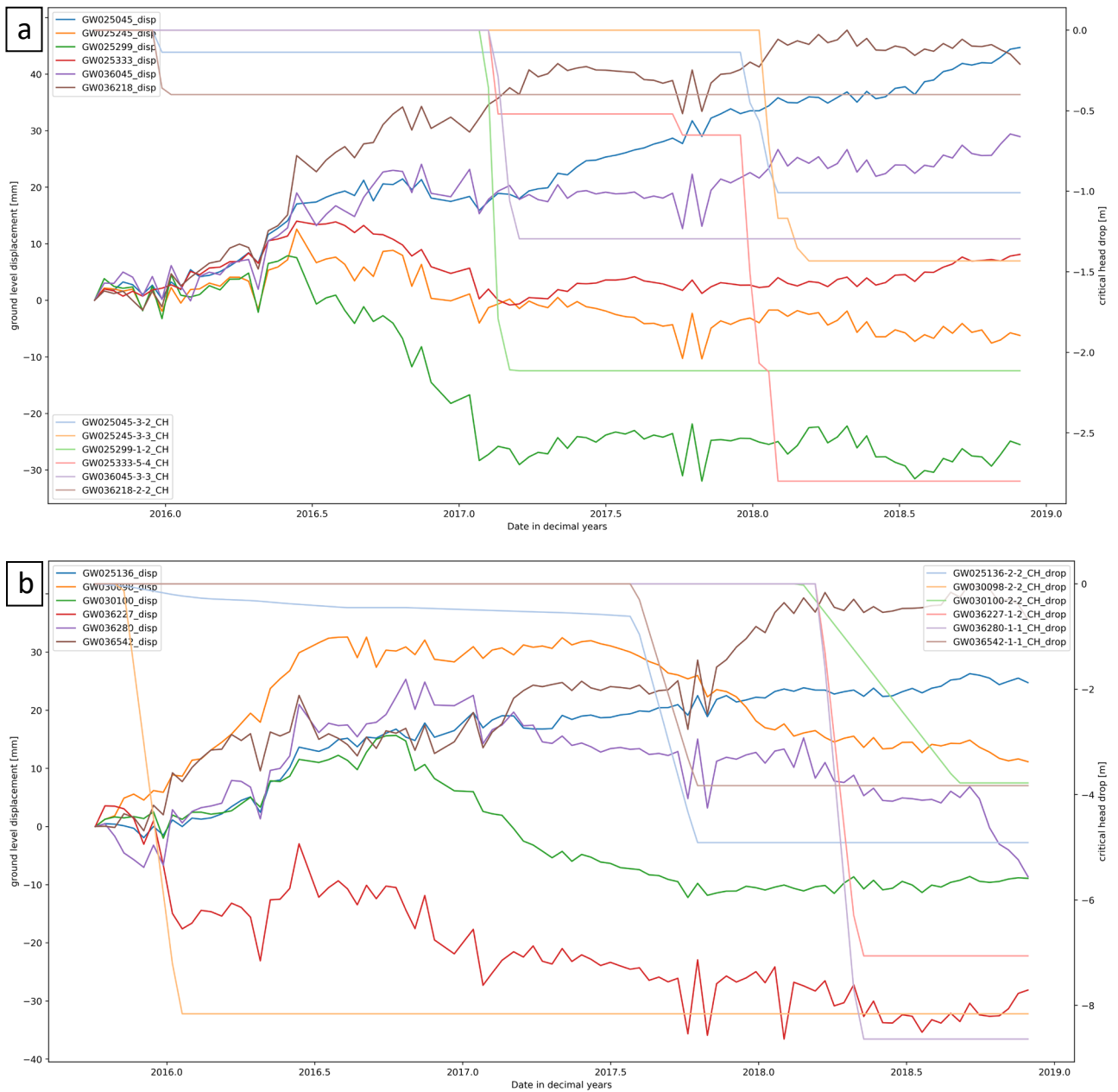


Figure 35 Time-series of deformation and critical heads of selected piezometers with logger data (a) or manual data (b) during the 3-year InSAR period

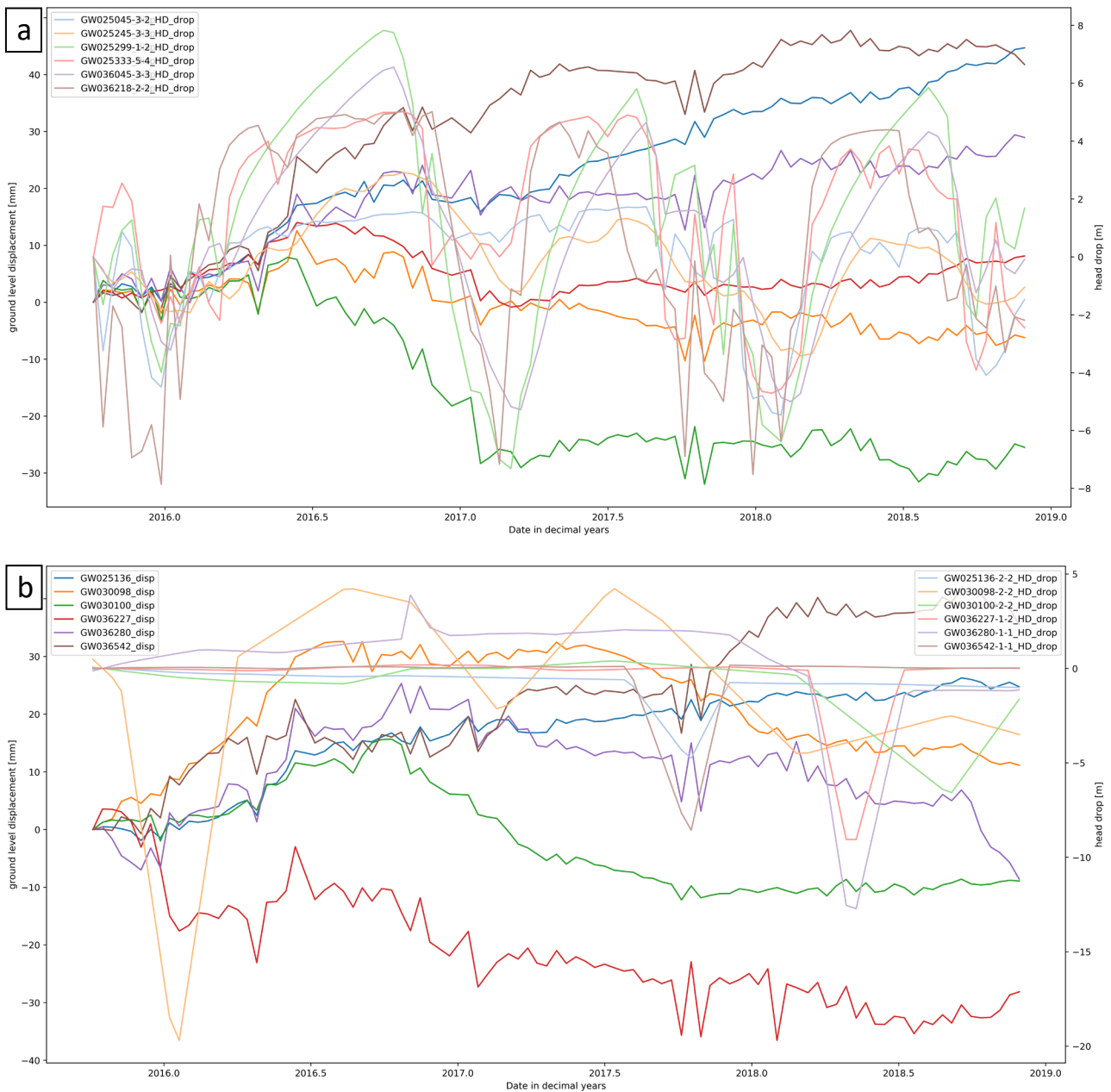


Figure 36 Time-series of deformation and heads of selected piezometers with logger data (a) or manual data (b) during the 3-year InSAR period

Among manually recorded water level hydrographs of a number of select piezometers with a maximum decline of critical head of up to 9 m (Figure 37b, ‘drop in critical head’ axis), some indicate compaction (e.g., GW036227-1-2, GW030100-2-2), some expansion (e.g., GW025136-2-2, GW036542-1-1) and some no trend (e.g., GW030098-2-2, GW036280-1-1) in the critical head versus deformation correlation scatter plot (Figure 35b; Figure 37b, ‘ground level displacement’ axis). Note that the InSAR velocity trends are integrated over the entire 3-year period, meaning a zero trend can obscure seasonal expansion and compaction that compensates each other. However, within the very short time-period of 3 years, even compaction around GW036227-1-2, GW030100-2-2 is not correlated with inelastic subsidence ($R^2 = 0.32$ and 0.19 in Figure 49 right) to the 2 or 3 isolated episodes of critical head drops as shown in Figure 34b.

Among the bores with logger data, the maximum decline of critical head reaches only around 3 metres over the 3-year InSAR period (Figure 35a; Figure 37a, ‘drop in critical head’ axis). Similarly

to the manually recorded heads, those also still show InSAR velocity trends that indicate both compaction (GW025299-1-2, GW025245-3-3) or expansion (GW025045-3-2, GW036045-1-1, GW036045-3-3) or a zero trend (GW025333-5-4) in the critical head versus deformation correlation scatter plot (Figure 35a; Figure 37a, 'ground level displacement' axis). Compaction is positively correlated with a drop in critical heads in only one bore (GW025299-1-2; $R^2 = 0.81$) (Figure 48 right). However, even this correlation is dominated by only one non-zero value of critical head drop. That is, similarly to the manual data, nearly no correlation could be found between inelastic subsidence and InSAR near bores with logger data.

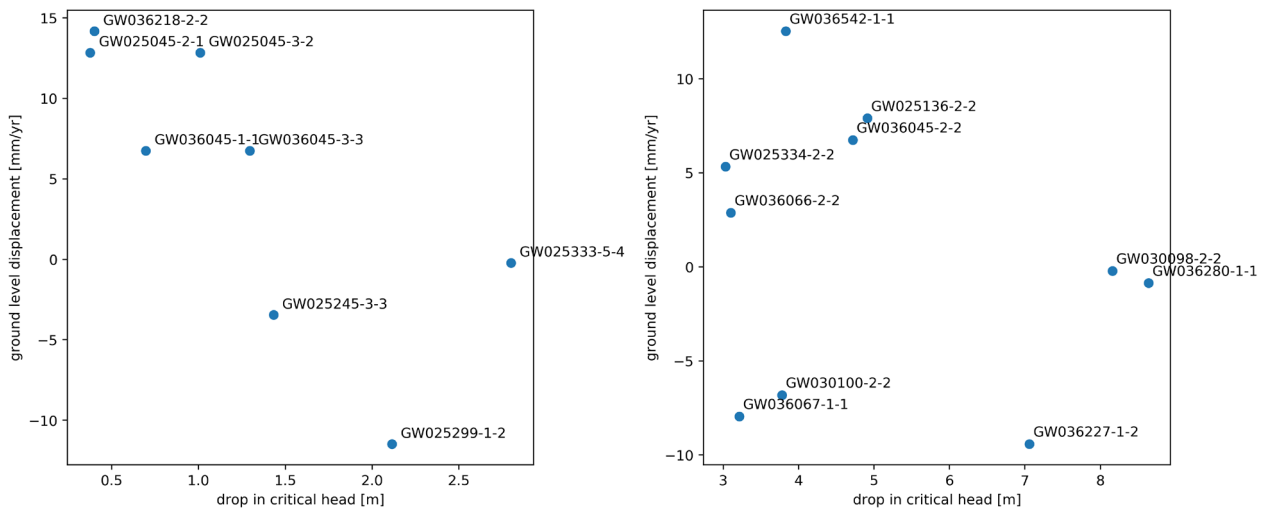


Figure 37 Relation between drop in critical heads and deformation trends during the 3-year InSAR Period for select piezometers with non-zero critical head drop for logger data (a) and select maximal drop in critical heads (> 3 metres) for manual data (b).

The remaining factors that may influence compaction or expansion are either elastic compaction and expansion or the swelling and shrinking of clays. A correlation between InSAR deformation and falling and rising water levels may indicate the former. However, such a correlation was only found for one bore with manual measurements (GW030098-2-2) ($R^2 = 0.45$; Figure 49 left and Figure 36b). One bore with logger data (GW025245-3-3) visually displays a positive correlation between water level fluctuation of ± 3 metres and around ± 10 metres of compaction and expansion (Figure 48 left and Figure 36a), albeit with a very low R^2 of 0.18. This mildly positive correlation between InSAR deformation and heads that are above previous pre-consolidation heads indicates the impact of recharge and drainage on elastic deformation.

Since most piezometers show no correlation between critical heads and deformation or between heads and deformation, we can infer that the prevailing factor influencing the 3-years of InSAR-derived deformation measurements in the Lower Namoi appears to be the swelling and shrinking of clay in vertosol soils. It is unknown, at this stage, if a longer InSAR time-series would allow better isolation of any potential groundwater-related deformation signal. However, it should be noted that any correlation analysis between time-series of water levels or critical heads that are resampled based on equal time-stepping of InSAR series is problematic due to the sparsity of manually recorded water level data and potential errors in the manual measurement or recording, which can lead to false critical heads.

3 Exploring spatial correlations

We spatially analyse the SBAS-InSAR results using two auxiliary sets of spatial data potentially able to explain the measured displacement patterns apparently not coinciding with groundwater-related boundaries (lithology or pressure change). As an approximation of the spatial distribution of the percentage of clay near the surface, we generated a soil clay content map defining the volumetric proportion of clay in the first meter of soil from 'modelled soil properties' available from eSPADE v2.0 (NSW and Office of Environment and Heritage (OEH) 2020), as depth-weighted average from 'Clay %, 0-30 cm' and 'Clay %, 30-100 cm.' eSPADE is a Google Maps-based information system that allows free access to soil and land information from across NSW. The modelling methods and data sources are described in NSW & OEH (2018).

3.1 Soil clay content

The soil clay content map is resampled over the InSAR-derived ground displacement map using a bilinear interpolation. A pixel-per-pixel scatter plot is drawn and allows to clearly observe that clay content below around 45% occurs almost only on the non-alluvial, non-quadernary surrounding of the Lower Namoi valley (compare Figure 38 with Figure 43 in Appendix A). Conversely, the quadernary alluvial aquifer is mostly covered by soils with clay content above 45%. The scatter plot's shape clearly illustrates the direct influence of surficial clay over InSAR displacement trend estimates. The range of InSAR-observed vertical displacement increases steadily with increasing clay content.

The influence of surficial clay over InSAR measurements for the entire period and for specific years (2016, 2017, 2018) is investigated in Figure 39. For each increment of 2.5% of clay content, percentiles of 5-50-95 are calculated and with corresponding percentile lines (in red). The lower and upper curves (5 and 95%) allow quantifying the deviation of InSAR results from the median expected for all incremental clay content values. As observed in previous sections, we note that observations from the full time-series are contaminated by measurements from 2016. Conversely, measurements from 2017 and 2018 show lower deviation, suggesting that limiting the observation to the dryer years (2017 and 2018) would strongly decrease the influence of surficial clays on InSAR observations.

It is important to note that no quantitative relation between InSAR results and clay content can be created from this analysis, as clay below the first meter of soil is unaccounted for and might also contribute to the overall measurement deviation. The clay estimates used here are taken as the best available spatial proxy of the quantity of clay in the surficial layers of soil potentially affected by expansion or compaction, which in turn affects InSAR measurements. In addition, this analysis relies on assuming that surficial clays are the only contributor to observed displacement. Indeed, no auxiliary data are available to help discriminate surficial displacements from groundwater-related displacements during the InSAR observation time-period. Anthropogenic activities might be spatially correlated with surficial clay content, and also impact InSAR measurements. This co-occurrence is unaccounted for. It is also important to keep in mind that the InSAR measurement is relative to the selected reference area, which also contains clays (around 25%).

The slopes of 5 and 95-percentiles curves are calculated by fitting a linear curve using a least-squares approach. By multiplying the slopes of the 5 and 95% curves with 50%, corresponding to the amount of clay occurring around Benchmark 27 and 28 (Figure 28; where the subsidence patch is located), we approximate the trend deviation related to surficial clays that limits the use of InSAR to detect the relatively small groundwater-related subsidence rates (in the order of 8 mm/yr) over the Lower Namoi region (Table 5). It also provides valuable information for applying InSAR in similar settings in terms of soil clay content and land cover/usage. This estimation assumes that the InSAR trend is solely related to the influence of climate variability and anthropogenic activities over surficial clays, and that no groundwater-related signal occurs during the InSAR period. Table 5 shows that a trend deviation of the order of around 5 cm/yr occurs in the wetter years (e.g. 2016) and that the deviation decreases to around 2 cm/yr for the driest years (e.g. 2017 and 2018). We note that the median trend deviation is positive throughout the study period, suggesting that uplifting area is more important in spatial extent than the subsiding area. It is important to note that this estimation only applies to annual trends, and that higher amplitude signals might occur seasonally. Hence the consideration of longer InSAR time-series would help in better isolating long-term ground displacement trends, potentially smoothing out the influence of climate variability and anthropogenic activities over surficial clays, and isolating higher proportions of groundwater-related displacements.

It is not possible to accurately quantify the minimum numbers of years (or SAR images) to detect the expected displacements of around 8 mm/yr, as it depends on numerous parameters such as the temporal and spatial stability of the subsidence signal (related to the highly varying critical head drop pattern; Figure 28) and all parameters affecting the InSAR sensing and its interpretation. However, it is reasonable to assume that by accounting for more years, the influence of surficial clays would be reduced, considering that the total mass and density of soil does not vary in the long-term. In addition, the subsidence signal would accumulate over certain locations, making it easier to detect through the InSAR inversion procedure.

It is observed that (1) surficial clay is the dominant source of noise in the InSAR-derived detection of groundwater-related deformation over the Lower Namoi, (2) longer time-series allow reducing the effect of annually-varying anthropogenic and climate influences on surficial clays and (3) the effect of surficial clay creates a near-symmetrical deviation from zero in the InSAR-derived ground deformation signal. We suggest using the half-width of the 5-95% percentile clay-related trend-deviation range as a conservative estimate of sensitivity of the InSAR technique to measure groundwater-related displacements. This sensitivity decreases to 29 mm/yr when considering three years including one wet year (2016), and to 21 mm when considering solely one dry year. It is reasonable to assume that using more than three years and accounting solely for dry years (without flooding events), this approximated sensitivity-threshold would decrease. It is unknown, however, if it would decrease down to the level of subsidence detected in the Lower Namoi region (around 8 mm/yr).

It can be considered that subsidence appears over the same location during the full length of an InSAR survey, and that the trend deviation induced by surficial clays would decrease with increasing time-series length. We recommend using at least 5 dry years for future InSAR measurements. However, it should be noted that, according to the critical head analysis presented earlier (Figure 28) in this report, the subsidence signal is expected to be highly variable in time, which would make it more difficult to detect with InSAR.

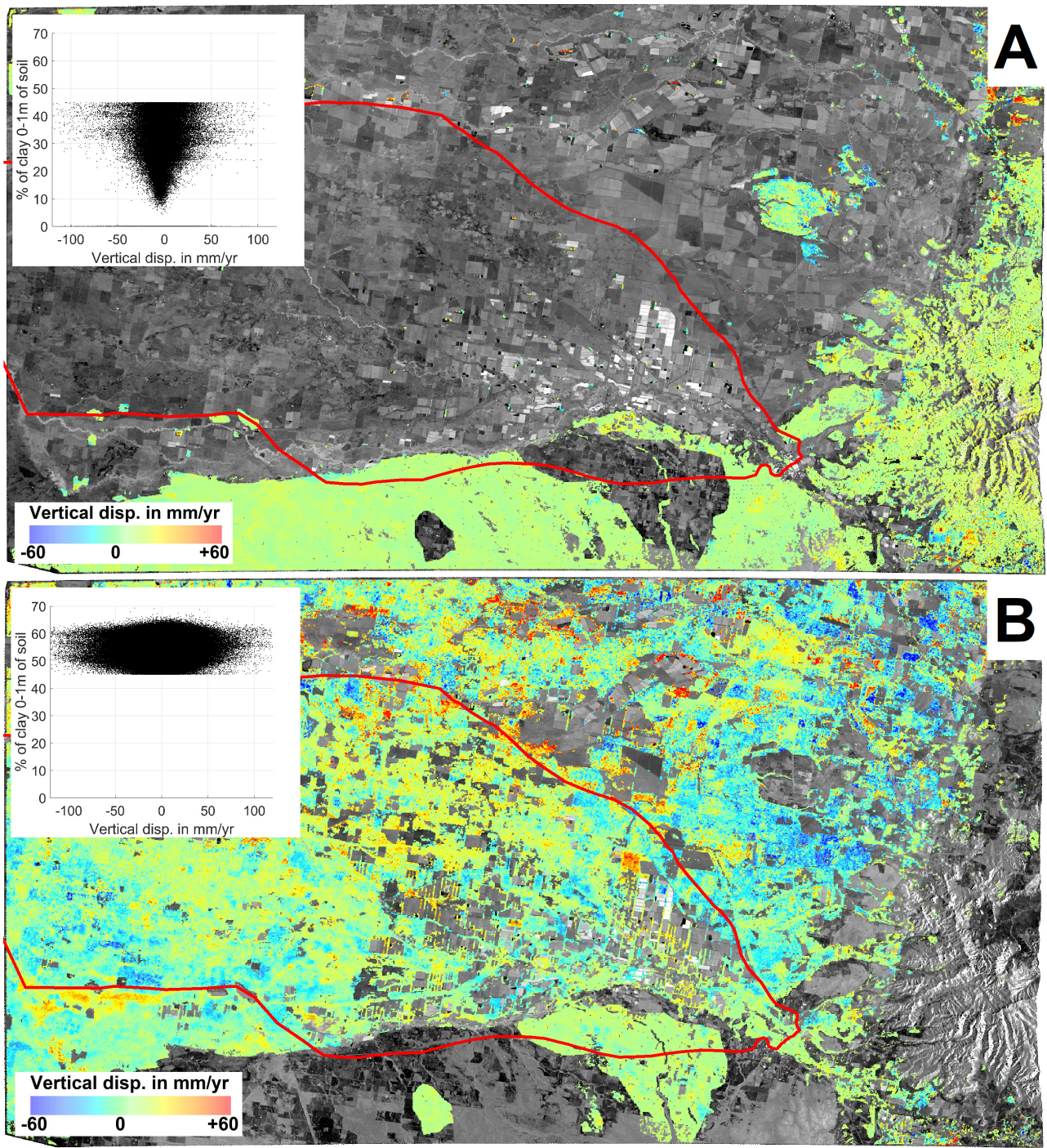


Figure 38 Ground displacements in areas where clay content in the first meter of soil contains less than 45% of clay (A), and more than 45% of clay (B). The figure highlights the importance of considering high proportions of clays, which typically occurs in the valley, where most of the water is extracted. The red line shows the boundary of the groundwater model.

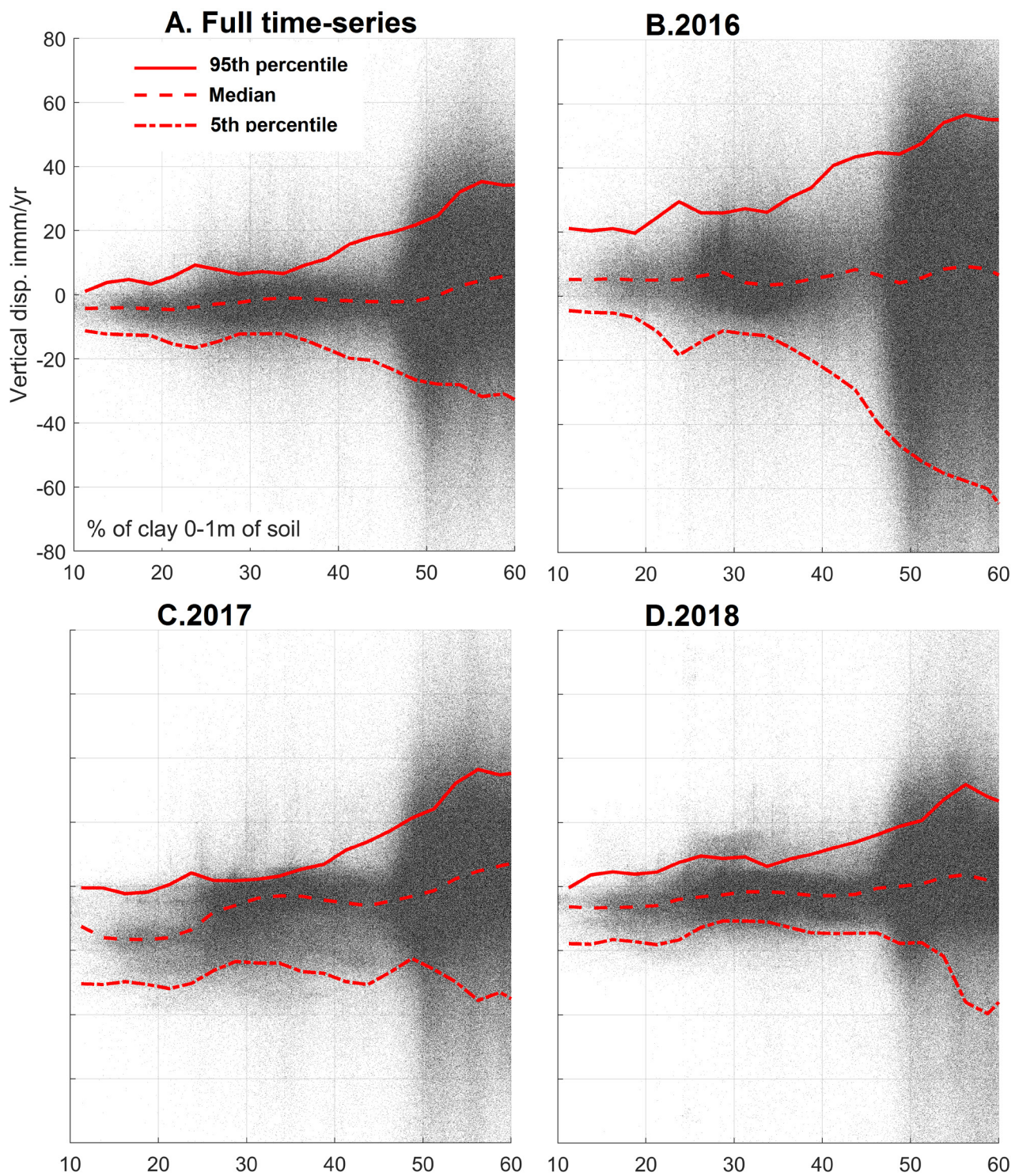


Figure 39 Absolute vertical displacement velocities as a function of the clay content in the first meter of soil for different periods considered in the InSAR time-series, with (in red) the 5, 50 and 95% percentile envelopes. The shape of the percentile curves (e.g. top graph) suggests a near-linear relation despite the shape of the scatter plot. The percentiles (red lines) are calculated for every 2.5% increment of clay content.

Table 5 Estimation of the trend deviation due to the clay content in the first meter of soil. The trend estimation (curve fitting) accounts for all clay content values between 15 and 60%. Trend of the 5-95% red lines shown on Figure 39. To detect subsidence around the Benchmark 27 and 28 (Figure 28), the error estimates need to account for 50% of clay in the surficial soil.

Time-period	5%	50%	95%	5-95% Range (50% clay)	Half-range (50% clay)	Half-range (60% clay; to cover 95% of the Lower Namoi)
Full time-series	-0.45	0.17	0.70	-22 to 35 mm/yr	29 mm/yr	34 mm/yr
2016	-1.28	0.07	0.85	-64 to 43 mm/yr	53 mm/yr	64 mm/yr
2017	-0.02	0.46	0.85	-1 to 43 mm/yr	22 mm/yr	26 mm/yr
2018	-0.29	0.21	0.56	-15 to 28 mm/yr	21 mm/yr	25 mm/yr

The ISBAS-InSAR technique includes (almost) the totality of the SAR signal reflection from the ground above a relatively low coherence threshold. Conversely, the PSI technique only interprets the SAR signal over structurally stable ground targets, which coincide with hard material and infrastructure, and high InSAR coherence. As the SAR signal reflected from the ground is greatly contaminated by the influence of surficial clays, it is of interest to assess the level of protection from this contamination offered by using the PSI technique (Figure 15). Figure 40 shows the relation between the vertical velocity measured over each ground target and the clay content for the two PSI processing results presented on Figure 15.

Figure 40A contains only 46,047 points which are distributed across the range of clay content, with no obvious relation. This PSI process (Figure 15A) was performed with the same SAR time-series as the main ISBAS-InSAR process presented in other sections. Hence the inclusion of a wet year (2016) into the process reduces the chance of obtaining coherent measurements points on the ground, which protects from the influence of clays. Unfortunately, as shown on Figure 15A, the point density of such processing is not adequate from monitoring subsidence throughout the whole Lower Namoi valley. Figure 40B presents a random selection of 100,000 points out of the 506,216 points obtained by PSI processing of the SAR images from 2017. This time, some bare soil locations were considered structurally stable and included as coherent measurement points, which increases the influence of surficial soils over the overall results. This analysis points at that a multiple-year PSI process would be adequate to monitor the subsidence over the Lower Namoi aquifer if the density of ground targets is artificially increased by installing corner reflectors in selected locations (e.g. near the benchmarks).

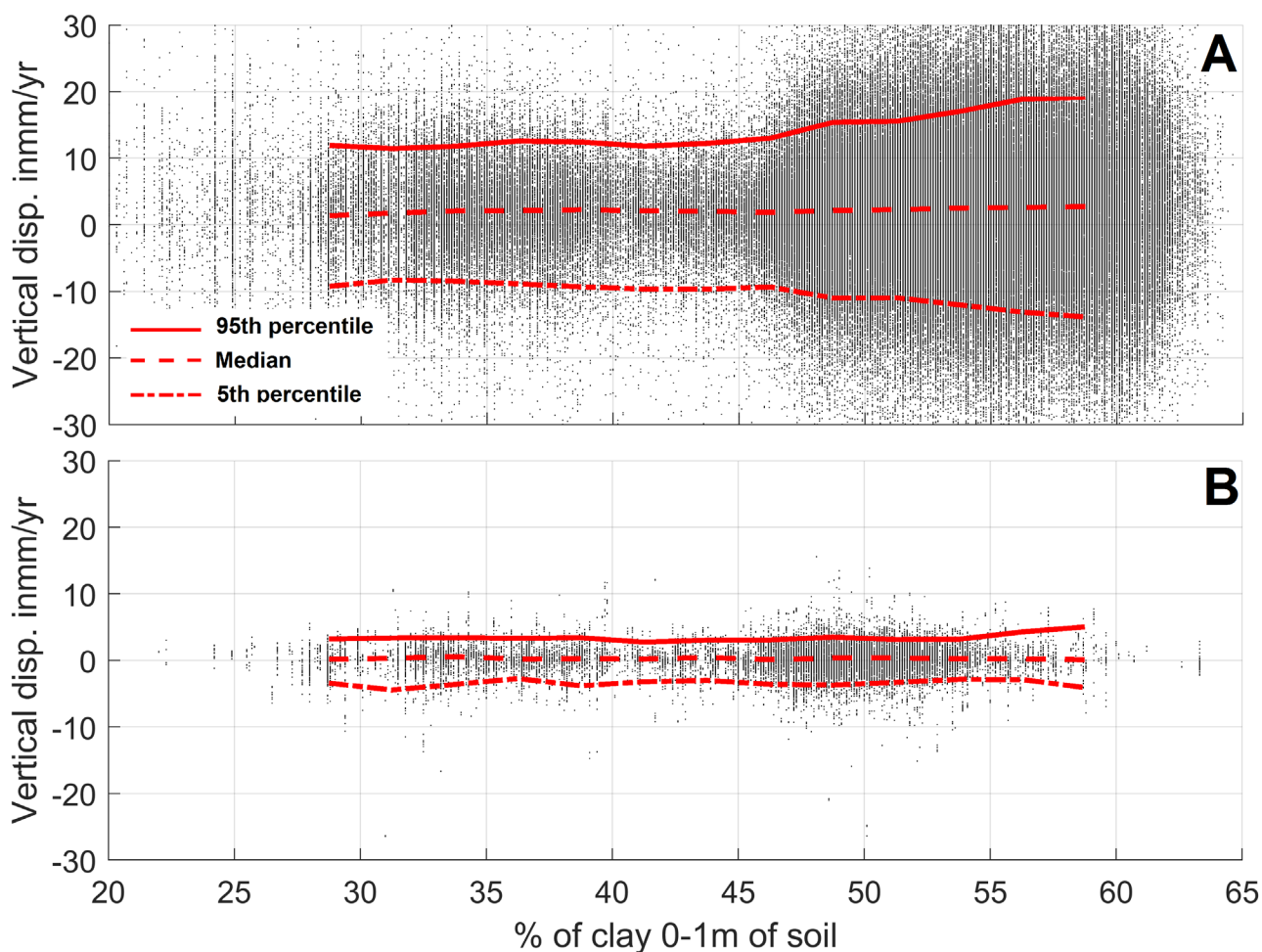


Figure 40 Correlation Relation between PSI-measured displacements and clay content for a multiple years PSI process (2015-2019; A) and a single (dry) year PSI process (2017; B). The low deviation observed on A indicates that only ground targets over built infrastructure (the only with high InSAR coherence in 2016) offers a relative protection to the influence of surficial clays. The percentiles (red lines) are calculated for every 2.5% increment of clay content. This figure was built from results shown on Figure 15.

3.2 Land use

A land use map was resampled over the InSAR-derived ground displacement map using a nearest neighbour interpolation, in order to respect the original land use classification. Table 6 presents statistics from the InSAR results per land use classes. Figure 41 shows the range of displacements measured over each land use classes occurring in the lower Namoi region.

Cropping, Irrigated cropping, and Grazing native vegetation, and Grazing modified pastures represent together around 90% of the surface area. Cropping and Irrigated cropping areas show particularly high values of standard deviation, highlighting the difficulty of the inferring groundwater-related displacements over such land usages implying constant modifications at the soil surface. Land use classes corresponding to presence of hard surfaces such as ‘Residential and farm infrastructure’ or ‘Services’ have a mean velocity close to 0 and a relatively low standard deviation. This gives confidence in the InSAR processing and supports the observation drawn from PSI that built infrastructure did not suffer from any major movements related to groundwater withdrawal during the 2015-2018 era. Figure 41 highlights classes 330, 430, 620 and 630, which

have a high noise level. They correspond to area with constant changes in relation to water fluxes (class 630 'River' and 620 'Reservoir/dam') or farming activities.

A possible correlation exists between the land use and the clay content in the first layer of soil presented earlier. This challenges the interpretation and limits our ability to discriminate which factor of the two is the most influential. Both factors seem to add up and play a role in the level of uncertainty observed in the InSAR measurements, as shown by the contrasting statistics (e.g. standard deviation) for each land use classes and the strong correlation between clay content and InSAR-displacements.

Table 6 Statistical analysis of the InSAR results per land use class. Classes representing more than 1% of the total coverage are marked in grey.

Land use class	class number	mean velocity (mm/yr)	median velocity (mm/yr)	Stdev (mm/yr)	% of InSAR coverage area	% of total coverage
Cropping	330	4.37	4.67	20.34	42.00	32.53
Grazing native vegetation	210	-2.31	-1.55	11.94	39.67	30.72
Grazing modified pastures	320	-1.30	-1.15	9.24	5.15	3.99
Irrigated cropping	430	-2.07	0.02	23.20	4.66	3.61
Nature conservation	110	-6.45	-4.83	11.39	3.77	2.92
Other minimal use	130	-3.17	-3.08	7.13	1.40	1.08
River	630	-4.12	-2.19	16.01	0.57	0.44
Residential and farm infrastructure	540	0.48	-0.24	7.89	0.48	0.38
Reservoir/dam	620	-3.72	-1.94	19.09	0.48	0.37
Transport and communication	570	0.94	-0.23	10.92	0.24	0.19
Marsh/wetland	650	0.47	-0.34	15.19	0.15	0.12
Manufacturing and industrial	530	2.74	2.17	8.01	0.10	0.08
Managed resource protection	120	-1.29	-0.97	4.92	0.07	0.05
Services	550	1.65	0.83	5.83	0.05	0.04
Mining	580	-1.58	-1.48	5.53	0.02	0.02
Utilities	560	3.49	3.44	3.24	0.02	0.01
Channel/aqueduct	640	-2.52	-0.73	14.11	0.01	0.01
Irrigated perennial horticulture	440	-3.19	-2.91	10.00	0.01	0.00
Waste treatment and disposal	590	-3.16	-1.48	3.91	0.00	0.00

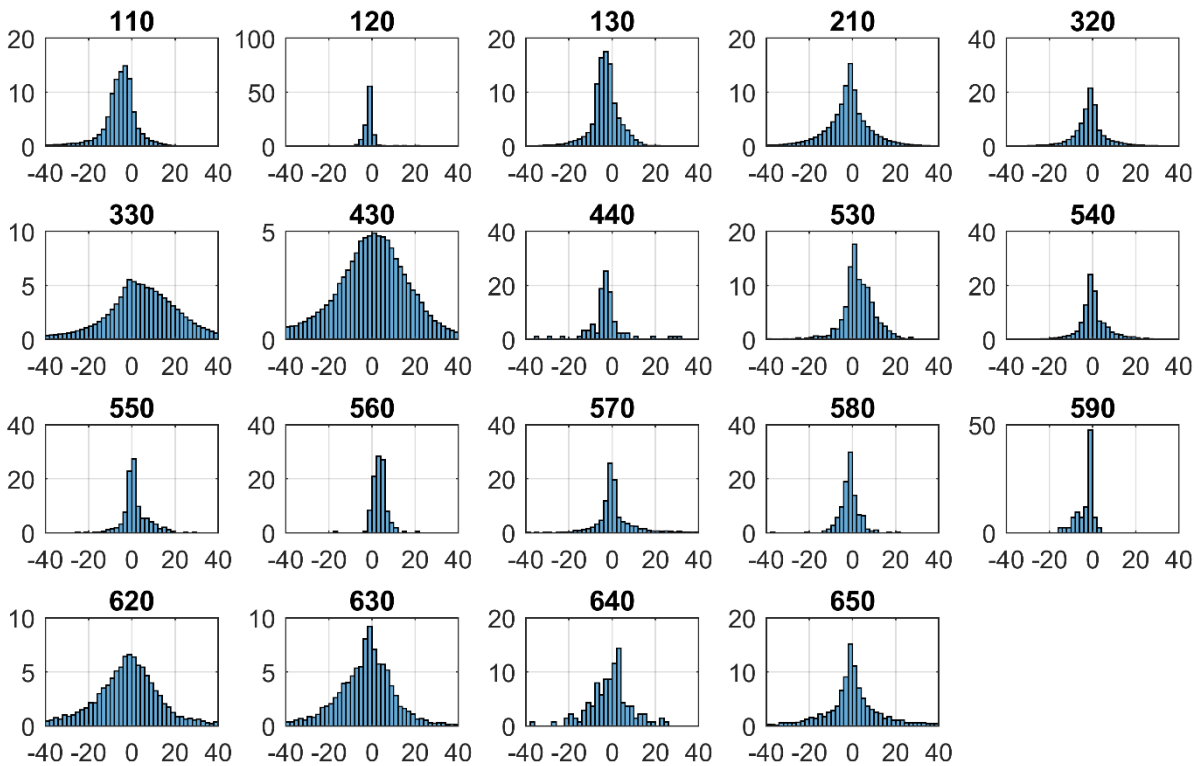


Figure 41 Histograms of InSAR-derived vertical displacement velocities for each land use class (see nomenclature in Table 6) in percentage of the total observation for each class. Classes 330, 430 (cropping areas) and 620, 630 (near water bodies) present noisier InSAR results.

4 Summary

In the Lower Namoi, the usability of subsidence-causing groundwater head changes to set local groundwater level management targets appears limited, because ground movement may also be influenced by seasonal swelling and shrinking of vertosol soils and specific for particular land-use classes. In order to derive relationships between head change and deformation derived from benchmark surveys, we assume the observations to be independent of swelling/shrinking of vertosols and land-use changes. Hence, only groundwater heads that represent aquifer dewatering were used to analyse potential temporal correlation with benchmark deformation (Section 2.1). In contrast, InSAR-derived ground movements are ignorant of the cause (swelling/shrinking clays, land cover, aquifer compaction/expansion) and, hence, require a 3-dimensional temporal correlation between InSAR deformation and these three factors (Section 2.2). The spatial distribution of the near-surface clay content is derived from eSPADE v2.0 (NSW & OEH 2020) and is used for the 3D temporal correlation analysis, but also for a statistical analysis of the spatial distribution of clay content and InSAR-derived ground displacement (Section 3.1). Lastly, to investigate the impact of certain land-use classes on seasonal or long-term land subsidence (Section 3.2) land use of 2017 from eSPADE was compared against SBAS-InSAR results and also observations drawn from PSI (Part III, section 4.3).

For the temporal correlation between groundwater heads and benchmark deformation, critical heads, at which preconsolidation might occur, were derived for piezometers with deepest drawdowns at 5 bores paired with benchmarks of subsidence rates of more than 2 mm/year

(BM25054, BM25144, BM25325, BM30222, BM30238). Significant groundwater depletion with associated drop in mean annual critical head occurs in the mid-1970s, early 1980s, and mid-1990s. After the 1990s, pre-consolidation heads remain stable indicating that measurements of the recent benchmark survey may indeed be related to dewatering activities in the mid-1990s. Meaningful simple linear relationships between head drop or critical head drop and benchmark subsidence cannot be formulated. However, exponential regressions appear to be more closely reflecting the reaction of subsidence to a drop in critical head which drives inelastic subsidence, particularly for two piezometers with deepest drop in critical head (GW030222-2-2, GW030238-2-2). The similar empirical exponential reaction of subsidence (22 cm and 37 cm over the total benchmark survey period) to drop in critical head (23 and 28 m) for these two piezometers most likely reflects the proximity of only around 3 km between them and, hence, similar hydrogeology, stratigraphy of aquitards and aquifers, as well as heterogeneity. A more distant piezometer, GW025325-5-6, shows a different behaviour with a lesser drop in critical heads of around 13 metres leading to the second biggest total subsidence of around 30 cm. Any such empirical relationship is specific for localized hydrogeologic conditions and for the 45-year period of benchmark observations. Therefore, any spatial extrapolation or temporal prediction of subsidence as a function of continuously dropping critical heads cannot be made based on those relationships. However, while a drop in critical head cannot be used as a quantitative proxy for potential subsidence through empirical relationships, it still serves a qualitative indicator for subsidence risk. Critical head drop alone cannot predict actual land subsidence because it also depends on localised hydrogeologic conditions which include the compressibility, thickness and storativity of the aquifer.

Over the entire period of water-level record keeping, critical heads of piezometers with deepest drawdowns within each bore do show significant drops in critical head in some areas. In contrast, during the InSAR period (03/10/2015 until 28/10/2018), a much lesser or no drop in critical heads of most of these piezometers can be found (including the 5 benchmarks with subsidence trends of >2 mm/yr) because previous pre-consolidation heads were established between the early 1980s to the mid-1990s. Therefore, a '3-way' correlation analysis between benchmark subsidence, InSAR deformation, and critical heads at those 5 benchmarks is not possible.

In order to temporally correlate groundwater heads or critical heads with spatially averaged InSAR deformation in the vicinity of the monitoring bores, time-series of heads and critical heads were resampled at uniform InSAR time steps. During the 3-year InSAR period, averaged InSAR deformation near some bores reaches up to ± 20 mm/year. However, most of the piezometers did not reveal any or only minimal drop in critical heads as a result of previous pre-consolidation prior to the 3-year InSAR period. Among the few piezometers that do reveal a decline in critical heads during the 3-year InSAR period, some do indicate compaction (e.g., manual: GW036227-1-2, GW030100-2-2; logger: GW025299-1-2, GW025245-3-3) as one would expect, but some show no trend (e.g. manual: GW030098-2-2, GW036280-1-1; logger: GW025333-5-4) or expansion (e.g., manual: GW025136-2-2, GW036542-1-1; logger: GW025045-3-2, GW036045-1-1, GW036045-3-3). However, even piezometers that do show compaction do not correlate well with a drop in critical heads (only for GW025299-1-2; $R^2 = 0.81$) i.e. are not, as expected, correlated with inelastic subsidence. That is, the averaged InSAR deformation near those piezometers may not be attributable to inelastic subsidence, but rather to either the impact of recharge and drainage on elastic deformation (i.e. expansion/compaction of fine-grained interbeds or aquitards above the

pre-consolidation head) or the swelling and shrinking of clays in the vertosol soils. However, correlation between InSAR deformation and falling and rising water levels above previous pre-consolidation heads was only found for one bore (GW030098-2-2; $R^2 = 0.45$). In conclusion, since most piezometers show no correlation between either critical heads and deformation nor between heads and deformation, we can infer that the prevailing factor for the short-term InSAR-derived deformation in the Lower Namoi appears is swelling and shrinking of clay in vertosol soils.

By assuming the InSAR deformation to be solely impacted by surficial clays, and indirectly by the parameter influencing its expansion and shrinking (anthropogenic activities, moisture content), it is possible to assess the related loss of precision of InSAR measurements toward detection of groundwater-related displacements. This assessment is of great value not only to improve InSAR result interpretation over the Namoi region, but also to improve the usability of InSAR over clay-rich areas. We observe that the trend deviation related to surficial clay decreases the precision of SBAS-InSAR down to around 2 cm/yr for the driest years and down to 5 cm for the wettest years. These rates are above the low subsidence rates detected through the benchmark surveys (up to 0.85 cm/yr).

Nevertheless, the SBAS-InSAR survey (Part II, Section 4.1) confirms that no subsidence patch beyond detection threshold occurs outside of the benchmark monitoring coverage. The PSI-InSAR survey (Part II, Section 4.3) confirmed that no particular subsidence pattern occurs along linear infrastructure such as roads. It is however observed that the area generally undergoes constant movements potentially due to the high clay content (mostly above 45%) of the soils in the region.

One way to increase the precision of the InSAR survey below the maximum subsidence rates detected through the benchmark surveys would be to install corner reflectors. These relatively inexpensive field installations allow to obtain highly-coherent measurement points where man-made infrastructure are not sufficiently dense. Garthewaite et al. (2015) presents the technical details and the requirements for such installation.

The SAR coherence and, as a result, the precision of SBAS-InSAR might also be correlated with land use, which, to some extent, might also be correlated with clay content. We analysed the distribution of InSAR-displacements for all land use classes. We note a particularly high standard deviation in InSAR measurements over “Irrigated cropping” and “Cropping” land use classes, in comparison with other land use class occurring in the study area. We also note that the standard deviation over “Grazing native vegetation” and “Grazing modified pasture” is significantly lower than over “Irrigated cropping” and “Cropping”. This shows that the clay content (assumed to be similar for all classes) is not the only contributing factor to the low InSAR coherence and precision occurring over cropping areas. It suggests that the low InSAR precision observe is a result of the combined effect of cropping activities (and related vegetation cycles) and the high clay content of the vertosols.

Part V Conclusions and Outlook

CSIRO and the NSW DPIE have assessed potential land subsidence over the Lower Namoi groundwater resource based on an analysis of available Synthetic Aperture Radar (SAR) imagery using SAR Interferometry techniques (InSAR), compared the InSAR data with surveyed benchmark data, as well as analysed the correlation between land subsidence and groundwater level hydrographs, soil clay content, and land use.

The primary purpose of the study is to provide a toolset for the determination or derived evidence of land subsidence or aquifer compaction in the Lower Namoi (and potentially for other NSW basins) that may be used for water level response management and as decision-support basis. Correlations between land subsidence and critical groundwater head change in hydrographs could be utilised to set local groundwater level management targets and thresholds to prevent or limit irreversible land subsidence and loss of aquifer transmissivity and storativity. The new 2019 Water Sharing Plan (WSP 2019) for the Upper and Lower Namoi Groundwater Sources (NSW, 2019) states that *“the Minister may, on presentation of evidence of land subsidence or aquifer compaction, restrict extraction from all water supply works (bores) nominated by access licences within a local impact area ... , to such an extent and for such time as to stabilise that subsidence or compaction.”* However, the presented methodology and findings also can serve as an early warning system for observed minor rates of land subsidence that do not yet warrant any restrictions. It could serve land holders and regulators to monitor the impact of incremental effects of further groundwater extraction on, potentially inelastic, deformation.

Long-term benefits of improved groundwater deformation data and monitoring methods are the use of InSAR as a subsidence monitoring tool in other cropping/farming areas of NSW and to inform and constrain (an) updated and upgraded Lower Namoi (and other NSW) groundwater model(s).

Availability of SAR images and InSAR processing

Retrieval of past ground displacement through InSAR techniques is dependent upon the availability of SAR images archives over the study region. Over most of the benchmark observation period, SAR images over the Lower Namoi are either absent in the 1970s or 80s or present in the 1990s and 2000s, but of insufficient spatial coverage or temporal density (ENVISAT and ERS SAR imagery). Since 2015, data from the Sentinel-1 mission have been available globally with a high temporal density of 12 days. A subset of a spatially continuous SAR image consisting of three merged 250km-wide Sentinel-1 images was analysed for the study area. The resulting SAR image time-series comprises 94 images acquired between October 2015 and November 2018. The stack of those images was processed using SARSCAPE 5.5 and the ISBAS-InSAR approach (Berardino et al., 2002; including the Intermittent-SBAS improvements from Sowter et al. 2013), which is usually superior to other InSAR techniques to overcome limitations due to spatial or seasonal changes in cropping or land cover, as present in the Lower Namoi, with associated lower or a highly varying InSAR coherence between temporally-close SAR images. Using the ISBAS-InSAR approach, we produced a space-time data-cube consisting of vertical displacement for each time-layer, but also blank areas where coherence thresholds mask out the noisiest sections of the image. This data-cube was used to compute yearly or multi-annual trends, as well as maps to observe the general displacement patterns in space and time. It was also used for comparison against displacement observed in-situ.

Results from InSAR processing

The trend map that uses this InSAR-derived data-cube revealed a clear distinction between the Lower Namoi quaternary alluvial basin and its more consolidated pre-quaternary surroundings with the respective higher (\pm max. 60 mm/yr) and lower (\pm around 10 mm/yr) amplitudes of ground movement. However, the displacements patterns detected by InSAR largely follow crop boundaries, which suggests that differences in cropping activities over clay-rich soils are a major controlling factor of ground level at the scale of 3-years of InSAR observation period. We observe oscillations across spatial transects of up to \pm 40 mm/yr. This effect is reduced to \pm 10 mm/yr by applying a 1D-linear spatial moving-mean filter, which reinforces the interpretation, assuming that the filter is large enough to encompass multiple crop-types.

Yearly amplitudes of displacement are particularly strong in 2016, which is a particularly wet year. It decreased from 2016 to 2018, suggesting a progressive recovery of the soils after 2016's floods. More generally, this shows the impact of climate variability over clays and as a consequence, over InSAR-derived displacements. Ground level decrease could be a result of erosion due to floods or to drying of the clays. Ground level increase could be a result of increased moisture content in the clays or elastic aquifer expansion following recharge. Such signals might also be exaggerated by agricultural work during these events or following years (e.g. reconstruction of trenches and canals), as regularly observed on the field.

A spatial averaging kernel was applied and six time-series of vertical displacement were presented. They show relative stability or a rising trend in the eastern part of the study area and varying (positive and negative) ground displacement in the western and central part. All series with significant rise or decline are superimposed with seasonal, most likely climate-related, patterns (particularly in 2016), which is analogous to an observation of Ross and Jeffery, 1991, who report '*widespread rise in ground surface (...) following two wet seasons.*' It is possible that the period selected for InSAR observation was dominated by such rise rather than groundwater-related displacements.

The other main type of InSAR processing workflow, Persistent Scatterer Interferometry (PSI), was also tested. Instead of including the low-coherence signal into a highly filtered phase-shift map (like SBAS/ISBAS does), it only analyses the temporal variations of SAR phase over highly coherent ground targets. It has the advantage of being significantly more precise. However, such processing chain is usually not used in vegetated (agricultural) settings, due to the low spatial density of coherent ground targets. We tested the PSI technique with a 1-year SAR time-series (2017), and with a 3-year SAR time-series (the same as for the ISBAS processing). We observed no particular movement patterns over linear infrastructure where coherent targets occur. However, as expected, the point-density over cropping areas is not sufficient for subsidence monitoring in the Lower Namoi. We note the potential of installing corner reflectors (as presented in Garthwaite et al., 2015) to solve that issue, both near benchmarks (for comparison/validation) and away from benchmarks to extend the spatial coverage of subsidence measurements.

Results from benchmark surveys

Benchmark data of a recent survey (conducted in April 2019 by SMK Consultants Pty Ltd for the NSW-DPIE Water Group as part of this project) were compiled together with previous data from 1974 to 1990 from Ross and Jeffery, 1991. Linear trends were calculated using all available data for each benchmark. As the time-series include a large time-gap between the last two surveys (2019 and 1990 or older), the resulting trends can be considered as long-term estimates relatively insensitive to seasonal variations.

There is uncertainty around the survey accuracy of this and previous surveys. We applied the pre-survey measurement accuracy around 25 mm for the 2019 survey and to previous surveys, assuming that historic surveys were not more accurate. When comparing two or more surveys, this margin doubles and, hence, the differential subsidence between two surveys outside the margin of error needs to be at least 50 mm to be detectable. Depending on the number of years between two surveys, the annualised margin of error for individual benchmarks differs when dividing the doubled error margin by the number of years, but is generally between 1 and 2 mm/yr.

Subsidence trends of only 8 of the 32 subsidence benchmarks are above this annualised margin of error of 1 to 2 mm/yr. When applying a more conservative error of 2 mm/yr to all benchmarks, the vertical displacement of only 5 benchmarks remains outside the margin of error. The maximum observed trend in one benchmark is 8.5 mm/yr. For this maximum trend to be beyond the annualised error, the period between surveys should at least be 6 years (50 mm measurement inaccuracy between 2 surveys / 6 years = 8.3 mm/yr). A denser temporal frequency will yield benchmark trends across the Lower Namoi that are below the detection threshold.

Displacements measured by comparing the last two surveys (2019 survey and the last one before that, usually but not always, from 1990) are generally less than the trend based on all available data, which could suggest a “slow-down” of the rate of decline. However, this conclusion cannot be fully supported, because the most recent displacement of the last few years is hidden within the ≥ 29 -year gap between the last two surveys.

Comparison between InSAR and benchmark surveying

Yearly trends of short-term vertical velocities derived from InSAR (3-year period from late 2015 until recent) and long-term benchmark survey data (up to 45 years from 1974 to 2019) allowed for a comparison of displacement from otherwise incompatible periods and methods. However, strong inter-annual and seasonal variations resulting from variations in climate and land management can influence the 3-year trend of the InSAR data, relatively more than the multi-decadal benchmark dataset.

Among the benchmark showing a measurable subsidence signal, one historically important benchmark (FW347) that shows nearly 40 cm since the inception of surveying is inversely correlated with the InSAR trend, which shows an uplift of around 5 cm at this location. However, given the incompatibility of the time-periods for InSAR and benchmarks, a short-term ‘InSAR’-derived uplift can be hidden within a 44-year ‘benchmark’ subsidence trend. Excluding FW347, one can observe a positive, albeit weak, relationship with InSAR vertical displacement of around 1.5 times the vertical displacement from benchmarks above the annualised margin of error.

InSAR and benchmark surveys indicated trends of minor vertical displacement of less than in 8 to 16 mm/yr, respectively. Correlation between the two is weak, suggesting either that InSAR measurements are affected by surficial movements (and benchmarks are not, by design), or that subsidence rates have changed, or both. Unlike long-term trends from benchmark surveys, short-term InSAR-trends are affected by noise from inter-annual variations that are influenced by cropping and agricultural practices, swelling/shrinking clays, and climate variability. This is supported by the InSAR-displacement trend map, which shows patterns respecting crop boundaries. The longer the InSAR periods are, the less is the derived displacement clouded by this noise.

Temporal correlations between deformation and heads

Selected piezometers with deepest drawdowns at benchmarks of subsidence rates above the measurement error show significant groundwater depletion with associated drop in mean annual head and critical head in the mid-1970s, early 1980s, and mid-1990s. For those piezometers, a well-correlated exponential reaction of benchmark subsidence to drop in mean annual critical head was found. However, this prediction of subsidence as a function of dropping critical heads is specific for localised hydrogeologic conditions and the 45-year period of benchmark observations and cannot be spatially or temporally extrapolated. Hence, a drop in critical head cannot be used as a proxy for actual land subsidence, but it still serves as an indicator for the risk of potential subsidence. In contrast, during the InSAR period, a much lesser drop in critical heads can be found due to prior consolidation. Therefore, a multi-factorial correlation analysis between benchmark subsidence, InSAR deformation, and critical heads is not possible.

During the 3-year InSAR period, spatially averaged InSAR deformation near some bores reaches up to ± 20 mm/year. However, most of the piezometers only reveal minimal or no drop in critical heads as a result of prior preconsolidation. Among the few piezometers that do reveal a decline in critical heads, some do indicate compaction, but some no trend or even expansion. However, even piezometers that do show compaction do not correlate well with a drop in critical heads, i.e. are not, as expected, correlated with or attributable to inelastic subsidence. Alternatively, a correlation between InSAR deformation and falling and rising water levels above previous pre-consolidation heads was only weak or non-existent. Hence, a potential impact of recharge and drainage on elastic deformation could also not be confirmed. In conclusion, since most piezometers show no correlation between either critical heads and deformation nor between heads and deformation, we can infer that the prevailing factor for the short-term InSAR-derived deformation in the Lower Namoi appears to be swelling and shrinking of clay in vertosol soils.

Spatial correlations between InSAR deformation and clay content

In order to understand the precision which can be expected from InSAR measurements to sense groundwater-related displacements, we analysed the correlation between InSAR-displacements and the clay content of the surficial layer of soil (top 1 m). The latter is expected to be the major source of bias toward detecting groundwater-related displacement. The ISBAS-InSAR technique, which is expected to have a nominal precision in the order of ≈ 5 -10 mm/yr, is potentially sensitive to surficial movements of the clay-rich vertosol soils, as it also incorporates into the phase-shift-to-displacement interpretation (inversion) procedure the low InSAR-coherence information occurring over cropping areas (corresponding in the Lower Namoi to soil and vegetation). The clay-rich vertosols and the intense cropping activities affect InSAR measurements, as demonstrated by the correlation between clay content and InSAR-displacements. Hence, the sensitivity of the ISBAS-InSAR technique to groundwater-related displacements decreases down to ≈ 2.5 cm/yr (considering a soil clay content of 60%) for the driest years. Around benchmarks with highest rates of subsidence soil clay content is of $\approx 50\%$. This corresponds to an InSAR noise of ≈ 2 cm/yr, which is more than twice the long-term subsidence rates detected on the benchmarks.

The PSI-InSAR technique, was tested by interpreting the phase shifts only on highly coherent ground targets, coinciding usually with hard and structurally stable surfaces. This largely isolates the noise from surficial clays, but also limits the measurement coverage to areas where built infrastructure occurs. As benchmarks are mostly surrounded by natural vegetation, the point-density obtained through PSI around benchmark is insufficient. We recommend the installation of

corner reflectors near benchmarks to assure the presence of coherent targets around the benchmarks in future InSAR surveys.

Implications for large-scale applications of InSAR over NSW

The project allows drawing observations on the usability of InSAR for other alluvial basins of NSW. A test was carried out over the Murrumbidgee area to complement the observations drawn over the Lower Namoi. The InSAR coherence is particularly low in the Lower Namoi and affected by the type of cropping activities and the clay-rich soils (in comparison with Murrumbidgee and to other cropping areas in Australia). This strongly challenges ISBAS-InSAR applications, which relies on interpreting a spatially-coherent SAR signal.

Subsidence above detection thresholds could be observed over the Murrumbidgee alluvium using similar processing parameters and input images as presented in this report. A recent InSAR test was also carried out using the Sentinel-1 scene to the West of the ones used for this study, which demonstrates that InSAR coherence there is better maintained in comparison to the Lower Namoi region, even over cropping areas. That is, the Lower Namoi is a particularly challenging for InSAR application and detection thresholds below ≈ 2 cm/yr may be possible in other areas of NSW.

Where InSAR coherence or result interpretation is challenged by the high clay content and the cropping/farming activities, we recommend the installation of corner reflectors. It usually consists in a three corrosion-proof metal sheets assembled together and positioned toward the satellite trajectory. It reflects a strong SAR signal that is coherent between acquisitions, which leads to highly accurate displacement measurements. A particular attention should be given to properly anchoring such reflectors into the ground, in a way to make the resulting SAR-derived displacement measurement insensitive to movements from the surficial clays.

Implications for GW modelling

Ground deformation using InSAR and benchmark surveys only indicate trends of spatially isolated, minor vertical displacement of less than in 8 to 16 mm/yr, respectively. This lack of spatially distributed historic deformation observations does not allow to calibrate simulated deformation or to estimate elastic and inelastic storage coefficients for the Lower Namoi groundwater model (LNM). However, deformation predictions within the LNM should be considered for future scenarios of groundwater depletion. This study provides a compilation of preconsolidation heads prior to development (e.g. during the late 1960s) and benchmark monitoring and demonstrates severe drops in critical heads during the mid-1970s, early 1980s, and mid-1990s. Using such data would require the LNM to include those periods unlike the current LNM, which starts in 1980.

Using the LNM for predictive subsidence modelling allows a probabilistic quantification of 'worst-case' modelled land subsidence that unlikely exceeds a threshold to predict critical drawdowns that result in inelastic compaction (based on the uncertainty of subsidence input parameters). A predictive LNM can also be used to determine where in space predictive uncertainty can be reduced by adding new InSAR and/or benchmark observations to the model. Finally, a predictive LNM can help manage the feedback and impacts of land subsidence (Schmid et al., 2014; Hanson et al., 2014, Boyce et al. 2020) on water-management related aspects, such as environmental assets, surface/ groundwater interaction, or the integrity of infrastructure (e.g. surface-water conveyance).

This approach of combining improved modelling methodology, observation data, and uncertainty analysis could be applied to other NSW-DPIE MODFLOW models in New South Wales that simulate

groundwater systems with significant groundwater extraction and spatially distributed subsidence above detection thresholds. For such studies, InSAR observations can be used for calibration and parameter estimation analogous to previous D-InSAR studies (Galloway et al., 1998; Hoffmann et al., 2003; Calderhead et al., 2011; Chaussard et al., 2014). The use of Point-InSAR for calibration and parameter estimation is documented in Hanson et al., 2014, and Faunt et al., 2016.

Appendix A **InSAR - Supplemental**

A.1 Vertical Displacement Trend Map

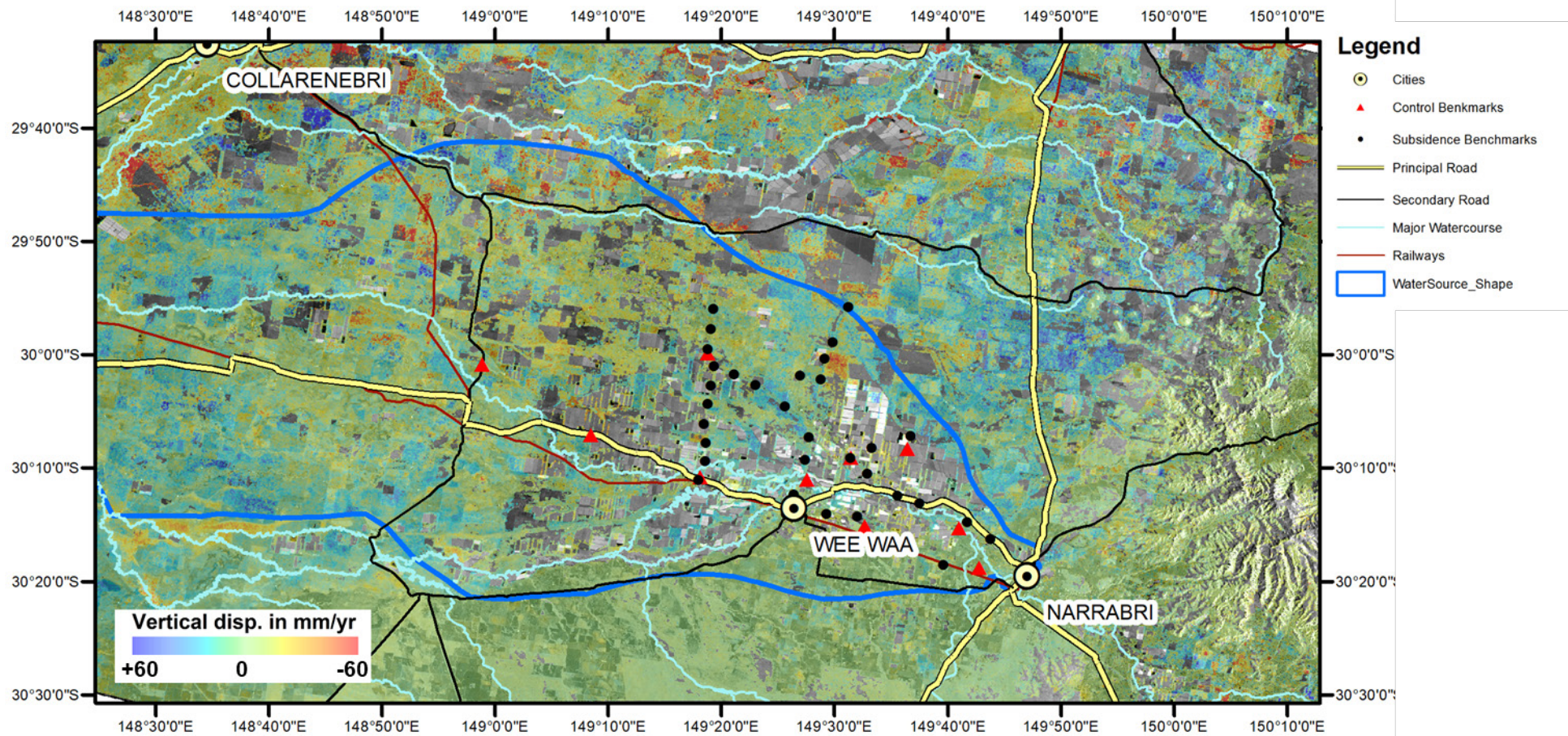


Figure 42 Vertical Displacement Trend in the Lower Namoi based on ISBAS-InSAR over a 3-year period (2016, 2017, 2018) with overlain Topography and location of Benchmarks

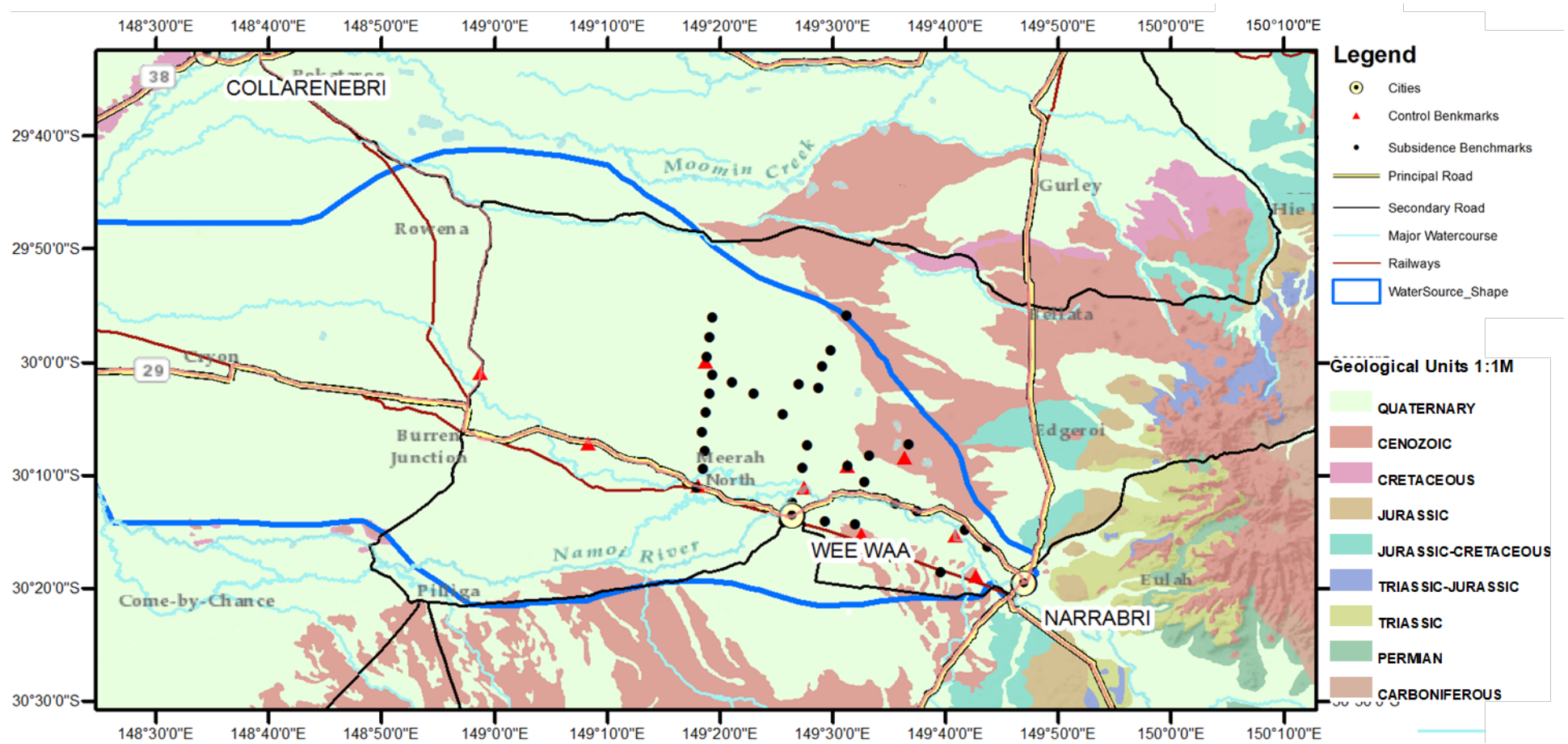


Figure 43 Generalised Surface Geology in the Lower Namoi for comparison with Vertical Displacement Trend in the Lower Namoi based on InSAR with overlain Topography and location of Benchmarks

Appendix B Benchmark Surveys - Supplemental

B.1 Area of Previous Benchmark Surveys after Ross and Jeffery, 1991

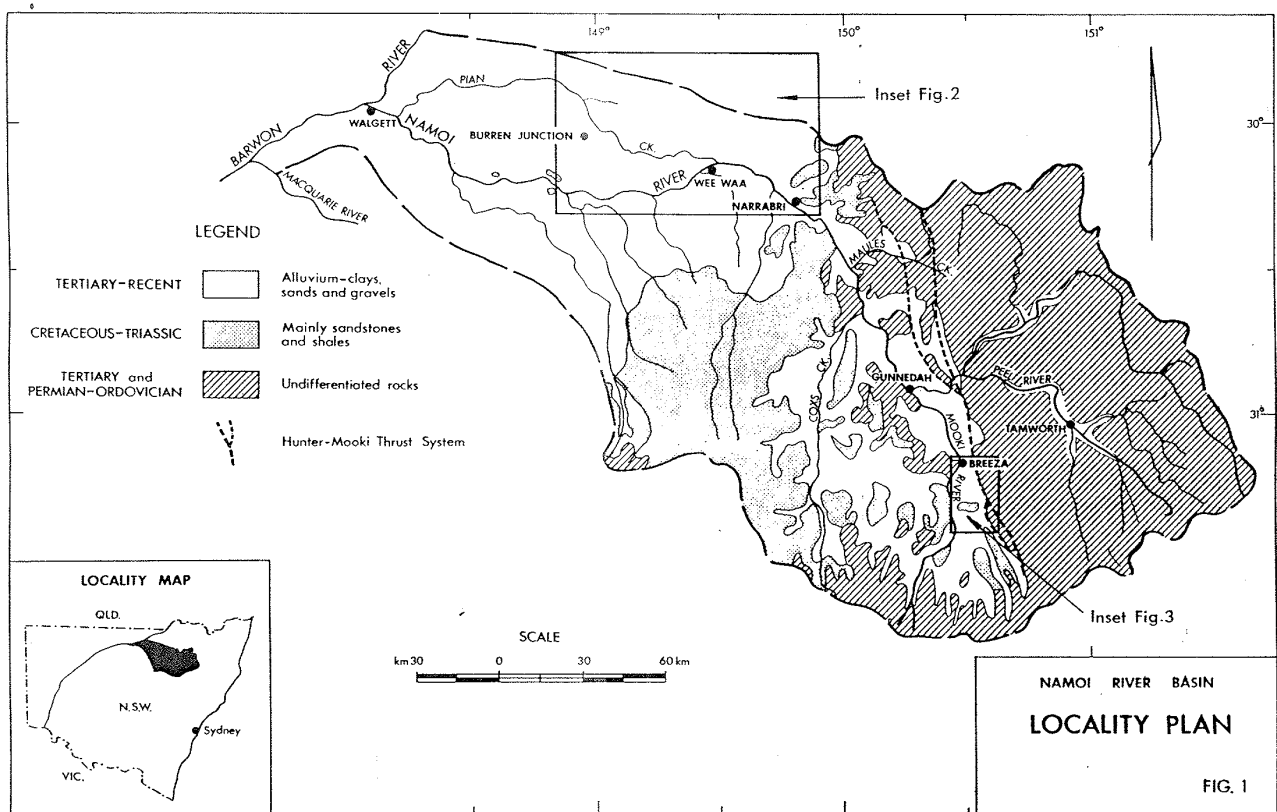


Figure 44 Locality Plan – Namoi River Basin (Ross and Jeffery, 1991)

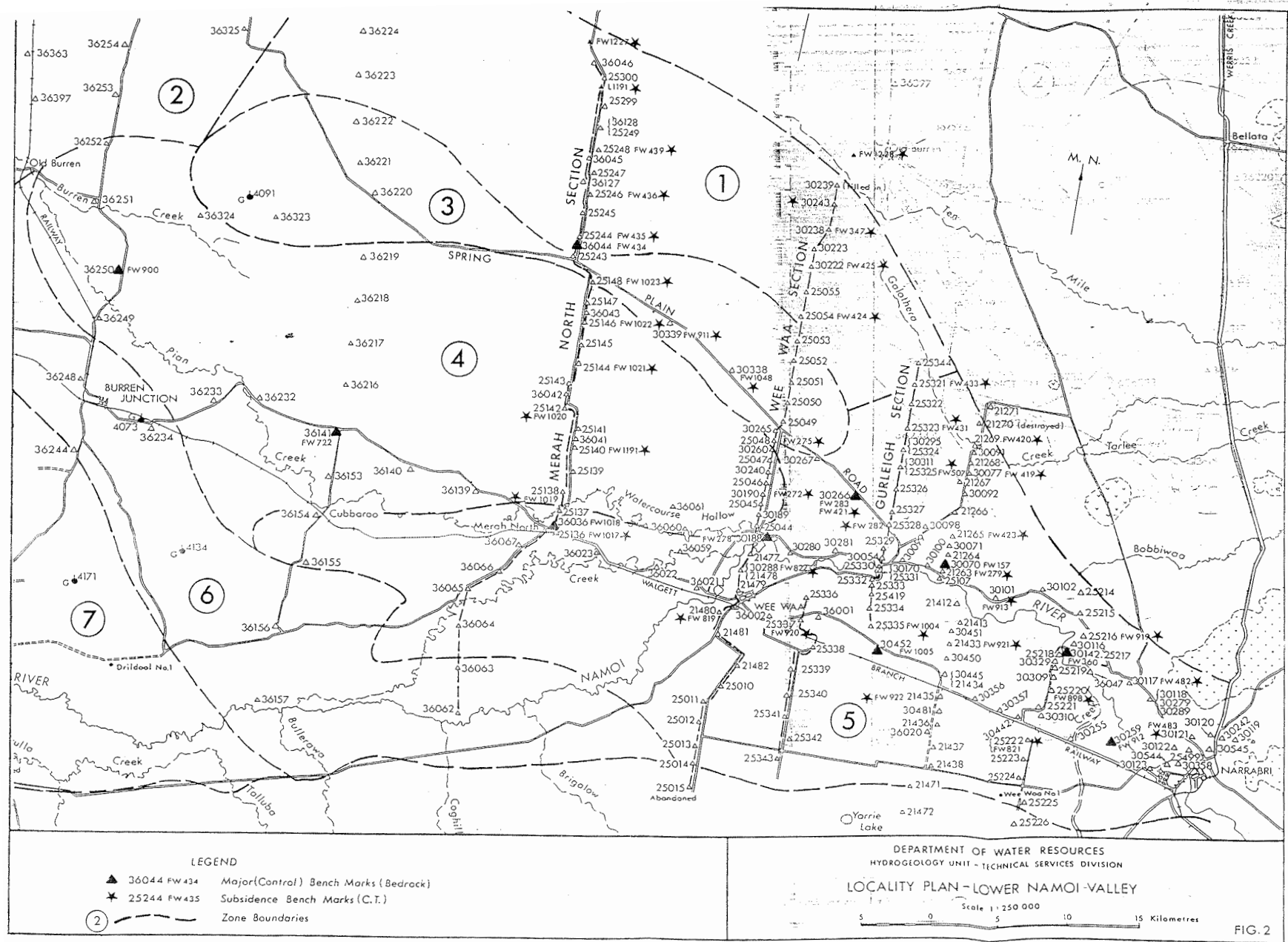


Figure 45 Locality Plan – Lower Namoi Valley (Ross and Jeffery, 1991)

B.2 Recent Benchmark Survey of April 2019

Table 7a Subsidence Benchmark Surveys 1974-1990 [m above AHD] (after Ross and Jeffery, 1991) and April 2019 - Results (Colour codes: see reverse side)

orig ID in Ross & Jeffery 1991	Bore Number	FW	Drillers Co-Ords Easting	Drillers Co-Ords Northing	EASTING	NORTHING	1974	1975	1978	1980	1981	1982	1987	1988	1990	2019	Total * [mm]
BM1228		1228			743346.844	6686214.113								182.796	182.786	182.824	28
BM21263	21263	279	749562	6655307	749560.428	6655334.038	199.822									199.784	-38
BM21265	21265	423	0	Bore Destroyed				198.994									N/A
BM21269	21269	420	751631	6664997	751654.886	6664984.168					197.847					197.839	-8
	21433	921	0	Bore Destroyed							201.028						N/A
BM21435	21435	922	748935	6646571	748926.879	6646602.936					204.883					204.88	-3
BM21480	21480	819	733694	6652792	N/A	N/A			190.19							190.198	8
BM25048	25048	275	737252	6665162	737234.065	6665179.574	190.072			190.052		190.072	190.057	190.057		190.046	-26
BM25054	25054	424	737024	6674502	739099.079	6674505.986		186.721		186.686		186.701	186.66	186.664	186.641	186.579	-142
BM25136	25136	1017	721424	6658499	721400.467	6658486.855				182.272						182.274	2
BM25138	25138	1019	722368	6661499	722413.35	6661526.028				182.485						182.46	-25
BM25140	25140	1191	722616	6664513	722623.178	6664538.676				182.268						182.247	-21
BM25142	25142	1020	722332	6667692	722360.512	6667569.615				181.724				181.762		181.709	-15
BM25144	25144	1021	722906	6670884	722945.438	6670846.799				180.066				180.096		179.988	-78
BM25146	25146	1022	723422	6673862	723480.374	6673879.582				179.796				179.831		179.763	-33
BM25148	25148	1023	723941	6676994	724030.19	6677003.59				178.411				178.411		178.346	-65
BM25216	25216	919	759411	6650764	759359.69	6650785.606					203.736					203.747	11
BM25220	25220	898	0	Bore Destroyed							206.483						N/A
BM25222	25222	821	755799	6643885	755794.817	6643891.429					209.554					209.556	2
BM25244	25244	435	723166	6679782	723193.129	6679817.022				176.994		176.992		176.983	176.989	176.954	-40
BM25246	25246	436	723714	6683036	723696.082	6683080.202				175.969		175.964		175.93	175.956	175.959	-10
BM25248	25248	439	724186	6686446	724140.868	6686391.151				175.104		175.104		175.045	175.079	175.068	-36
BM25300	25300		#N/A	#N/A	N/A	N/A										N/A	N/A
BM25321	25321	433	0	Bore Destroyed							192.445			192.415	192.455	N/A	N/A
BM25323	25323	431	0	Bore Destroyed							194.695			194.633	194.694		N/A
BM25325	25325	507	746074	6663243	746088.831	6663235.07					195.307			195.215	195.233	195.007	-300
BM25328	25328	282	745363	6659007	745348.79	6658998.544					197.054			197.065	197.055	196.995	-59
BM25333	25333		744368	6655178	N/A	N/A										N/A	N/A
BM25335	25335	1004	743897	6652045	743849.012	6652045.064					197.078					197.053	-25
BM25337	25337	920	739494	6652534	739477.193	6652568.895					194.496					194.465	-31
	30077	419	751072	6662791							198.646						N/A
BM30101	30101	913	752636	6653973	752657.44	6654028.677					201.361					201.324	-37
BM30117	30117	482	762635	6647975	762583.083	6647983.083					209.136					209.129	-7
	30121	483	766600	Bore Destroyed				211.094									N/A
BM30190	30190	272	736610	6661479	736577.031	6661431.617	191.7	191.7		191.691		191.69				191.682	-18
BM30222	30222	425	739784	6677973	739726.795	6677934.928		185.203		185.137		185.129	185.048	185.058	185.031	184.978	-225
BM30238	30238	347	741016	6680547	740977.353	6680541.58		184.379		184.327		184.344	184.198	184.224	184.168	184.005	-374
BM421	30266	421	743013	6661647	743009.118	6661586.637		195.005		195.002		194.996	194.996		194.994	194.949	-56
BM30288	30288	822	734857	6655909	734871.055	6655859.828			191.251							191.237	-14
BM30338	30338	1048	735272	6669025	733959.723	6670274.296				187.35						187.377	27
BM30339	30339	911	730567	6673376	729826.033	6673805.175				183.286						183.295	9
NAIL IN BITUMEN	NAIL IN BITUMEN				733731.714	6652724.649											190.418
STAR PICKET	STAR PICKET				726792.202	6675624.284											180.659

Data Sources:	
	2019-05-03 STATIC RTK FINAL MGA Z55
	Benchmark Details April 2019_.xls
	data from Ross and Jefferey 1991
	original survey year from Ross and Jeffery 1991
	* Total in [mm]: calculated total movement since initial survey

Comments of consultant (SMK Pty Ltd):

- “NOTE: HEIGHT DATUM AVERAGED FROM BEDROCK RLS AVAILABLE IN REPORT 'Ground Subsidence and Bore Collapse associated with Groundwater Withdrawals - Namoi Valley NSW Feb 1991'
- NOTE: HORIZONTAL DATUM - MGA GRID ZONE 55 GDA94”

Table 7b Subsidence Benchmark Surveys 1974-1990 (after Ross and Jeffery, 1991) and April 2019 – Notes, Location, Condition (Colour codes: see reverse side)

orig ID in Ross & Jeffrey 1991	Bore Number	FW	NOTES	Location Details	Condition (other than rust / paint)	Bore Condition Rating
BM1228		1228		1.6km past Jews Lagoon Crossing on nth west fence line		5
BM21263	21263	279			lock needs cutting	4
BM21265	21265	423				0
BM21269	21269	420	BENCHMARK HIT AND LEANING		no lock	3
	21433	921				0
BM21435	21435	922		CSIRO Road		2
BM21480	21480	819	UNDER THICK TREE COVER / NO CO-ORD SURVEYED - LEVELLED ONLY	west Side rd just past Edaen Lane		4
BM25048	25048	275		1m north of Helebah front gate (in off road)		3
BM25054	25054	424		Kevin Schwager a few days before access 428 667 541 access from road at northern end	No monument	2
BM25136	25136	1017	NO LOCK		no lock	2
BM25138	25138	1019			monument off lock not working	3
BM25140	25140	1191	LOCK JAMMED		lock not working	4
BM25142	25142	1020	CUT LOCK		lock not working	2
BM25144	25144	1021	CUT LOCK		lock not working	2
BM25146	25146	1022			lockwood lock	4
BM25148	25148	1023			monument off lock not working	3
BM25216	25216	919	NO LOCK	turn off hwy at large cement tank - unknown property owners	no lock	4
BM25220	25220	898				0
BM25222	25222	821	NO LOCK	Kiandool Ln		2
BM25244	25244	435	CUT LOCK		lock not working	4
BM25246	25246	436			no lock	4
BM25248	25248	439	CUT LOCK		lock not working	4
BM25300	25300		NO BM LOCATED			0
BM25321	25321	433	NO BM LOCATED			0
BM25323	25323	431				0
BM25325	25325	507	LOCK JAMMED OPEN		lock not working	2
BM25328	25328	282	LOCK JAMMED OPEN	Nth east cnr Greenbah Rd		4
BM25333	25333		NO BM LOCATED			0
BM25335	25335	1004		Call Merv "Eskdale" property - 42895425. Access to bore past shed to boundary then left along fence line		4
BM25337	25337	920		1m down Lynches Rd and on West, near rd sign		2
	30077	419			lock not working	4
BM30101	30101	913			lock needs cutting	2
BM30117	30117	482	BENCHMARK HIT AND LEANING	South side of Hwy		1
	30121	483				0
BM30190	30190	272			needs new lock	4
BM30222	30222	425		Kevin Schwager a few days before access 428 667 541 access from road at northern end		2
BM30238	30238	347				3
BM421	30266	421			needs new lock	2
BM30288	30288	822		Myalla Lane		2
BM30338	30338	1048	NO LOCK	1.6km west of Wee Waa Cotton Gin (Waiwera Ln) Nth side rd on fence line (not as per coords)		3
BM30339	30339	911		7.km west Wee Waa Cotton Gin (Waiwera Ln) sth side rd on fence line under tree (not as per coords)		3
NAIL IN BITUMEN	NAIL IN BITUMEN		PLACED TO OBTAIN LEVEL OF BM 21480			
STAR PICKET	STAR PICKET		PLACED FOR SURVEY CONTROL			

Files used:	
	2019-05-03 STATIC RTK FINAL MGA Z55
	Benchmark Details April 2019_.xls
	data from Ross and Jefferey 1991
	original survey year from Ross and Jefferey 1991

Bore Condition:	no. of bores	
0 Bore destroyed or no benchmark located	8	
1 Benchmark has been damaged - possible error in result	1	
2 Benchmark has had dirt encroached due to cropping activities	12	
3 Benchmark uncovered with no visible impact to site	7	
4 No visible reason for impact to result for benchmark	12	
5 No notes or comments	1	
	9	not used
	32	used
	41	sum

Appendix C **InSAR-Benchmark Comparison – Supplemental**

- C.1 Detailed Comparison of trends of vertical displacement for each subsidence benchmark with InSAR velocities derived at benchmark locations.

Table 8 Comparison of annualised trends of vertical velocities for each subsidence benchmark with InSAR velocities derived at benchmark locations (in mm/yr).

ID map	Name	Location [MGA GRID ZONE 55 GDA94]		Benchmark Year of		Total [mm]	Benchmark Vertical Displacement [mm/yr]			InSAR Velocity 3-year trend [mm/yr]			InSAR Velocity trend [mm]		
		Eastings	Northing	first survey	last before 2019		2019 - first	between 2019 – last	between 2019 – first	linear trend using all avail. data	InSAR LOS Vel.	InSAR VV (no buffer)	InSAR VV (15 x 15)	Trend 2016	Trend 2017
1	_FW1228	743346.8	6686214.1	1988	1990	28	1.31	0.90	1.08	12.98	16.70	8.34	4.27	11.17	12.55
2	BM21263_FW279	749560.4	6655334.0	1974	1974	-38	-0.84	-0.84	-0.84	-0.84	-1.07	-2.08	12.95	-4.36	-0.57
3	BM21269_FW420	751654.9	6664984.2	1981	1981	-8	-0.21	-0.21	-0.21	NA	NA	1.94	12.31	6.76	7.27
4	BM21435_FW922	748926.9	6646602.9	1981	1981	-3	-0.08	-0.08	-0.08	-5.05	-6.41	-5.10	4.39	-3.39	-3.43
5	BM21480_FW819	733733.9	6652752.0	1978	1978	8	0.20	0.20	0.20	-0.55	-0.71	-1.85	3.25	-1.11	-0.18
6	BM25048_FW275	737234.1	6665179.6	1974	1988	-26	-0.35	-0.58	-0.48	8.65	11.13	9.36	16.58	9.69	7.25
7	BM25054_FW424	739099.1	6674506.0	1975	1990	-142	-2.14	-3.23	-3.10	4.59	5.91	-0.29	-5.49	-5.78	6.74
8	BM25136_FW1017	721400.5	6658486.9	1980	1980	2	0.05	0.05	0.05	9.39	12.21	9.27	20.59	6.70	3.49
9	BM25138_FW1019	722413.3	6661526.0	1980	1980	-25	-0.64	-0.64	-0.64	18.61	24.20	18.90	39.63	12.79	12.51
10	BM25140_FW1191	722623.2	6664538.7	1980	1980	-21	-0.54	-0.54	-0.54	-8.05	-10.48	-5.33	11.12	-10.13	1.92
11	BM25142_FW1020	722360.5	6667569.6	1980	1988	-15	-1.71	-0.38	-0.76	0.60	0.78	0.95	18.07	-1.41	-1.82
12	BM25144_FW1021	722945.4	6670846.8	1980	1988	-78	-3.48	-2.00	-2.42	-6.22	-8.10	-1.48	1.46	3.55	-1.47
13	BM25146_FW1022	723480.4	6673879.6	1980	1988	-33	-2.19	-0.85	-1.22	3.99	5.20	4.03	9.21	2.30	-6.95
14	BM25148_FW1023	724030.2	6677003.6	1980	1988	-65	-1.67	-1.67	-1.79	0.01	0.01	-8.83	6.12	-5.17	-18.57
15	BM25216_FW919	759359.7	6650785.6	1981	1981	11	0.29	0.29	0.29	6.53	8.22	3.38	17.97	0.71	5.06
16	BM25222_FW821	755794.8	6643891.4	1981	1981	2	0.05	0.05	0.05	1.05	1.32	-1.22	11.18	-4.90	-1.84
17	BM25244_FW435	723193.1	6679817.0	1980	1990	-40	-1.21	-1.03	-1.02	-1.81	-2.36	-1.88	-4.24	-5.66	2.14
18	BM25246_FW436	723696.1	6683080.2	1980	1990	-10	0.10	-0.26	-0.05	-6.75	-8.82	-6.82	-1.12	-9.15	-4.90
19	BM25248_FW439	724140.9	6686391.2	1980	1990	-36	-0.38	-0.92	-0.72	3.09	4.04	2.45	12.62	1.75	1.66
20	BM25325_FW507	746088.8	6663235.1	1981	1990	-300	-7.79	-7.89	-7.60	-4.75	-6.06	-8.53	28.60	-16.50	-20.31
21	BM25328_FW282	745348.8	6658998.5	1981	1990	-59	-2.07	-1.55	-1.80	-2.39	-3.05	-0.87	14.86	-4.14	0.78
22	BM25335_FW1004	743849	6652045.1	1981	1981	-25	-0.66	-0.66	-0.66	5.28	6.73	1.07	3.60	-0.18	4.37
23	BM25337_FW920	739477.2	6652568.9	1981	1981	-31	-0.82	-0.82	-0.82	-2.70	-3.46	-5.19	-0.30	-4.58	-1.65
24	BM30101_FW913	752657.4	6654028.7	1981	1981	-37	-0.97	-0.97	-0.97	-7.81	-9.90	-7.95	6.39	-7.26	-1.21
25	BM30117_FW482	762583.1	6647983.1	1981	1981	-7	-0.18	-0.18	-0.18	-0.45	-0.56	-3.32	2.44	-1.94	1.25
26	BM30190_FW272	736577	6661431.6	1974	1982	-18	-0.22	-0.40	-0.36	16.91	21.73	15.11	21.00	19.78	12.55
27	BM30222_FW425	739726.8	6677934.9	1975	1990	-225	-1.83	-5.11	-4.54	-14.01	-18.03	-16.30	10.17	-15.61	-7.41
28	BM30238_FW347	740977.4	6680541.6	1975	1990	-374	-5.62	-8.50	-8.52	22.96	29.54	14.93	23.50	13.42	1.20
29	BM30266_FW421	743005.6	6661586.6	1975	1990	-56	-1.55	-1.27	-1.30	-11.74	-15.02	-8.68	2.88	-6.21	-2.91
30	BM30288_FW822	734871.1	6655859.8	1978	1978	-14	-0.34	-0.34	-0.34	1.11	1.42	-3.49	6.39	-4.29	2.22
31	BM30338_FW1048	733959.7	6670274.3	1980	1980	27	0.69	0.69	0.69	9.19	11.86	10.37	18.44	10.46	10.16
32	BM30339_FW911	729826	6673805.2		1980	9	0.23	0.23	0.23	5.50	7.14	4.70	12.38	7.59	0.96

- C.2 Comparison of InSAR Vertical Displacement with Benchmark trends using no measurement inaccuracy at all

- C.3 Comparison of InSAR Vertical Displacement with Benchmark trends using a measurement inaccuracy of 1 mm/yr

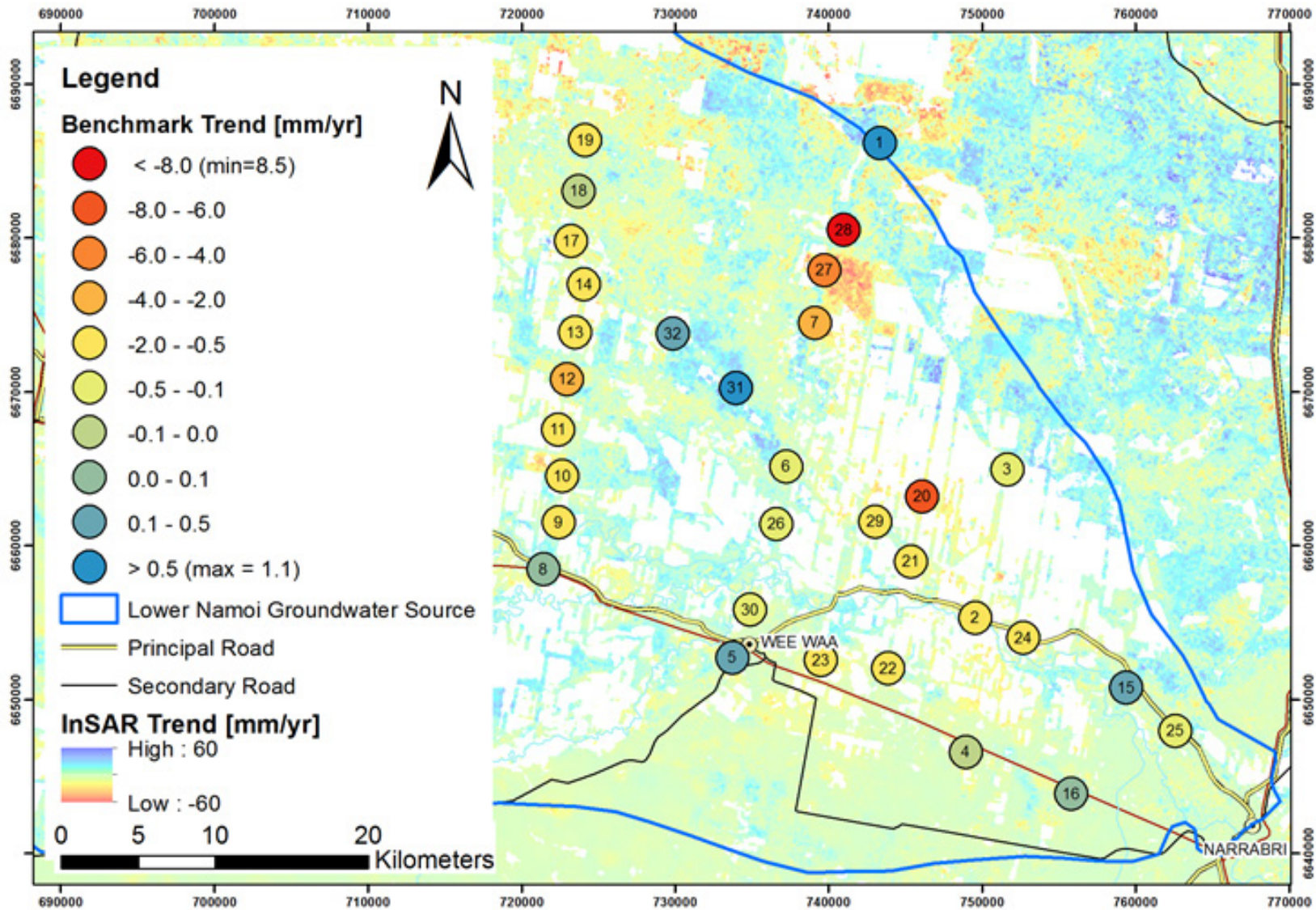


Figure 46 Comparison of InSAR vertical displacement with benchmark trends using no measurement inaccuracy at all (white areas: below coherence threshold)

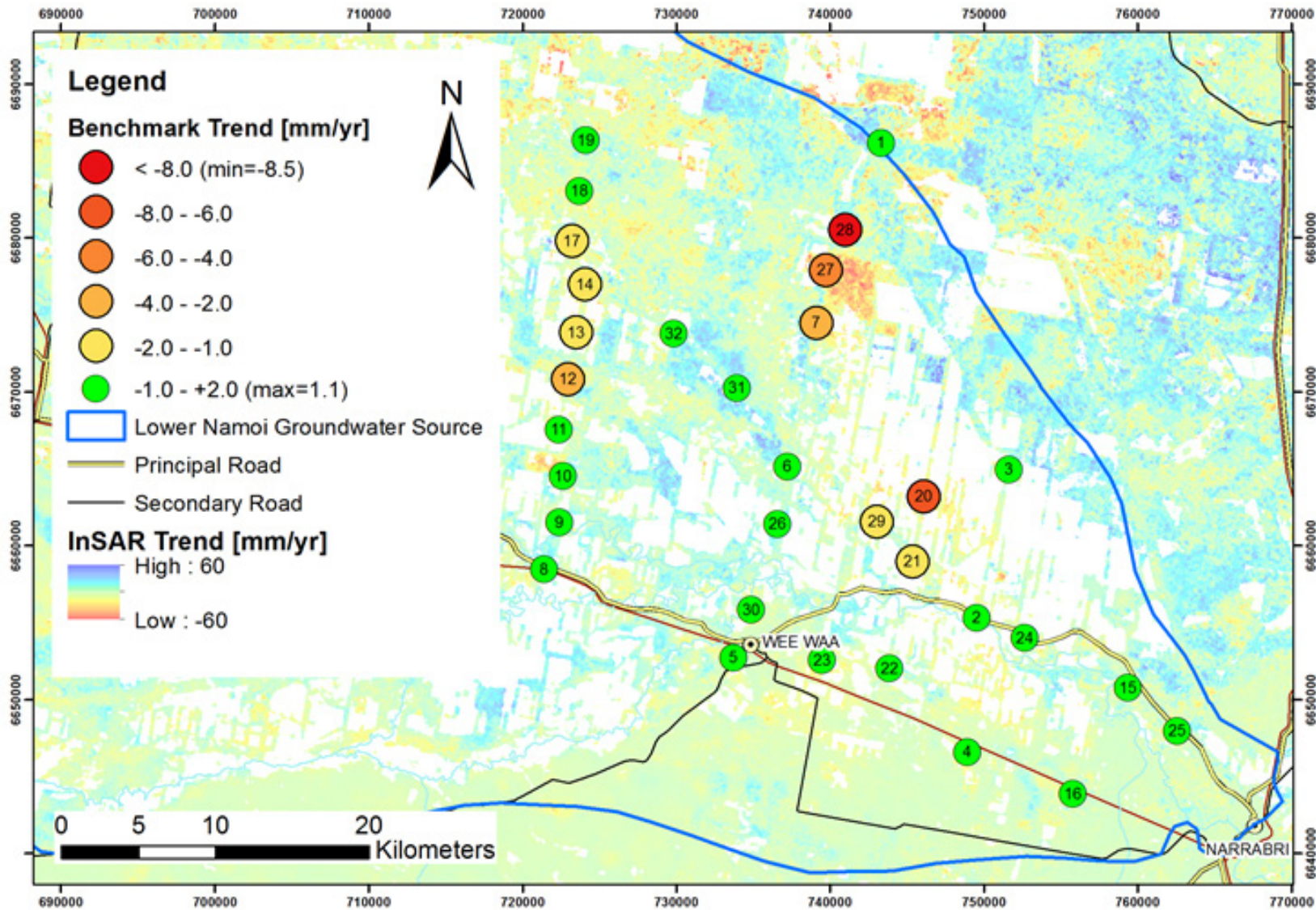


Figure 47 Comparison of InSAR vertical displacement with benchmark trends using a measurement inaccuracy of -1 mm/yr (white areas: below coherence threshold)

Appendix D **Correlating Ground Movement with Auxiliary Data – Supplemental**

- D.1 Correlation between drop in head or critical head and deformation trends during the 3-year InSAR Period for select piezometers for logger data.
- D.2 Correlation between drop in head or critical head and deformation trends during the 3-year InSAR Period for select piezometers for manual data

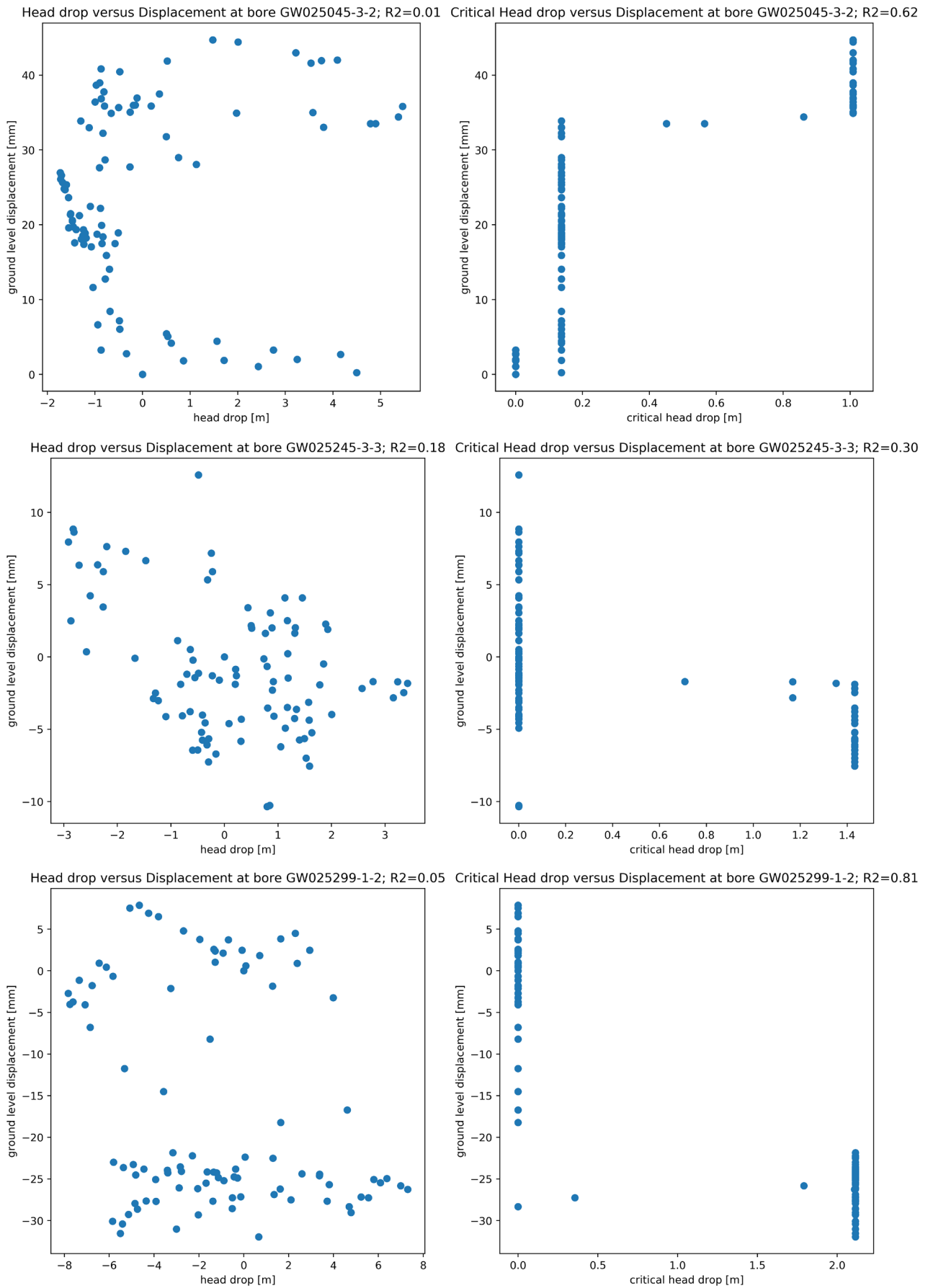


Figure 48 Correlation between drop in head (left) or critical heads (right) and deformation trends during the 3-year InSAR Period for select piezometers with non-zero critical head drop for logger data.

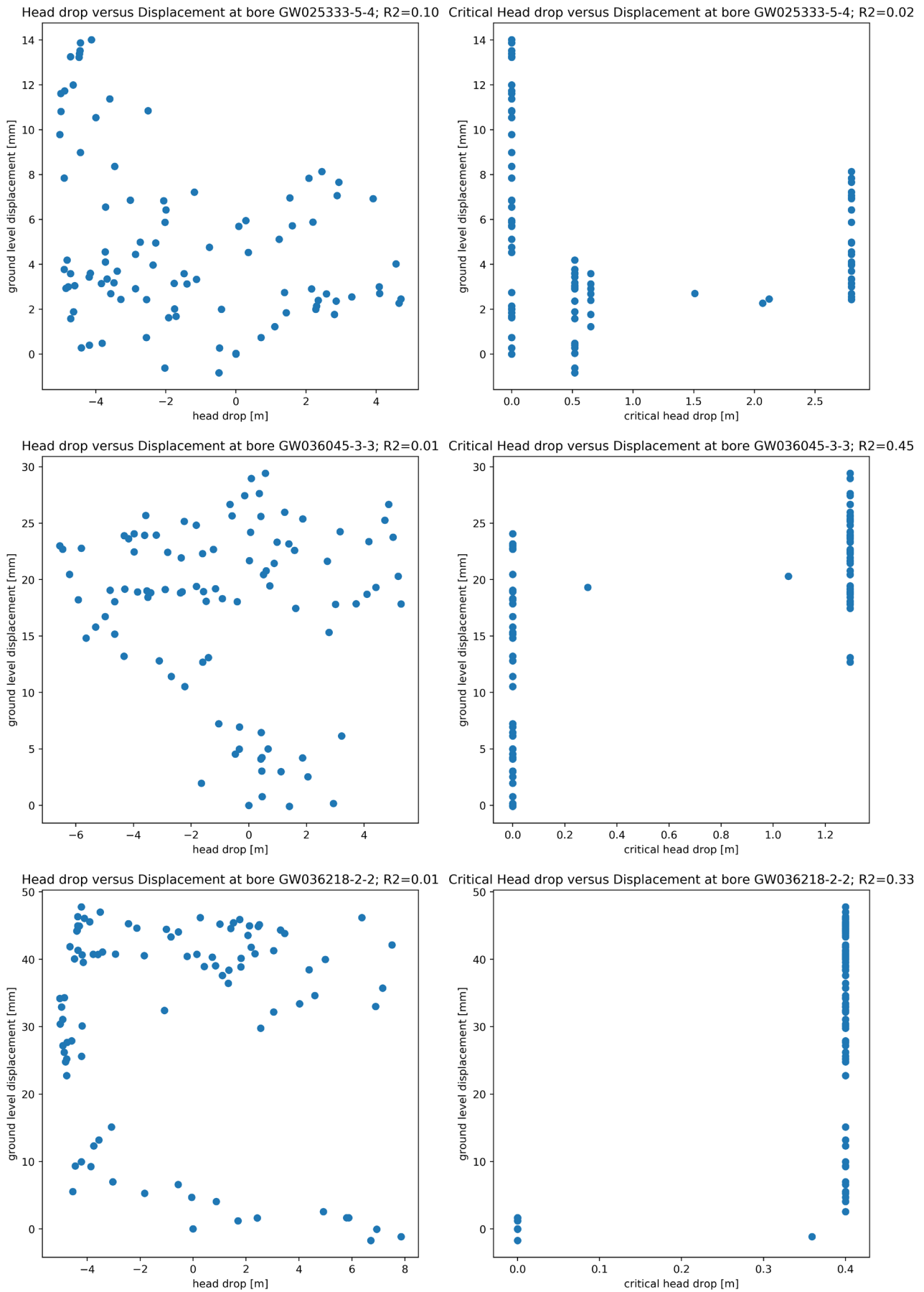


Figure 48 (cont.) Correlation between drop in head (left) or critical heads (right) and deformation trends during the 3-year InSAR Period for select piezometers with non-zero critical head drop for logger data.

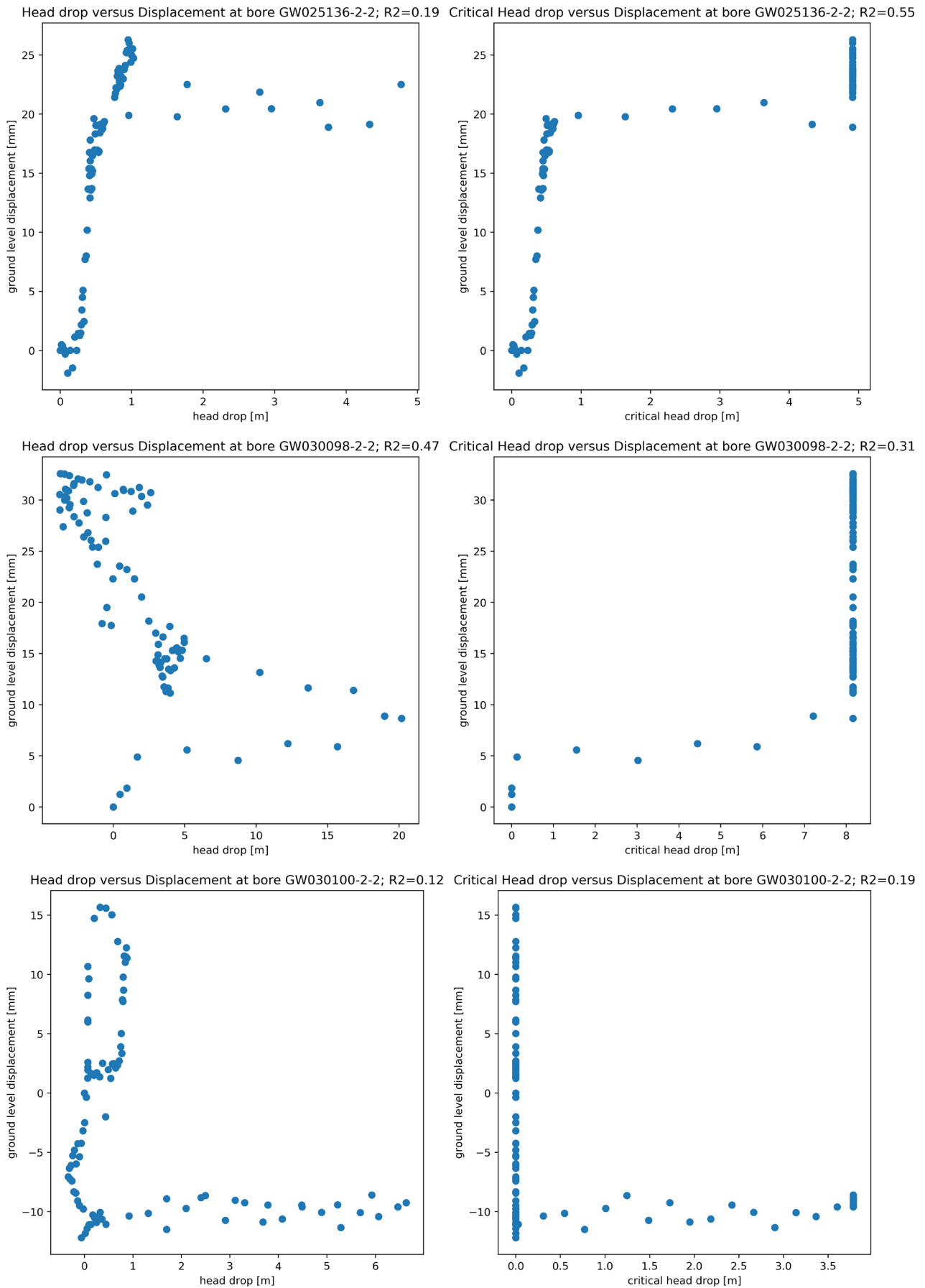


Figure 49 Correlation between drop in head (left) or critical heads (right) and deformation trends during the 3-year InSAR Period for select maximal drop in critical heads (> 3 metres) for manual data.

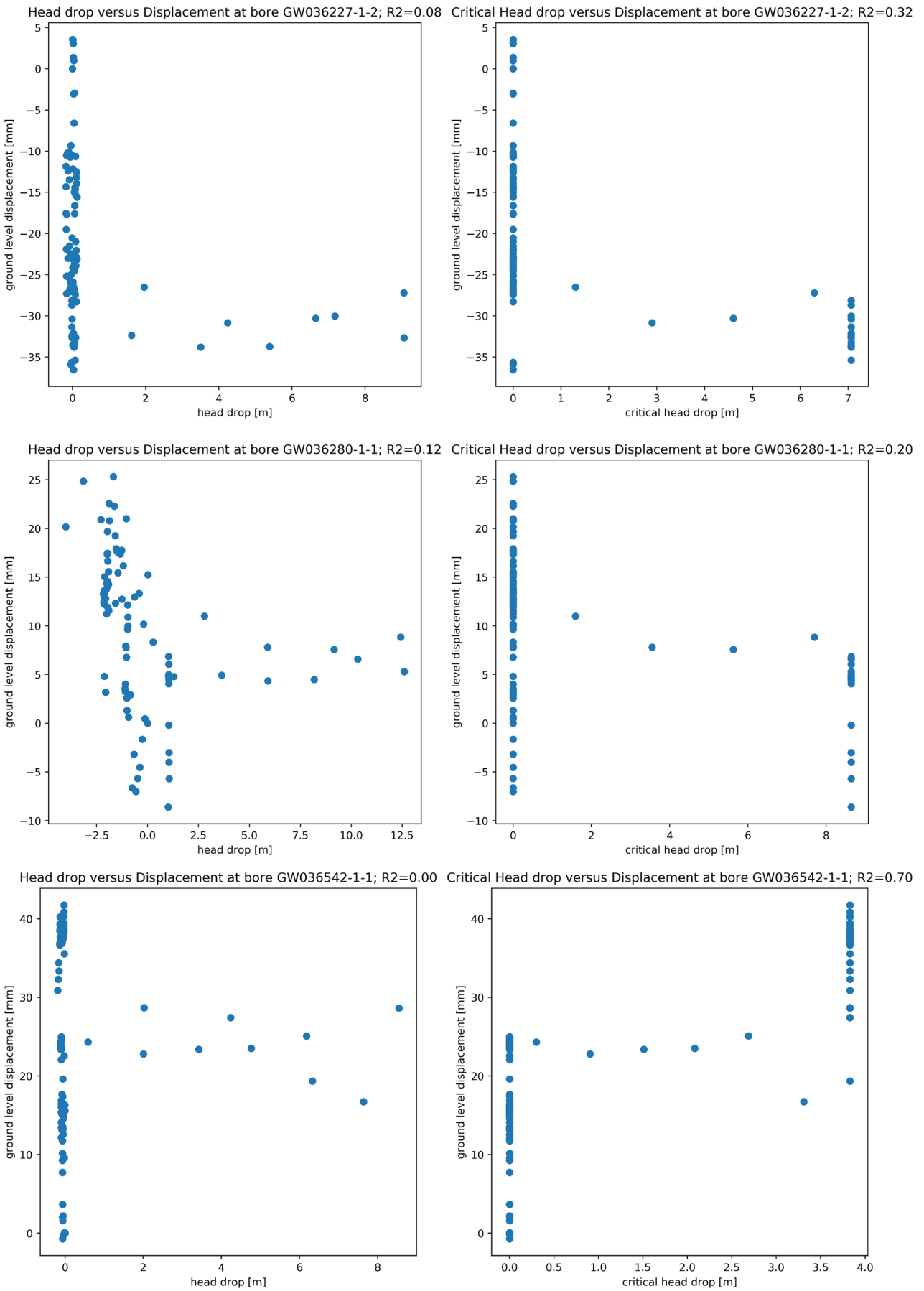


Figure 49 (cont.) Correlation between drop in head (left) or critical heads (right) and deformation trends during the 3-year InSAR Period for select maximal drop in critical heads (> 3 metres) for manual data

References

- Ali, A, Merrick, NP, Williams, RM, Mampitiya, D, d’Hautefeuille, F, and Sinclair, P (2004) Land settlement due to groundwater pumping in the Lower Namoi Valley of NSW. In Proceedings of 9th Murray Darling Basin Groundwater Workshop, Bendigo, Australia.
- Boyce, SE, Hanson, RT, Ferguson, I, Schmid, W, Henson, W, Reimann, T, Mehl, SM, and Earll, MM (2020) One-Water Hydrologic Flow Model: A MODFLOW based conjunctive-use simulation software: U.S. Geological Survey Techniques and Methods 6–A60, 435 p., <https://doi.org/10.3133/tm6a60>.
- Berardino, P, Fornaro, G, Lanari, R, and Sansosti, E (2002) A new algorithm for surface deformation monitoring based on small baseline differential SAR interferograms. *IEEE Transactions on Geoscience and Remote Sensing*, 40(11), 2375–2383. <https://doi.org/10.1109/TGRS.2002.803792>
- Calderhead, AI, Therrien, R, Rivera, A, Martel, R, and Garfias, J (2011) Simulating pumping-induced regional land subsidence with the use of InSAR and field data in the Toluca Valley, Mexico. *Advances in Water Resources*, 34(1), 83-97.
- Castellazzi, P, Arroyo-Domínguez, N, Martel, R, Calderhead, AI, Normand, JCL, Gárfias, J, and Rivera, A (2016) Land subsidence in major cities of Central Mexico: Interpreting InSAR-derived land subsidence mapping with hydrogeological data. *International Journal of Applied Earth Observation and Geoinformation*, 47. <https://doi.org/10.1016/j.jag.2015.12.002>
- Castellazzi, P, Garfias, J, Martel, R, Brouard, C, and Rivera, A (2017) InSAR to support sustainable urbanization over compacting aquifers: The case of Toluca Valley, Mexico. *International Journal of Applied Earth Observation and Geoinformation*, 63. <https://doi.org/10.1016/j.jag.2017.06.011>
- Chaussard, E, Bürgmann, R, Shirzaei, M, Fielding, EJ and Baker, B (2014) Predictability of hydraulic head changes and characterization of aquifer-system and fault properties from InSAR-derived ground deformation, *J. Geophys. Res. Solid Earth*, 119, 6572–6590, doi:10.1002/2014JB011266.
- Faunt, CC, Sneed, M, Traum, J, and Brandt, JT (2016) Water availability and land subsidence in the Central Valley, California, USA. *Hydrogeol J* 24, 675–684 (2016) doi:10.1007/s10040-015-1339-x
- Ferretti, A, Prati, C, and Rocca, F (2001) Permanent scatterers in SAR interferometry. *IEEE Transactions on Geoscience and Remote Sensing*, 39(1), 8–20. <https://doi.org/10.1109/36.898661>
- Galloway DL, Hudnut KW, Ingebritsen SE, Phillips SP, Peltzer G, Rogez F, and Rosen PA (1998) Detection of aquifer system compaction and land subsidence using interferometric synthetic aperture radar, Antelope Valley, Mojave Desert, California. *Water Resour Res* 1998;34:2573–85.

- Garthwaite, MC, Nancarrow, S, Hislop, A, Dawson, J, Lawrie, S, and Thankappan, M (2015) The Design of Radar Corner Reflectors for the Australian Geophysical Observing System: a single design suitable for InSAR deformation monitoring and SAR calibration at multiple microwave frequency bands. Record 2015/03. Geoscience Australia, Canberra.
- Hanson, RT, Boyce, SE, Schmid, W, Hughes, JD, Mehl, SM, Leake, SA, Maddock, TIII, and Niswonger, RG (2014) One-Water Hydrologic Flow Model (MODFLOW-OWHM): U.S. Geological Survey Techniques and Methods 6–A51, 120 p., <https://dx.doi.org/10.3133/tm6A51>.
- Hanson, RT, Flint, LE, Faunt, CC, Gibbs, DR, and Schmid, W (2014) Hydrologic models and analysis of water availability in Cuyama Valley, California: U.S Geological Survey Scientific Investigations Report 2014–5150, 150 p., <http://dx.doi.org/10.3133/sir20145150>
- Hoffmann J, Galloway D, Howard AJ (2003) Inverse modeling of interbed storage parameters using land subsidence observations, Antelope Valley, California. Water Resources Res 2003;39(2):1231.)
- Kirby, JM, Bernardi, AL, Ringrose-Voase, AJ, Young, R, and Rose, H (2003) Field swelling, shrinking, and water content change in a heavy clay soil. Soil Research, 41(5), 963-978.
- Martel, R., Castellazzi, P., Gloaguen, E., Trépanier, L., & Garfias, J. (2018). ERT, GPR, InSAR, and tracer tests to characterize karst aquifer systems under urban areas: The case of Quebec City. Geomorphology, 310. <https://doi.org/10.1016/j.geomorph.2018.03.003>
- Massonnet, D., & Feigl, K. L. (1998). Radar interferometry and its application to changes in the Earth's surface. Reviews of Geophysics, 36(4), 441–500. <https://doi.org/10.1029/97RG03139>
- NSW & OEH (2018) Digital soil mapping of key soil properties over New South Wales Version 1.2; <https://www.environment.nsw.gov.au/-/media/OEH/Corporate-Site/Documents/Land-and-soil/digital-soil-mapping-key-soil-properties-nsw-180489.pdf> - accessed 09/01/2020.
- NSW & OEH (2020) <https://www.environment.nsw.gov.au/eSpade2Webapp> - accessed 09/01/2020
- NSW (2019) Water Sharing Plan for the Upper and Lower Namoi Groundwater Sources 2019 under the Water Management Act 2000. Melinda Pavey, Minister for Water, 24 June 2019. <https://legislation.nsw.gov.au/regulations/2019-304.pdf>; accessed 02/07/2019.
- NSW-DPIE (2019) Risk Assessment for the Namoi Alluvium Water Resource Plan (GW14); Published by NSW Department of Industry; First published June 2019; https://www.industry.nsw.gov.au/__data/assets/pdf_file/0003/230808/schedule-d-draft-namoi-alluvium-risk-assessment-wrpa.pdf; accessed 04/07/2019.
- Ringrose-Voase A (2019) verbal communication
- Ross JB and Jeffery L (1991) Ground Subsidence and Bore Hole Collapse associated with Groundwater Withdrawals—Namoi Valley NSW, Technical Services Division, Hydrogeology Unit.
- Schmid, W, Hanson, RT, Leake, SA, Hughes, JD, and Niswonger, RG (2014) Feedback of land subsidence on the movement and conjunctive use of water resources. Environmental modelling & software, 62, 253-270.

Sowter, A, Bateson, L, Strange, P, Ambrose, K, & Syafiudin, MF (2013) DInSAR estimation of land motion using intermittent coherence with application to the South Derbyshire and Leicestershire coalfields. *Remote Sensing Letters*, 4(10), 979–987.
<https://doi.org/10.1080/2150704X.2013.823673>

Water Management Act 2000 (NSW) s. 324, retrieved from
<https://www.legislation.nsw.gov.au/#/view/act/2000/92/chap7/part1/div2/sec324>

CONTACT US

t 1300 363 400
+61 3 9545 2176
e csiroenquiries@csiro.au
w www.csiro.au

AT CSIRO, WE DO THE
EXTRAORDINARY EVERY DAY

We innovate for tomorrow and help improve today – for our customers, all Australians and the world.

Our innovations contribute billions of dollars to the Australian economy every year. As the largest patent holder in the nation, our vast wealth of intellectual property has led to more than 150 spin-off companies.

With more than 5,000 experts and a burning desire to get things done, we are Australia's catalyst for innovation.

CSIRO. WE IMAGINE. WE COLLABORATE.
WE INNOVATE.

FOR FURTHER INFORMATION

LAND AND WATER
Wolfgang Schmid
t +61 8 9333 6793
e wolfgang.schmid@csiro.au

FOR FURTHER INFORMATION

LAND AND WATER
Pascal Castellazzi
t 61 4 5237 2066
e pascal.castellazzi@csiro.au